INVESTIGATION OF SEMI-EMPIRICAL BATTERY AGING MODELS OF ELECTRIC VEHICLES

A Thesis Submitted to
the Graduate School of
İzmir Institute of Technology
in Partial Fulfilment of the Requirements for the Degree of

MASTER OF SCIENCE

in Mechanical Engineering

by
Gülşah YARIMCA

December 2023
İZMİR

We approve the thesis of **Gülşah YARIMCA**

Examining Committee Members:

Prof. Dr. Erdal ÇETKİN
Department of Mechanical Engineering, İzmir Institute of Technology

Assist. Prof. Dr. Kasım TOPRAK
Department of Mechanical Engineering, İzmir Institute of Technology

Assoc. Prof. Dr. Mehmet Akif EZAN
Department of Mechanical Engineering, Dokuz Eylül University

5 December 2023

Prof. Dr. Erdal Çetkin
Supervisor, Department of
Mechanical Engineering
İzmir Institute of Technology

Prof. Dr. M. İ. Can DEDE
Head of the Department of
Mechanical Engineering

Prof. Dr. Mehtap EANES
Dean of the Graduate School

ACKNOWLEDGMENTS

I would like to express my heartfelt gratitude to the individuals who played instrumental roles in the successful completion of my master's thesis. Their unwavering support, guidance, and encouragement have been invaluable.

First, I would like to express my deepest gratitude to my advisor Prof. Dr. Erdal ÇETKİN for his extraordinary mentorship, valuable opinions, encouragement and patience.

I am deeply grateful to my father, Abdullah YARIMCA, my mother, Meltem YARIMCA, and my sister, Ayça Büşra YARIMCA, who have always been with me throughout this academic study and provided their endless support. Their belief in my abilities has been a constant source of inspiration, and I am truly blessed to have such a supportive foundation.

I would like to express my special thanks to Erkan PAKSOY, who significantly contributed to the development and improvement of this thesis with his invaluable expertise and contributions.

Moreover, I extend my sincere gratitude to my lab friends whose camaraderie, discussions, and shared experiences have enriched my academic and personal growth. Their support and encouragement have been a constant source of motivation.

I express my gratitude to the European HORIZON-HELIOS project partners, particularly Anders Christian Solberg JENSEN from Danish Technological Institute, for generously providing crucial test results.

Also, I would like to thank my thesis defence committee members Assist. Prof. Dr. Kasım TOPRAK, Assoc. Prof. Dr. M.Akif EZAN for their valuable suggestions and encouragements.

ABSTRACT

INVESTIGATION OF SEMI-EMPIRICAL BATTERY AGING MODELS OF ELECTRIC VEHICLES

Batteries have been the focus of attention due to their numerous advantages in distinct applications such as recently on Electric Vehicles A limiting factor for adaptation by industry is related to the aging of batteries over time. Characteristics of battery aging vary depending on many factors such as battery type, electrochemical reactions and operation conditions. Aging could be considered in two sections according to its type: calendaring and cycling. This thesis presents a review of empirical and semi-empirical modelling techniques and studies of aging. It focuses on the trends observed across different studies for two types of aging and highlights the limitations and challenges of various models. It introduces three different models for semi-empirical modelling based on Arrhenius Law from the literature for calendar aging, which cover all three important factors for calendar aging: temperature, stage of charge, and time. Moreover, four more models are developed based on these three factors and the Arrhenius law to contribute to the literature. To examine the usability and compatibility of these models, we selected five different experimental sets based on different chemistries and operating conditions from the literature. We also added calendar aging experiments carried out within the scope of our HORIZON-Helios European Project and examined a total of six experimental sets. The Helios Project dataset is split into 70% training data and 30% prediction data to measure the ability to predict future capacity loss. For this purpose, linear regression and genetic algorithm methods were used to determine the parameters of each semi-experimental model by minimizing the mean square error value between the prediction results and experimental capacity data. As a result, it was seen that the numerical solution obtained using the genetic algorithm gave better results than the analytical solution obtained by linear regression.

The objective of this thesis is to present comprehensive and accurate models by examining the compatibility of models proposed in the literature models developed in our research with experimental sets. 7 Semi-Empirical Models (SEM), based on a fixed set of defined parameters, have obtained satisfactory estimates of calendar obsolescence for

given storage conditions. SEM-3 and 7 were able to predict capacity loss with low errors. In particular, SEM-3 had the lowest RMSE in most experimental sets. While model errors are generally close to each other, Redondo-Iglesias et. al model and Model 7 have lower errors, similar to SEM-3. When all data sets are examined, it is seen that the lowest and highest RMSE values in the model predictions are 0.036 and 3.91, respectively.

Keywords: Electric Vehicles Battery, Battery Aging, Calendaring and Cycling Aging, Calendaring Aging Modelling

ÖZET

ELEKTRİKLİ ARAÇLARIN YARI-AMPİRİK BATARYA YAŞLANMA MODELLERİNİN İNCELENMESİ

Piller, son dönemde Elektrikli Araçlar gibi farklı uygulamalardaki sayısız avantajlarından dolayı ilgi odağı olmuştur. Endüstrinin adaptasyonunu sınırlayan faktörlerden biri de pillerin zaman içinde yaşlanmasıyla ilgilidir. Yaşlanma, türüne göre iki bölümde ele alınabilir: Takvim ve döngüsel yaşlanma. Bu iki yaşlanma tipi için farklı çalışmalar arasında gözlemlenen eğilimlere odaklanarak, ampirik ve yarı-ampirik modelleme tekniklerinin ve eskime çalışmalarının bir incelemesi sunulmaktadır. Daha sonra takvimsel yaşlanma için literatürden Arrhenius Yasası'na dayalı yarı-ampirik modelleme kullanan üç farklı model sunulmuştur. Ayrıca literatüre katkı sağlamak amacıyla Arrhenuis Yasası'na bağlı 4 farklı model daha geliştirilmiştir. Bu modellerin kullanabilirliği ve uyumluluğunu incelemek için literatürden birbirinden farklı kimyalara ve çalışma koşullarına bağlı 5 farklı deney seti seçilmiştir. HORIZON-Helios Avrupa projesi kapsamında gerçekleştirilen takvimsel yaşlanma deneyleri de eklenmiş olup toplamda 6 adet deney seti incelenmiştir. Helios Projesi veri seti, gelecekteki kapasite kaybını tahmin etme yeteneğini ölçmek için %70 eğitim, %30 tahmin verisiyle bölünmüştür. Bu amaçla, yarı-ampirik modellere ait parametreleri belirlemek için Doğrusal Regresyon ve Genetik Algoritma kullanılmıştır. Bunun sonucunda genetik algoritma kullanılarak elde edilen modellerin doğrusal regresyonda elde edilen modellere göre daha iyi sonuçlar verdiği görülmüştür. Bu tezin amacı, literatürdeki ve geliştirilen modellerin, deney setleriyle uyumluluğunu inceleyerek kapsamlı ve doğru modeller sunmaktır. Bir dizi tanımlanmış parametreye dayanan 7 yarı-ampirik modelleme, belirli depolama koşulları için takvim eskimesi konusunda tatmin edici tahminler elde etti. Özellikle Model-3 çoğu deney setinde en düşük kök kare ortalama hatasına (RMSE) sahipti. Literatürdeki verilerin kullanıldığı model hataları genel olarak birbirine yakın olmakla birlikte Redondo-Iglesias vd. modeli ve Model-7, Model-3'e benzer şekilde daha düşük hatalara sahiptir. Tüm veri setleri incelendiğinde model tahminlerinde en düşük ve en yüksek RMSE değerlerinin sırasıyla 0,036 ve 3,91 olduğu görülmektedir.

Anahtar Kelimeler: Elektrikli araç bataryası, Batarya yaşlanması, Takvimsel ve döngü yaşlanması, Takvimsel yaşlanma modellemesi

TABLE OF CONTENTS

LIST OF FIGURES

Figure **Page**

LIST OF TABLES

Table **Page**

LIST OF SYMBOLS

Nomenclature

EV	Electric Vehicle
SoC	Stage of charge
DoD	Depth of discharge
C-rate	Dis/charge current divided by nominal battery capacity
DoD	Depth of discharge
DoC	Depth of cycle
SEI	Solid electrolyte interphase
E_a	Activation Energy [$kJ.mol^{-1}$]
LCO	Lithium cobalt oxide
LFP	Lithium iron phosphate
NMC	Lithium nickel manganese cobalt oxide
Q_{loss}	Capacity Loss
T	Temperature [K]
t	Days
A	Exponential factor
R	Gas constant [mol^{-1} K^{-1}]
k	Boltzmann Constant [eV K^{-1}]
a,b,c,d	Fitting Parameters
SEM	Semi-Empirical Model
MAE	Mean Absolute Error
RMSE	Root-mean-square-error
MAPE	Mean Absolute Percentage Error

Greek letters

α, β, γ	Fitting parameters

CHAPTER 1

INTRODUCTION

The majority (almost 80%) of global energy demand is supplied from fossil fuels [1]. The emissions associated with them is responsible for environmental pollution and climate change. Enabling the use of renewable energy sources in transportation is being embodied in electric vehicles in recent years with an accelerated pace. Thus, the emissions related with transportation would be decreased greatly to decelerate environmental pollution and climate change [2]. Furthermore, some additional benefits of electric vehicles (EVs) in comparison to the conventional internal combustion vehicles are enhanced sustainability, diversification of energy sources, quiet operation (noise pollution), and low operating costs [3,4].

The advantages of EVs over the traditional transportation solutions and support of legislations around the world have accelerated the transition to EVs. Therefore, it is evident EVs will become widespread in the upcoming decade. Thus, the importance of batteries is becoming essential more than ever. There are many distinct types of batteries used in electric vehicles depending on their chemistry, shape, characteristics etc. Li-ion (Lithium Ion) batteries are the most preferred ones for EVs where NiMH (Nickel Metal Hydrate) and Pb-acid (Lead-Acid) [5].

NiMH batteries have high energy density, high power, fast charging feature, long life, wide operating temperature range, and completely closed maintenance features. NiMH batteries have a lower energy storage capacity than Li-ion batteries. NiMH batteries can experience a memory effect if not properly charged and discharged, which can lead to a reduced usable capacity over time [6].

Pb-acid batteries are one of the oldest and are known for their reliability and low cost. They have lower charging efficiency compared to lithium-ion batteries. In addition, they have relatively low energy storage (energy/weight and energy/volume ratio) capability [7].

Lithium-ion batteries are the most used energy sources in current electric vehicles thanks to their advanced technological benefits comparison to other types [8]. Lithium-ion batteries have many advantages such as high power, high charge rate, high capacity, no

memory effect, low self-discharge, and improved safety performances. In addition to these features, due to their relatively low cost, they are demanded for automotive and aerospace applications [9,10]. In addition, heating, performing optimally in a limited temperature range and limited life cycle are disadvantages of Li-ion batteries. The most of commercial Li-ion cells use intercalating compounds as active materials. The negative electrode (anode) is usually graphite. There are six distinct types of lithium-ion batteries: Lithium Cobalt Oxide (LCO), Lithium Manganese Oxide (LMO), Lithium Iron Phosphate (LFP), Lithium Nickel Manganese Cobalt Oxide (NMC), Lithium Nickel Cobalt Aluminum Oxide (NCA), Lithium Titanate Oxide (LTO) [11]. Mobile electronic devices often powered by high-energy-density lithium polymer batteries, LCO ($LiCoO_2$) cathode with a graphite anode. LFP ($LiFePO_4$), LMO (Li2MnO3 or $LiMn_2O_4$ spinel), NCA, NMC and LTO are widely used in EVs due to their high energy density in comparison to other chemistries [12]

Battery cell performance and useful capacity decrease over time while internal resistance increases due to the aging of batteries [13–16]. Batteries in EVs and hybrid electric vehicles (HEVs) should be replaced as their capacity decreases to 70% (80% is considered as the limit for some) of the original capacity. Therefore, critical measures should be taken to design battery packs for HEVs/EVs [17,18].

Aging is caused by various chemical mechanisms that affect the electrolyte, electrodes, separator, current collectors, and separator (Figure 1) [19]. The predominant cause of capacity degradation, as acknowledged by many authors, is attributed to the loss of active lithium[20–22]. This viewpoint is grounded in the belief that the deterioration of both the cathode and anode occurs at a significantly slower rate compared to the utilization of accessible active lithium. Consequently, the key factor limiting capacity is the lithium inventory itself. The primary loss of active lithium predominantly arises from the electrolyte's reduction occurring at the anode's surface, culminating in the creation of an insulating solid electrolyte interphase (SEI) in close proximity to the anode surface [23]. At relatively high state of charges (SoC) and temperatures, SEI dissolves which increases the anode impedance [24,25]. In addition to the effect of SEI growth on the aging of negative electrode, lithium plating and binder decomposition play an integral role. The aging mechanism in the positive electrode is dominated by active material degradation, mechanical breakage and electrode separation [13]. Table 1 documents the factors affecting aging, the chemical and physical mechanisms of aging, and the effects it causes [26]. This

table can provide insight into the cause-effect relationship and the battery aging event cycle.

Battery aging can be classified in two major categories: cycle and calendar aging. Calendar aging occurs when the battery is at rest, (i.e., lack of charge/discharge cycle) and cycle aging occurs when the battery is experiencing charging/discharging cycles. However, all the cells experiencing charge/discharge cycles also age due to calendric effects which requires both effects of cycle and calendar aging should be combined to offer a more realistic approach.

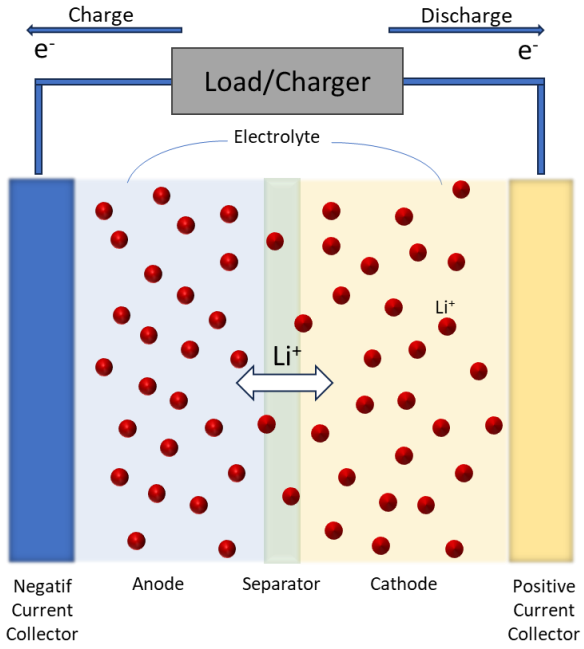

Figure 1 Lithium-ion battery schematic [27].

Battery aging is a complex process as many factors interact with each other while both environmental conditions and user characteristics (drive cycle profile) also play a role on aging. Establishing appropriate aging predictions is essential to ensure the efficient use of battery cells as well their safe operation [28]. Battery capacity degradation depends on charge output, time and operation parameters such as SoC, temperature, current amplitude and depth of discharge (DoD) [29–32]. Even though many external factors play a role on the aging mechanism, the most dominant one is the effect of temperature on the aging as it triggers some chemical reactions and accelerate the reaction speed of others on degradation. Fast charging and discharging are among the most critical factors that cause a sudden temperature increment in battery cells which increases degradation.

Furthermore, extreme conditions such as overcharging, over-discharging and relatively high ambient temperature (generally accepted as more than 30°C) decrease battery life a lot faster in comparison to normal use conditions. Likewise, the current increment accelerates aging (degradation) which also increases the probability of failure during a cycle [33].

The majority of theoretical models predicting battery aging are based on physical relationships. Therefore, experimental and computational aging studies on battery cells are simultaneously documented to reveal EV batteries' aging mechanisms and capacity degradation. This thesis aims to summarize the capacity degradation of batteries, factors affecting battery life, and experimental-semi-experimental prediction models for calendar and bicycle aging. In Chapter 2, experimental studies on calendar and cycle aging are examined. This chapter begins with an overview of relevant aging mechanisms and stress factors for battery types commonly used in calendar aging studies. Then, the studies are analyzed and a general conclusion is made, and the degradation models are examined in detail in Chapter 3. In Chapter 4, the model methods and validation studies of the models determined for calendar aging are examined. In Chapter 5, the data sets taken from the literature and our project are explained in detail. In Section 6, model parameters are fitted to these experimental sets, and the results are discussed. In Chapter 7, the conclusions drawn from the entire study are discussed.

Table 1. Factors affecting aging, chemical and physical mechanisms, and the effects it causes [26].

Degradation Mechanism	Cause	Degradation Mode
SEI growth	Time High temperature High SoC Current load	Loss of lithium inventory
SEI decomposition	High temperature High SoC Current load	Loss of lithium inventory
Electrolyte decomposition	High temperature High SoC	Loss of lithium inventory
Binder Decomposition	High temperature High SoC	Loss of active anode material Loss of active cathode material
Graphite exfoliation	High SoC Current load	Loss of active anode material
Structural disordering	Current Load	Loss of active cathode material
Lithium plating	Low temperature Stoichiometry Low SoC	Loss of lithium inventory Loss of active anode material
Loss of electric contact	Current load Mechanical stress Low SoC	Loss of active anode material Loss of active cathode material
Electrode particle cracking	Current load Mechanical stress	Loss of active anode material Loss of active cathode material
Transition metal dissolution	Stoichiometry Low SoC	Loss of active cathode material
Corrosion of current collectors	Low SoC	Loss of active anode material Loss of active cathode material

CHAPTER 2

LITARETURE SURVEY

The literature on cycling aging and calendar aging was reviewed, encompassing experimental studies. Firstly, an examination of experimental studies focusing on calendar aging was conducted. It commenced with an overview of the pertinent aging mechanisms and stress factors associated with battery types commonly utilized in calendar aging research. Subsequently, experimental studies concerning bicycle aging were explored. The same procedures outlined for calendar aging are applicable to cycling aging within this section.

2.1. Calendar Aging

Calendar aging includes all aging mechanisms that are in the resting state of battery cells, i.e., absent of charge and discharge cycle [34]. Over time, the chemical reactions occurring within the battery cells during storage gradually degrade the active materials on the electrodes and the electrolyte, leading to a reduction in the battery's energy storage capacity. These reactions can lead to the formation of a SEI layer, electrolyte decomposition, and changes in electrode materials over time.

Several interconnected factors contribute to calendar aging in EV batteries. Calendar aging is affected greatly from SoC, temperature and the time elapsed [35]. Temperature plays a critical role in calendar aging. High temperatures accelerate the chemical reactions within the battery, leading to the breakdown of its components and a faster decline in its capacity and performance. However, extremely low temperatures can also adversely affect the battery's efficiency and overall performance [36,37]. SoC is another critical factor influencing calendar aging. Storing a battery at high SoC levels for prolonged periods can increase calendar aging. On the other hand, storing the battery at very low SoC levels can also lead to degradation due to other chemical reactions that occur at low charge levels. Time itself is a significant contributor to calendar aging. As time passes, even if the battery is not actively used, chemical reactions within the cells continue to take place.

This section aims to explore various experimental studies in the literature that have produced noteworthy findings on the subject of battery calendar aging. Our primary focus will be on highlighting the influence of temperature and SoC to gain a better understanding of their impact on battery longevity. The ultimate objective of this analysis is to derive valuable insights that can enhance the lifespan of batteries, leading to improved performance and efficiency.

2.1.1. Effect of Temperature on Calendar Aging

Temperature significantly impacts battery calendar aging, which refers to the gradual capacity loss and reduced lifespan of a battery over time. When exposed to high temperatures, several adverse effects can occur, all of which contribute to a shorter battery lifespan and reduced overall performance. In this subsection, we focus on temperature parts in calendar aging studies found in the literature, providing illustrative examples from various battery chemistries [38,39]. Electrochemical reactions are primarily responsible for the aging of battery cells which affects their life cycle of them. However, temperature play an integral role in electrochemical reactions; therefore, the effect of temperature on life cycle is essential. Abnormal ambient temperatures (25-30°C) negatively impact battery safety, functionality and aging. Both low and high temperatures have distinct effects on battery performance [40,41].

Wang et al. [42] conducted extensive tests on NMC+LMO cells with a capacity of 1.5 Ah, focusing on their calendar life performance over 400 days at 10% DoD and temperatures of 10°C, 20°C, 34°C, and 46°C, uncovering the pronounced impact of lithium inventory loss on capacity degradation. The findings demonstrated the highest capacity reduction at 46°C, which was a 22% capacity reduction. In order to elucidate the exhaustive impact of temperature, a time-dependent model was formulated, incorporating the Arrhenius correlation. While the model exhibited slight predictions for the temperature of 20°C, it tended to overestimate the capacity loss at higher temperatures of 34°C and 46°C.

A study by Ecker et al. [43] examined the aging of lithium-ion batteries by combining the electric-thermal model with a semi-empirical aging model. Over a period of 60 weeks, they conducted accelerated tests on 6 ah NMC batteries, taking into account temperature (25°C, 35°C, 50°C, and 65°C) and SoC (20%, 50%, 80%, and 100%). The test outcomes

revealed that at the 65°C storage temperature, unexpected chemical reactions occurred at lower temperatures, and some cells stored at 65°C exhibited gassing processes. These reactions caused the cell to die rapidly at 65°C. Furthermore, the test results demonstrated that the reduction in capacity exhibited an exponential dependence on voltage and temperature.

Omar et al. [44] performed calendar life tests on LFP pouch battery cells with a nominal capacity of 7 Ah. Batteries were examined at four distinct temperatures (10°C, 25°C, 40°C, 60°C) for various SoC (25%, 50%, 100%) for 28-280 days. Their results conclude that the effect of high storage temperatures is detrimental to the life of battery cells and that the storage temperature has a greater effect on aging of batteries than the SoC. They highlighted that the optimal storage conditions for LFP batteries are at a temperature in the vicinity of 25°C. They also document that the aging increases 120% at 20°C, 135% at 40°C and 138% at 60°C. In another study that provides evidence supporting the notion that temperature exerts a more significant influence on aging than SoC, Grolleau et al. [45] examined the aging behavior of commercial LFP cells with a nominal capacity of 15 Ah. Cells were stored for 450 days at nine distinct conditions: three nominal SoCs (30%, 65%, 100%) for three temperatures (30°C, 45°C, 60°C). While the capacity loss of cells stored at 45°C reached 20% in 450 days, the capacity loss of cells stored at 60°C reached 20% in 150 days. They developed a model capable of predicting cell degradation under various SoC and thermal storage conditions. It was seen from the good agreement between the prediction and the capacity loss that the rate of capacity reduction depends only on the storage conditions and not on the aging history.

Kassem et al., [46] an investigation into the aging of 8 Ah LFP cells was presented, considering their storage under three distinct temperature conditions (30°C, 45°C, and 60°C) and various SoC levels (30%, 65%, and 100%) during up to 8 months. Following the storage period, the trend of reduced capacity was observed in all cells except those preserved at 30°C and particularly severe aging was noted at a storage temperature of 60°C. The study suggested a direct correlation between the extent of capacity loss and the storage temperature, and cyclic lithium loss constituted the primary contributor to capacity reduction. They suggested that lithium loss was due to side reactions occurring at the anode. Cells aged at 45°C or 60°C exhibit both reversible and irreversible capacity losses, with the magnitude of these losses being quite similar at 45°C. However, at 60°C, the irreversible losses notably surpass the reversible ones.

Sarasketa-Zabala et al. [47] performed storage tests on 2.3 Ah LFP cells at different temperatures (30°C, 40°C and 50°C) and different SoC values (30%, 70%, 90%) for 300-650 days. They created a model using a combination of storage temperature and SoC parameters based on the Arrhenius law. The research revealed that prolonged storage time and exposure to high temperatures over 40°C triggered additional aging effects, causing the primary degradation mechanism to shift to a combination of LLI and LAM. Furthermore, the LAM aging phenomenon greatly accelerated the decline in cell performance. The model's predictions closely matched the experimental results, with the model's error consistently below 1% during the entire experimental period.

Werner et al. [48] reported the calendar aging of an NCA cell as a function of temperature (40°C, 50°C and 60°) and SoC (20-100%) under open circuit conditions, considering self-discharge for 21 months. The voltage was monitored continuously during storage periods, and high temperatures and high SoC levels were found to lead to significant self-discharge, particularly at 100% SoC with a storage temperature of 60°C. An empirical model was formulated to describe the cell's degradation. This study also takes into account a possible path dependence on temperature. The results show that there is no dependence of the cells on historical temperature conditions.

Eddahech et al. [49] conducted a study elucidating calendar aging outcomes for four distinct Li-ion battery chemistries. In the study, prismatic 5.3 Ah LMO+NMC, prismatic 12 Ah NMC, cylindrical 8 Ah LFP and cylindrical 7 Ah NCA battery cells are used. These batteries were subjected to storage at three varying temperatures (30°C, 45°C, and 60°C) and maintained at three different SoC levels (30%, 65%, and 100%). The research aimed to discern disparities in the behaviors of Li-ion battery chemistries, revealing the sensitivity of lithium batteries containing Manganese (particularly LMO and NMC) to elevated temperatures. In contrast, LFP batteries demonstrated an extended calendar life and robust thermal stability. Additionally, NCA cells were identified as striking a balance between extended life cycles and high-performance efficiency measurements.

Geisbauer et al. [50] conducted a study on six different chemistries of lithium-ion batteries (NCA, NMC, LFP, LCO, LMO, and LTO) under three different ambient temperatures (18.5°C, 50°C, and 60°C) and three various SoC (2%, 38%, and 100%) for calendar aging. The researchers conducted experimental measurements on six lithium-ion batteries with nominal capacities ranging from 1.3 to 2.6 Ah for a duration of 120 to 150 days. The results showed that capacity loss was most severe at 60°C and higher

storage voltages, even for titanate oxide cells. NMC, NCA, and LTO cells exhibited the most severe capacity degradation at 60°C. At 60°C and the highest storage voltage, NMC and NCA cells did not show any open-circuit voltage as the current interruption mechanisms were triggered. In most cases, extreme conditions, such as 100% SOC and higher temperatures (such as 60°C), will result in increased capacity loss. In general, the effects of calendar aging are more severe in 60°C storage than in 50°C storage.

Similar to the impact of elevated temperatures, lower temperatures also exert adverse effects on battery capacity and internal resistance. Additionally, it's important to acknowledge that the influences of low and high temperatures on battery performance can exhibit variations. Jaguemont et al. [51] presented the results of aging tests conducted on a 100Ah prismatic LFP battery cell under low-temperature conditions. Accelerated aging experiments were performed on four cells to investigate the influence of low temperatures on Li-ion batteries. Three of these cells underwent a standardized driving cycle at three different temperature settings (-20°C, 0°C and 25°C), while a calendar test was conducted on a single battery at -20°C, with a SoC maintained at the mid-range (50%) for 400 days. The study found that the end-of-life criterion, defined as 80% of the nominal capacity, was met after 415 hours of storage, equivalent to 17 days at -20°C. The results underscored the imperative need to account for the impact of cold temperatures on the lifespan of battery packs.

Maures et al. [52] introduced a calendar aging model for 2.5 Ah NCA Lithium-ion batteries, emphasizing the pivotal role of time and temperature. Their investigation spanned a temperature range from -20°C to 55°C at a SoC of 95% for approximately 200-300 days, highlighting the quantification of degradation processes such as conductivity loss (CL), active material loss (LAM), and lithium inventory loss (LLI). They modeled these decay processes using an equation derived from the Arrhenius law. Consequently, they found that the aging based on LAM and LLI coefficients can be described by the Arrhenius's law. LLI is linked to the formation of SEI and follows Arrhenius law. However, at lower temperatures, especially at -20°C, a different degradation mechanism, lithium plating, becomes more significant. Despite this change, they suggested that the Arrhenius law still applies.

2.1.2. Effect of SoC on Calendar Aging

SoC significantly influences the calendar aging of lithium-ion batteries, which refers to the degradation occurring over time, regardless of usage. SoC plays a critical role in this process, impacting the battery's overall lifespan and performance. High SoC, where the battery is maintained close to 100%, can accelerate calendar aging. This is because elevated SoC levels can trigger unwanted chemical reactions within the battery, leading to the degradation of electrode materials and capacity reduction. High SoC can also lead to mechanical stress within the battery due to material expansion, potentially causing damage. Conversely, low SoC, close to 0%, over extended periods can also contribute to calendar aging.

Schmalstieg et al. [53] introduced a comprehensive aging model derived from accelerated aging tests conducted on 2.05 Ah NMC batteries at varying temperatures (35°C, 40°C, and 50°C) and SoC levels ranging from 0% to 100% for range of 160-500 days. Analyzing the experimental results, they noted that the SoC value with the least pronounced impact on calendar aging is 50%. Mathematical functions were fitted using these data to describe capacity fade, employing a two-step fitting process for calendar aging. After using an electric-thermal model to generate battery SoC and voltage, they proposed a semi-empirical model based on the Arrhenius law to predict battery future calendar aging, revealing that aging speed increased linearly with voltage during calendar aging tests.

Zheng et al. [54] conducted a comprehensive investigation into the degradation characteristics of high-power 1.06 Ah LFP batteries exposed to various temperatures (25°C, 40°C, and 55°C) and different SoC levels (30%, 60%, and 100%) for 10 months. The study specifically focused on samples stored at 30%, 60%, and 100% SoC at 55°C, employing a combination of electrochemical techniques and postmortem analysis. Their findings revealed that the most severe capacity loss occurred when batteries were stored at 55°C with a SoC of 100%. Notably, the batteries exhibited substantial performance deterioration when subjected to high SoC conditions. Under high SoC and 55°C storage conditions, they observed significant lithium-ion loss at the LFP cathode, along with a minor reduction in capacity at the graphite anode. Also, for lithium-ion LFP cells, Redondo-Iglesias et al. [55] proposed to use Eyring acceleration model for calendar aging modeling. Eyring's law extends Arrhenius's law to other stress constraints. The model was

validated in an experimental setup on 2.3 Ah LFP batteries at temperatures of 30°C, 45°C, and 60°C and with SoC values of 30%, 65%, and 100% for 500-800 days. This model, which is not common, has been proposed to express the aging laws of batteries in some recent studies [56,57] Cells may experience self-discharge (SoC shift) during idle operation. Therefore, In this study calculations were made by taking into account the SoC shift during calendar aging tests. As a result, while the estimation error was 2% in the Eyring law model, the error becomes 4.8% if SoC estimation shift is not considered. Therefore, SoC shift consideration increases the accuracy compared to the applied classical models.

In another study, a different path was followed by taking into account non-static conditions as well as static conditions. Su et al. [58] examined the aging of 3 Ah NMC batteries under both static and non-static conditions, investigating the pathway dependence of lithium-ion cells. They conducted 12 assessments involving three different temperatures (45°C, 53°C, and 60°C) and four SoC levels (40%, 60%, 80%, and 95%) for 240 days. During the non-static storage tests, both temperature and SoC change over time throughout the testing procedure. Results showed that the mode of cell senescence remained consistent across temperatures, but a notable acceleration was observed at 95% SoC, deviating from patterns at lower SoCs. An empirical model was then employed to describe cell senescence in static storage tests. The derived model was able to predict the capacity reduction with a maximum error of 1% for 240-day static storage tests and a maximum of 3% error for 180-day non-static storage tests.

Naumann et al. [59] presented a comprehensive calendar aging study conducted at different temperatures (0°C, 25°C, 40°C, and 60°C) and SoCs ranging from 0% to 100% using 2.3 Ah LFP batteries with a test duration of 29 months. When examining the experimental results, it was observed that capacity fades increased with higher storage SoCs, but the ratio remained relatively constant in the middle SoC range (37.5-62.5%). Similar SoC behavior had previously been demonstrated by Keil et al. [60] in different lithium-ion cells with graphite anodes, and it was attributed to stages in the graphite anode potential. Utilizing the measurement data, the article presents a semi-empirical aging model for capacity loss that is valid for all storage conditions (static and dynamic conditions). When compared against validation data points, the absolute model errors for capacity loss remained below 2.2% for all dynamic validation tests.

Xu et al. [61] studied the effects of irregular battery operation on battery degradation. The study considered several fundamental theories of battery degradation, including SEI

film formation and the Arrhenius law relation. In order to develop a model, storage tests were performed on LMO cells at various SoC (60%, 80%, 100%) levels and temperature of 25°C. Storing the battery at 100% SoC caused a more significant capacity reduction than storing it at 60% SoC. However, they found that the effect of SoC on capacity fade becomes more pronounced as storage time increases, i.e., especially after the 2nd year.

Similarly, a study by Montaru et al. [62] addressing the decrease in capacity at high temperatures with high SoC values develops a model for capacity degradation. They document a dual tank aging model [63,64] which combines a physics-based model for SEI growth and an empirical model for electrode capacity degradation. Model validated on LMO+NMC Li-ion cells with 43 Ah nominal capacity at various SoC (0%, 30%, 65%, 80%, 100%) and temperatures (0°C, 25°C, 45°C, 60°C) for 380-700 days. They noticed that at high temperature (45°C), the increasing capacity reduction with the growth of SEI thickness was significant at higher SoC ranging from 65% to 100%. The model demonstrates the evolution of lithium contents, electrode potentials, and electrode capacities. The model showed satisfactory accuracy (maximum 3.1%).

Hoog et al. [65] proposed a semi-empirical combined lifetime model for 20 Ah NMC cells. Two variables were considered in their test matrix: SoC (20-80%), temperature (25-45°C). Their numerical model predicted combined lifespan with less than 5% accuracy relative to the experimental results. Analyzing the results of storage tests conducted over a 16–17-month period of calendar aging, it was evident that cells stored at SoC levels exceeding 80% tended to reach their defined End-of-Life (EOL) earlier than those stored at lower SoC levels (<50%). Conversely, an initial increase in capacity was observed when cells were stored at a low charge state, attributed to electrochemical grinding. This observation indicated that side reactions did not impact SEI growth.

Calendar senescence analysis involves a recurring process of calendar aging and cell characterization. Historically, the impact of cell characterization on the outcomes of calendar aging studies has been generally considered insignificant. Krupp et al. [66] in this calendar aging study involving NMC cells with a capacity of 64 Ah, they utilized additional periodic characterization measurements to quantify and rectify the impact of control on capacity loss attributed to calendar aging. In the calendar aging tests, batteries were subjected to three different temperatures (23°C, 40°C) and various SoC (50%, 70% and 90%) values over a period of 450 days. The observed aging behaviors displayed some deviations from previous studies, notably in the relationship between SoC and capacity

loss. Rather than a linear dependence, a constant capacity loss was identified between 70% SoC and 90% SoC, which was attributed to the influence of cathodic and combined side reactions.

Finally, a study combining different battery chemistries in a single study was examined. Keil et al. [60] documented calendar aging of three 18650 lithium-ion cells with distinct cathode materials (NCA, NMC, LFP). Experiments were carried out at several temperatures (25°C, 40°C, 50°C) for 16 SoC values from 0% to 100% for 270-300 days. They showed that there is no linear relation between calendar aging and SoC. In addition, the anode potential has a significant effect on capacity weakening. Capacity fade during storage is significantly affected by the intermediate anode potential, which typically occurs between 30% and 60% SoC for NMC and NCA cells and between 40% and 70% SoC for LFP cells. When SoC values are below 30 - 40%, the capacity decreases while the anode potential increases.

2.1.3. Summary of Calendar Aging

When a battery is stored in calendar mode, it can experience irreversible loss of capacity. This loss may be sped up or slowed down based on storage conditions, with temperature being the most significant factor, followed by SoC. As detailed in Chapter 2, various experimental studies in the literature have explored the impact of these parameters on calendar aging behavior. Some studies focus solely on time and temperature, while others propose correlations for aging behavior that consider time, SoC, and temperature. A summary of the studies analyzed in this review is presented in Table 2.

Aging mechanisms happen in lithium-ion batteries during calendar aging, which is natural deterioration over time, regardless of usage. It has been observed that the three main mechanisms that temperature, SoC, and time cause calendar aging in Li-ons are loss of lithium inventory, loss of active material in the electrodes, and loss of electrical conductivity [42,52]. Lithium inventory loss occurs due to side reactions that consume Li-ions, such as the formation of SEI on the surface of graphite negative electrodes, electrolyte degradation processes, and binder dissociation. These side reactions destroy Li-ions permanently and cause a gradual decrease in capacity. Loss of active material is typically caused by decomposition of the electrolyte, irreversible phase transition, and cracking of the electrode particles during storage. The loss of electrical conductivity is

related to the deterioration of the collectors and connectors. Lithium inventory loss and active material loss are the dominant modes of calendar aging[40].

SEI growth is particularly affected by SoC, temperature, and storage time. Continuous expansion of the SEI layer results in loss of lithium inventory and increased internal impedance. As the SEI layer thickens, some active materials such as the electrolyte become less electrochemically active, resulting in negative electrode active material loss, which accelerates calendar aging [47,62].

The degradation of batteries may exhibit varying chemical reactions at high and low temperatures. High temperatures over 40°C can cause lithium loss, resulting in less available lithium for intercalation and inducing capacity fade. One notable effect is the acceleration of chemical reactions within the battery. High temperatures can lead to increased chemical activity, causing the breakdown of active materials and the formation of unwanted compounds. This phenomenon ultimately results in a reduction in the battery's capacity and performance, which means that an EV's range on a single charge will diminish more rapidly in hotter climates [42–49]. The lifespan of cells is negatively affected by high temperatures, regardless of their chemistry. However, certain chemistries may be more sensitive to temperature changes than others. For instance, the NMC + LMO mixture shows a significant increase in degradation rates at temperatures between 40 °C and 60 °C, particularly at high SoC [42,62]. In contrast, NCA chemistry experiences only a minor change in degradation rates across the same temperature range[48]. The effect of temperature on LMO chemistry is similar to that of the NMC + LMO mixture, but pure LMO cells showed one less aging effect compared to blended NMC + LMO cells [49,60].

On the other hand, cells containing NMC, on their own, have poor high-temperature performance and are susceptible to rapid degradation [43,50,53].

Low temperatures below 10°C can cause a loss of active material or less available active material for diffusion, which modifies the battery chemistry. At low temperatures, the lithium coating on the anode becomes more important and contributes to battery degradation differently than other degradation mechanisms [52,59,67]. Particularly for LFP and NMC cells, aggressive capacity degradation was observed in the low-temperature field. LTO cells, on the other hand, are less sensitive to low and high storage temperatures than NMC, LCO, LFP and NCA cells. Among LCO batteries, it seems to be the most sensitive to low temperature and SoC changes compared to other batteries [50].

Table 2. Overview of calendar aging studies reported in the literature.

Study	Chemistry	Capacity (Ah)	Storage Time (Days)	Parameters	
				Temp. (°C)	SoC (%)
Eddahech et al. [49]	NMC, LMO, NCA and LFP	5.3, 5.3, 12 and 8 respectively	1000-1200	45 and 60	65 and 100
Geisbauer et al. [50]	NCA, NMC, LFP, LCO, LMO and LTO	1.3 to 2.6	120-150	18.5, 50 and 60	2, 38 and 100
Keil et al. [60]	NCA, NMC, and LFP	2.8, 2.05 and 1.1 respectively	270–300	25, 40, and 50	0 to 100
Wang et al. [42]	NMC+LMO	1.5	400-600	10, 20, 34 and 46	50
Montoru et al. [62]	NMC+LMO	43	380-700	0, 25, 45 and 60	0, 30, 65, 80 and 100
Sarsketa-Zabala et al. [47]	LFP	2.3	300-650	30, 40 and 50	30, 60 and 90
Omar et al. [44]	LFP	7.	28-280	10, 25, 40 and 60	25, 50 and 100
Grolleau et al. [45]	LFP	15	420-480	30, 45 and 60	30, 65 and 100
Kassem et al. [42]	LFP	8	230	30, 45 and 60	30, 65 and 100
Zheng et al. [54]	LFP	1.06	280	25, 40 and 55	50, 60 and 100
Redondo-Iglesias et al. [55]	LFP	2.3	500–800	30, 45 and 60	30, 65 and 100
Jaguemont et al. [51]	LFP	100	400	-20	50
Naumann et al. [59]	LFP	2.3	810	0, 25, 40 and 60	0 to 100
Ecker et al. [43]	NMC	6	420	25, 35, 50 and 65	20, 50, 80 and 100
Schmalstieg et al. [53]	NMC	2.05	330-520	35, 40 and 50	0, 10, 20, 30, 50, 60, 70, 80, 85, 90 and 95
Su et al. [58]	NMC	3	240	45, 53 and 60	40, 60, 80 and 95

(cont. on next page)

Table 2. (cont.).

Hoog et al. [65]	NMC	20	470	25, 35 and 45	20 to 80
Krupp et al. [66]	NMC	64	450	23 and 40	50, 70 and 90
Werner et al. [48]	NCA	3.2	590	40, 50 and 60	20, 35, 50, 65, 80, 90 and 100
Maures et al. [52]	NCA	2.5	200-300	-20, 25 and 55	95
Xu et al. [61]	LMO	1.1	1800-3600	15, 25, 35, 45 and 55	60, 80 and 100

SoC level is also a stress factor contributing to aging during calendar mode. Cells stored at the same temperature but different SoCs age at different rates. Higher battery degradation effects are expected at high SoC levels (SoC >80%), caused by a potential disequilibrium on the electrode/electrolyte interface, promoting secondary or side chemical reactions. Additionally, batteries are chemically stressed when they are maintained at high SoC, causing degradation of the electrode materials over time [53,57–62,68]. During calendar mode, the accelerated aging tests focused on examining how temperature and SoC affect cell performance in terms of capacity degradation [44,46,53,60]. The results showed that high SoC values not only speed up the aging process but also capacity degradation effects are non-linear over time. Additionally, It has been observed that capacity degradation increases as storage SoC increases, but the rate remains relatively constant in the mid-SoC range according to studies [59,60].

The aging rate in NMC cells was found to increase at 100% SoC, while NCA cells experienced an aging rate increase at SoC values above 90% [60,65,66]. Senescence in LFP cells, on the other hand, is affected by SoC but not as significantly as in NMC and NCA cells [49]. In contrast, LCO chemistry degrades rapidly when the cell is charged and kept at a temperature of 40-50°C. However, reducing the SoC slightly can significantly reduce the degradation rate. Additionally, compared to other batteries, LCO batteries are the most sensitive to changes in low temperature and SoC [50]. Comparing these results with LFP degradation rates, it is evident that LFP chemistry has a slightly lower degradation rate under the same conditions (high temperature and SoC). However, the degradation rate remains fairly constant despite changes in SoCs at a given temperature. Therefore, it can be concluded that temperature has a greater impact on degradation within LFP cells [47,54,69]. There is not as much literature available on the calendar aging of LTO-based cells compared to other types of batteries. However, it is understood that cells with LTO are

less affected by temperature and SoC than NMC and NCA cells. It is worth noting that LTO cells tend to degrade more quickly when at a low SoC compared to a high SoC. This could be due to the depletion of limited lithium inventory, particularly at low potentials [50].

In addition, when examining battery aging, larger lithium-ion cells may have different performance and aging patterns compared to smaller ones, even if they have the same cell chemistry. These distinctions stem from variations in factors like current density, design, geometry, and spatial irregularities in electrical potential. In the above two studies conducted under similar conditions ([45], [46]), the relative capacity of the 15 Ah LFP cell is 0.55 under 250-day 65 °C and 100% SoC storage conditions, while it is 0.68 for the 8 Ah capacity LFP cell.

2.2. Cycling Aging

Battery cycling aging in electric vehicles is a critical consideration in their long-term performance and reliability. The cycling mode corresponds to the irreversible loss of capacity that occurs during the charging and discharging of a battery. Over time, the battery's capacity gradually decreases, impacting its ability to store and deliver energy efficiently. In addition to temperature and SoC, various other stress factors become pertinent during cycling, including the rate of discharge or charge, often referred to as the C-rate, and the SoC ranges (ΔSoC) throughout a cycle [70–72]. The ΔSoC represents the degree of variation in SoC experienced during a single cycle.

This section aims to explore various studies in the literature that have produced noteworthy findings on the subject of battery cycling aging. Our primary focus will be on highlighting the influence of temperature, SoC and C-rate to gain a better understanding of their impact on battery longevity. The ultimate objective of this analysis is to derive valuable insights that can enhance the lifespan of batteries, leading to improved performance and efficiency.

2.2.1. Effect of Temperature on Cycling Aging

The effect of temperature on cycling aging is a critical factor that significantly influences the long-term performance and lifespan of rechargeable batteries, such as

lithium-ion batteries commonly used in various applications. Elevated temperatures, whether due to environmental conditions or internal heat generated during charging and discharging, can have detrimental effects on batteries. Firstly, increased temperature accelerates the chemical reactions within the battery, leading to more rapid degradation of the electrode materials, the electrolyte, and the formation of solid electrolyte interface (SEI) layers. These reactions contribute to capacity fade and reduced cycle life [40].

Conversely, lower temperatures can slow down chemical reactions and reduce the rate of cycling aging. However, excessively cold temperatures can also have adverse effects on battery performance, such as increasing internal resistance and decreasing the battery's ability to deliver power effectively. To maximize the lifespan and performance of batteries, manufacturers and battery management systems often incorporate temperature control mechanisms to maintain the battery within an optimal operating temperature range. This range varies depending on the specific battery chemistry and application but typically falls between 25°C to 30°C [38,39].

A study conducted by Han et al. [73] examined the effects of cycle aging on five types of commercial Li-ion cells: 20 Ah LTO/NMC, 60 Ah and 11 Ah graphite/LFP, and 35 Ah and 10 Ah graphite/LMO. The batteries underwent charging at 1/3C and discharging at 1.5C, undergoing 90 cycles at both 45°C and 5°C. This allowed the cells to experience high and low temperatures without the influence of SoC. This process was repeated a total of 1000 cycles to expose the cells to high and low temperatures without the effect of SoC. However, for the LTO/NMC cell, there was almost no loss of battery capacity and LTO anode active material inside the battery, but there was obvious loss of NMC cathode active material. The aging diagnosis for LMO and LFP cells showed that both experienced a loss of lithium inventory and anode active material. The LFP cells experienced a 20% capacity loss in 200-300 cycles, while the LMO cells experienced a loss in 420 cycles.

Yang et al. [74] investigates unbalanced discharging and aging caused by temperature differences among parallel connected cells. Cycling experiments were conducted on 2.2 LFP cells for up to 1000 cycles at ambient temperatures of 25°C and 40°C. Cells were charged at 3C and discharged at 5C. They estimated the capacity reduction of lithium-ion batteries by Arrhenius approach during a charge/discharge cycle [68,75]. Their conclusion is that the increase in capacity loss is directly proportional to the increased temperature difference between the cells in the battery packs connected in

parallel. Therefore, in order to increase the battery life, the temperature difference between the cells must be minimized as much as possible.

Baghdadi et al. [76] conducted a cycling study for 5.3 Ah LMO+NMC and 7Ah NCA cells. Their model development relies on SIMSTOCK and SIMCAL project, which includes the effects of temperature (40°c, 45°C and 50°C), SoC (20% and 40%) and current (1C and 2C) on aging [77,78] They relied on a chemical ratio approach based on Dakin degradation model [79]. They conclude that the aging rate increases exponentially as SoC, temperature (40°C, 45°C, and 50°C) and current increase. Cycling at relatively low temperature values accelerate overall aging. Notably, the aging rate exhibited a significant increase when temperatures decreased within the range of -5°C to 25°C and when temperatures increased within the range of 25°C to 60°C.

Hoog et al. [65] presented cycling a aging study on 20 Ah NMC cells for 3000 cycle that four variables were considered in their test matrix: Mid SoC (35%, 50%, 65% and 80%), temperature (25°C, 35 and 45°C), DoD (20-100%) and C-rate (from C/3 to 2C). In terms of temperature, they showed that at 100% depth of discharge (DoD), higher operating temperatures have a more pronounced effect on the lifetime of the cell. Specifically, the cells exhibited a faster deterioration, reaching end-of-life more rapidly at 45°C compared to 25°C. This observation aligns with findings in the existing literature, which demonstrate that at lower temperatures ($T < 25°C$), lithium plating leads to accelerated capacity fade in NMC-based cells.

Wu et al. [80] examined the effect of low temperatures and cycling charging on battery degradation. For this purpose, a test setup was created for 5Ah LFP batteries with various charge C-rates (0.3C, 0.5C) at temperatures of -10°C and -20°C. They documented a significant degradation of up to 35% in the batteries. They documented at low temperatures that the lithium-ion losses turned into lithium coating and do not reconnect to anode structure but form dendrites. Dendrite formation caused a further reduction in ohmic resistance, ultimately leading to a decrease in capacity.

Also, Burow et al. [81] investigated the aging of 25Ah prismatic NMC Li-ion cells at low temperatures (5°C-20°C). Capacity loss started after the 200th cycle. From post-mortem analysis, they uncover that the primary aging mechanism is due to lithium plating. Furthermore, observed that the distortion examined at the anode was not distributed homogeneously.

In another study conducted at low temperatures, Rauhala et al. [82] examined the challenges of implementing large lithium-ion battery systems in countries with cold climates, with a focus on the reduced cycle life of LFP cells at low temperatures (room temperature, 0°C, and -18°C). The study involves an extensive post-mortem analysis of 2.3 Ah cylindrical cells that were subjected to simulated battery electric vehicle usage patterns. Their results show that lithium loss is due to lithium coating on the electrode and SEI growth. They document that lithium coating and SEI formation were observed at 0°C on the graphite electrode while only lithium coating was observed at -18°C.

2.2.2. Effect of SoC on Cycling Aging

SoC plays a crucial role in determining the cycling aging of rechargeable batteries, such as lithium-ion batteries commonly found in electric vehicles. SoC indicates the level of charge of a battery, typically expressed as the percentage of its maximum capacity. It impacts cycling aging because different SoC levels expose the battery to varying levels of stress and chemical reactions during each cycle.

When a battery is cycled at high SoC levels, meaning it is frequently charged to near its maximum capacity and discharged to a low level, it experiences more stress due to the higher voltage and increased chemical activity. High SoC values can lead to more severe aging because they accelerate degradation due to the relation between electrode potentials and the rate of parasitic side reactions [61]. Moreover, the cathode structure can suffer permanent damage when SoC of a cell is high [83].

Todeschini et al. [84] developed an experimentally validated capacity degradation model for LFP batteries. They conducted an aging campaign using six 2.3 Ah LFP battery cells, with the goal of simulating real battery usage in a low-charge state during cycling conditions. The temperature was maintained at a constant 55°C, and they created an experimental matrix consisting of nine different tests with varying SoC levels (0-10%, 0-30%) and different C-rates (2C, 4C and 8C) up to 4000 cycles. When examining the experimental results, it became evident that the SoC range associated with the most significant aging was within 0-30%. The most rapid aging was observed specifically in the test condition with 0-30% SoC at 8C, resulting in a decrease to 80% of the battery capacity after 4000 cycles. Conversely, the least aging occurred at 0-10% SoC at 2C. Subsequently, they presented a semi-empirical model that links SoC and C-rate factors in

which battery cells are tested to predict capacity degradation. Comparing the proposed model with experimental data, the average error rate is only 0.24%.

Cordoba-Arenas et al. [85] developed a semi-empirical cycle life model for 15 Ah LMO+NMC cells. To gain insights into the aging process, they conducted a series of 16 distinct cycling experiments over a span of 3 months, considering minimum SoC levels (25%, 35% and 45%), charging rates (C/3, 3C/2 and 5C), and temperatures (10°C, 30°C and 45°C), while also accounting for charge sustaining/depleting ($0 < \text{Ratio} < 1$). The outcomes of these experiments revealed that the rate of capacity fade increased with rising minimum SoC values, with a more pronounced effect observed when SoC_{min} exceeded 35%. When they compared the capacity fade model with the experimental data, it exhibited an almost perfect fit, as indicated by the RMSE of 0.0047%.

Lithium-ion batteries are used in various applications for energy storage and may not always experience complete charging and discharging cycles. Saxena et al. [86] investigated the effect of partial charge-discharge cycles on the capacity loss of 1.5 LCO pouch cells. The study was carried out under different SoC ranges (0-100%, 20-80%, 40-60%, 40-100% and 0-60%) and discharge currents (C/2, 2C) up to 800 EFC. Since cells under partial SoC intervals do not complete full cycles, accurately defining the number of cycles is not possible. Hence, the cycle life performance of the cells was evaluated using equivalent full cycles (EFC). The results showed that average SoC values during the first 500 full cycles played a crucial role in cell disruption. However, ΔSoC intervals between 600-800 full cycles had a more significant impact on degradation. 20-60% SoC range and cells cycled at C-rate of C/2 exhibited the least capacity loss. Then, they developed a model of battery degradation based on partial and full charge cycles. The model describing this degradation is based on the power law model [87,88] which is compatible for the full number of cycles in the first 500 cycles.

In different research that studied various SoC ranges, Gao et al. [89] conducted cycling life tests on 8 Ah NMC at 25 °C and 6C with SoC ranges of 0–20%, 20–40%, 40–60%, 60–80%, 80–100% and 0–100% up to 3400 EFC. The results showed that among five ranges with 20% discharge depth, the cycle below 0-20% causes less capacity loss, while the cycle below 80%-100% causes more capacity loss. They found that the degradation behavior of the batteries was similar in the remaining three intervals. They revealed that the most effective aging mechanism in batteries below 20% DoD is lithium loss.

Wikner and Thiringer [90] investigated the impact of aging at various SoC levels in an electric vehicle. The tests were performed with Li-ion cells consisting of 26 Ah LMO+NMC. These cells were subjected to life cycle tests for a duration of three years with SoC varying at 10% intervals, various temperature (25°C and 35°C) and C-rate (1C, 2C and 4C). An empirical battery model was generated based on the degradation observed during the experiments. The findings indicate that reducing SoC to 50% can increase the lifetime of the vehicle battery by 44-130%, considering aging from discrete types of driving only at high SoCs. The study also reveals that high SoC accelerates aging more than low SoCs. Moreover, batteries with high SoC and experience various C-rates experience accelerated aging relative to high C-rates for a given SoC.

Gantenbein et al. [91] focused on the capacity loss caused by lithium loss, which is permanently linked to the SEI on the graphite surface. They conducted cycling experiments on a 2.6 Ah NCA cell at various SoC ranges (5–25%, 25–45%, 45–65%, 65–85% and 75–95%), covering discrete graphite potential ranges. The results revealed that lithium-ion loss was the dominant aging mechanism in each cycling life test. Over 4000 test cycles, the cells lost 2.5% active cathode material and 3.5% active anode material, while 7.5% active lithium-ion was lost. The maximum value for capacity and active lithium-ion loss was observed in the 65-85% SoC range.

Benavente-Araoz et al. [92] conducted an extensive study involving quasi-realistic aging tests on 2.5 Ah NCA lithium-ion cylindrical cells. The cells were partially cycled at four different cut-off voltages and ΔSoC (65–95%, 35–65%, 20–50%, and 20–95%) over 700-1000 cycles. Cells cycled with high cut-off voltages and wide ΔSoC (20% to 95%) were severely affected by material degradation and electrode shift. High cut-off voltage and narrow ΔSoC (65% to 95%) caused greater electrode degradation but negligible cell unbalance.

In a multi-year cycling investigation by Preger et al. [93], LFP, NCA, and NMC cells were subjected to different SoC values (40-60%, 20-80%, and 0-100%), temperature (15°C, 25°C and 35°C) and C-rate (0.5C, 1C, 2C and 3C). When compared to LFP cells, both NCA and NMC cells exhibited a more pronounced shift in capacity degradation as they transitioned from partial to complete SoC, a finding consistent with prior research. This transition can be attributed to the higher operating voltages of metal oxide cathodes (with 100% SoC corresponding to 4.2 V for NCA and NMC, in contrast to 3.6 V for LFP), which may promote electrolyte oxidation. Notably, NCA and NMC cells exhibited rapid

capacity fade in cycle aging studies when operated at 100% SoC. In addition, the LFP cells had significantly longer cycle life spans compared to NCA and NMC cells under tested conditions: 2500-9000 EFC vs 250-1500 EFC and 200-2500 EFC, respectively.

Naumann et al. [94] conducted a thorough 29-month study on the cyclic aging of lithium-ion cells. They examined the development of capacity in 2.85 Ah LFP cells under different conditions, including temperature (25°C and 40°C), C-rate (0.2C, 0.5C, and 1C), depth of cycle (DoC) (1%, 5%, 10%, 20%, 40%, 80%), and SoC_{mean} (25%, 50%, and 75%). Results from the 19 test points showed that capacity loss was strongly affected by DoC and SoC. Test points with lower DoC initially had higher rates of capacity degradation, but this leveled off as the number of cycles increased. Larger DoC led to higher ultimate capacity losses at higher cycle numbers, as expected. In terms of capacity, cycling around DoCs =20% around SOC =50% resulted in higher aging than low and high SoC ranges. A semi-empirical model was developed based on the static cycle aging study to predict capacity loss for the influence of C-rate, DOC, and Ah-throughput.

2.2.3. Effect of Current rate on Cycling Aging

The current rate at which a rechargeable battery is charged and discharged has a significant impact on its cycling aging, which refers to the gradual degradation and capacity loss that batteries experience over repeated charge and discharge cycles. The current rate, often expressed in terms of C-rates, determines how quickly electrons are transferred between the battery's electrodes during these processes. When a battery is subjected to higher current rates, it undergoes more rapid charge and discharge cycles. This increased electron flow can lead to several detrimental effects on the battery. Firstly, it generates more heat due to higher internal resistance, which can accelerate chemical reactions within the battery and promote the growth of SEI layers. These reactions can contribute to capacity loss and reduced cycle life. Secondly, the increased stress on the battery's materials, particularly the electrode materials, can lead to mechanical wear and tear, further deteriorating the battery's performance over time.

Conversely, charging and discharging a battery at lower current rates results in slower, gentler electron transfer. This reduces the heat generated, lowers the likelihood of SEI layer growth, and minimizes stress on the battery's components. Consequently, batteries cycled at lower current rates tend to exhibit slower cycling aging and retain their

capacity and performance for a longer duration. Battery aging is influenced by various factors, including SoC levels, charging/discharging cutoff voltages, temperature and the current rate. Notably, the current rate has a direct effect on battery temperature due to internal losses. Particularly, higher charging and discharging currents lead to a significant increase in battery temperature.

Wang et al. [95] established cycle-life model to investigate the capacity degradation induced by cycling in an LFP battery. To create this model, they performed an extensive cycle test (exceeding 2000 cycle numbers) with lifetime data of LFP cells with a capacity of 2.2 Ah. This matrix encompassed three key parameters: temperature (ranging from -30 to 60°C), DoD (ranging from 90% to 10%), and discharge rate (measured in C-rate, ranging from 2 to 10). The experimental results demonstrated that at lower C rates, capacity loss was significantly influenced by both time and temperature, with the DoD effect being comparatively less pronounced. However, at higher C rates, the impact of charge/discharge rates became more significant, with noticeable cell heating during cycles involving high discharge rates.

Wang et al. [42] conducted thorough tests on NMC+LMO cells with a 1.5 Ah capacity in their next work. The tests were conducted at different temperatures (10°C, 20°C, 34°C and 46°C) and C-rates (0.5C, 2C, 3.5C, 5C and 6.5 C) for 2000-5000 cycles at 10% constant DoD. The Tests conducted on the cycle life indicate that lower temperatures and higher C-rates lead to more mechanical breakdown and cycle life loss. results are shown in Figure 2. At 10°C, the capacitance decrease showed a clear dependence on the C rate, but the difference between the C rates for the ambient temperature of 34°C and 43°C decreased, indicating a reduced dependence. It is possible to explain this observation as the result of voltages induced by diffusion at the negative graphite electrode during fast discharge. When the lithium diffusion kinetics in the graphite negative are inhibited at low temperatures, the effect of rate becomes more prominent. In addition to the calendar models, we described in Chapter 2, they created an empirical cycle aging model from the experimental results obtained by subtracting calendar tests from life tests. For most of the conditions, the predicted values are within ±5% of the measured values for capacity loss.

Omar et al. [69] conducted experiments on LFP batteries with a nominal capacity of 2.3Ah to examine cycle aging under different current rates (1C, 5C, 10C and 15C), operating temperatures (-18°C, 0°C,25°C, and 40°C) and discharge depths up to 3000

cycles. The objective was to assess the long-term performance of LFP battery cells under diverse discharge constant current rates. The results of the investigation notably highlight the adverse consequences associated with elevated current rates on battery characteristics. Specifically, it was observed that the battery's cycle life was limited to only 560 cycles when subjected to the highest C-rate of 15C.

Sarasketa-Zabala et al. [96] performed cyclic tests on 2.3 Ah LFP cells at different C-rate (1C, 2C and 3.5C) and different DoD values (5%, 10%, 30%, 50%, 60% 100%) and derived a semi-empirical model. Experiments were always performed at 303K and 50% mean SoC for cycling aging for 2000-6000 EFC. In the current study, static cycling was found to have a more pronounced impact on cell behavior than dynamic operation. Notably, under dynamic cycling conditions, the predictive model demonstrated a root-mean-square error of only 1.75%. When cycling at a low 10% depth of discharge, the duration of cycling (measured in Ah-throughput) emerged as a more influential factor than the C-rate. However, at an intermediate 60% depth of discharge, the C-rate's influence was heightened, though the observed trends did not align with the conventional theory suggesting that higher C-rates lead to increased degradation rates, a pattern observed in the 10% DoD test.

Groot et al. [97] conducted a comprehensive study on the cycle life of LFP cells, exploring various charging and discharging C-rates. The lifespan of 2.3Ah LiFePO4/graphite cells was evaluated by testing under varying conditions, including charge and discharge rates from 1 to 4C, temperatures ranging from 23 C to 53 C, and 60% or 100% SoC. This research aims to quantify aging in terms of capacity loss under conditions typical of high-power automotive applications, involving high charge/discharge rates, elevated temperatures, and wide state-of-charge ranges. Notably, when these cells underwent symmetric cycles at C-rates ranging from 1C to 3.75C, and across the full SoC spectrum, the observed aging was heavily influenced by both current rate and temperature. Looking at the experimental data, it was observed that the combination of 1 C- rate discharge and 3.75 C-rate loading caused faster degradation compared to symmetric cycles with 3.75 C-rate in both directions. That is fast charging coupled with slow discharging significantly reduced cycle life compared to symmetric cycling in all cases studied.

Wu et al. [98] presented a battery aging study on 5 Ah LCO+NCA pouch cells to investigate the effect of various discharge rates (1C, 2C, 3C) and temperatures (10°C, 25°C, 40°C) on the cycle life. Compared to cells in other aging studies in the literature,

these pouch cells are more sensitive to low temperatures and less sensitive to discharge rates. Sensitivity to low temperature is due to cathode deterioration. Even at discharge rates as high as 5C, the number of cycles of 3000-5000 can be reached before a 20% reduction in capacity occurs. It allows capacity utilization at higher discharge rates due to less thermal and mechanical stress in their geometry.

Petit et al. [99] developed an experimental cyclic capacity model for 2.3 Ah NCA and LFP cells, considering stress factors like temperature (ranging from 5 to 30°C) and current (ranging from 1/6C to 4C) for cycle aging. Their findings indicated that higher charging currents expedited battery degradation and increased capacity loss due to cyclic aging, with this effect more pronounced in simulations involving charge rates below 4C. Additionally, they observed that prolonged exposure of batteries to high SoC resulting from fast charging also increases capacity loss. This study effectively demonstrated the influence of fast charging on battery aging, revealing notable distinctions between NCA/C and LFP/C battery technologies. Specifically, NCA/C-based battery has been found to be more susceptible to cyclic aging and ages earlier when exposed to high charge rates.

Barcellona and Piegari [100] analyzed the aging of a 10Ah LCO battery to examine how cycling aging is affected by the current rate. To isolate the impact of temperature, increase from that of the current rate on the aging process, their study employed Peltier cells to control and maintain battery temperature within a safe range of 20°C to 30°C during testing, especially for high currents (0.8C, 2.5C and 5C). The test results revealed that capacity fade remains independent of the current rate for moderate rates (up to 5C) and initial capacities of up to 95%, provided that the battery temperature is maintained within the appropriate range, and the cell is not subjected to excessive voltage stress.

Saldana et al. [101] presented a simple but realistic degradation model for a 63Ah NMC battery cell in a commercial EV. This model was created from experimental data under different temperatures (25°C, 45°C), C-rate (0.3786C, 0.4812C and 0.6710C) and DoD (20%, 40%, 60%, 80%) for the desired 1800 number of cycles. The model found an average capacity fade estimation error of 1.2% under distinct temperatures, C-rates, and DoDs for the desired number of cycles. This observation underscores that, among the variables considered, C-rate, in addition to temperature, exerts the most substantial influence on battery degradation, whereas DoD exhibits a linear relationship with degradation, particularly in the context of capacity fade.

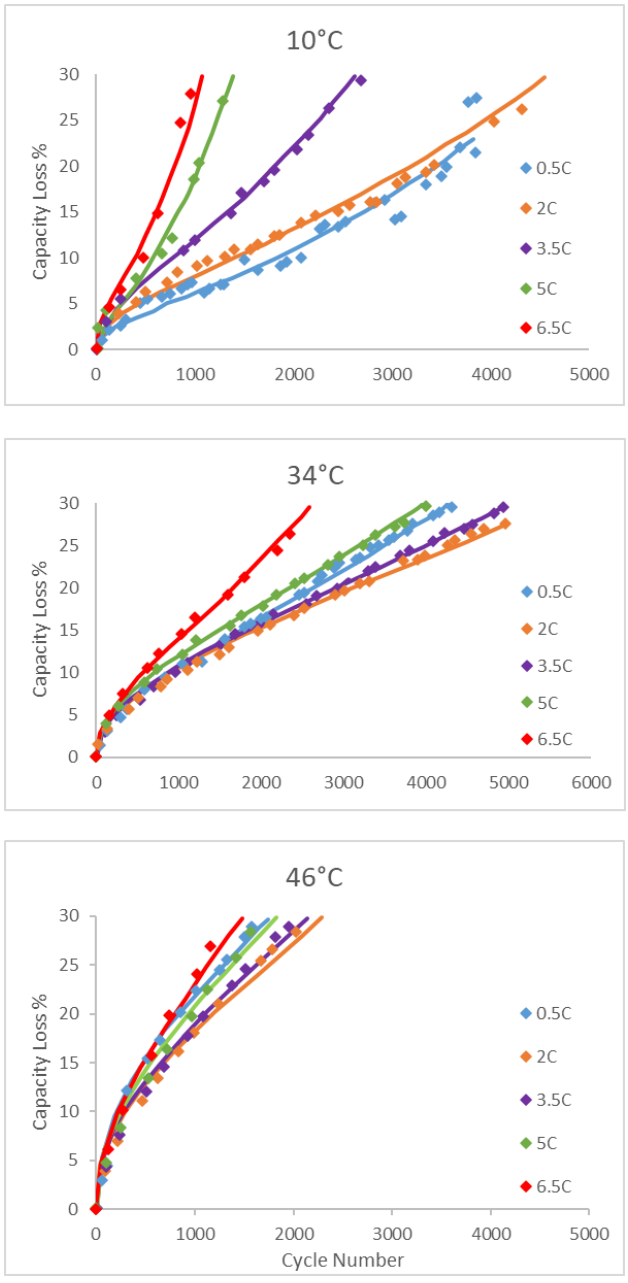

Figure 2. Cycling capacity loss at different temperatures (10 C, 34 C and 46 C respectively) for different discharge rates (0.5 C, 2 C, 3.5 C, 5 C, 6.5 C) [42].

2.2.4. Summary of Cycling Aging

Cycling aging in EVs refers to the gradual deterioration of the battery pack over time due to repeated charge and discharge cycles. This phenomenon is primarily associated with the use of lithium-ion batteries, which are common in EVs and several parameters influence cycling aging. The primary factors include the number of charge and discharge cycles the battery undergoes, the range of SoC during these cycles, the operating temperature, and the charging and discharging rates. The cumulative effect of these factors leads to capacity fade, where the battery can store less energy over time, reducing the EV's driving range. As detailed in Chapter 3, various experimental studies in the literature have explored the impact of these parameters on cycling aging behavior. Cycling aging behaviors can be interpreted differently depending on the parameters studied. For example, while some studies investigate the impact of combining temperature and SoC, other studies propose correlations between aging and the combination of temperature and C-rate. In order to provide a comprehensive overview of the research conducted, a summary of the detailed examined studies has been meticulously compiled in Table 4.

Battery cycle aging can occur during both charging and discharging. It is caused by various factors such as the battery's level, usage patterns, temperature conditions, and current demands. Additionally, the factors mentioned in calendar aging also apply to studies of cyclic aging, as they have a similar impact on battery performance. Because these aging phenomena occur during both batteries use and when it is not. Thus, this article will delve deeper into the C-rate and ΔSoC (or SoC_{mean}) factors that contribute to bicycle aging, in addition to the factors already discussed in calendar aging.

Because at high SoC and at higher temperatures ($T > 25°C$), the cathode undergoes degeneration [102–104].

Cycling aging impacts several critical parameters, including capacity, voltage, internal resistance, state of charge range, and overall performance. Over time, the battery's ability to store energy diminishes, reducing the driving range and affecting power delivery. Internal resistance increases, slowing down charging and decreasing efficiency. Temperature sensitivity plays a crucial role, with high temperatures accelerating degradation. Additionally, charging time and rate may become affected, and warranties often cover significant capacity degradation. As a result, proper maintenance and

charging habits are essential for prolonging an EV battery's lifespan and preserving its performance[105].

Similar to the calendar mode, elevated temperatures exceeding 30°C and high %SoC levels surpassing 70% tend to foster degradation and the growth of the SEI, resulting in diminished battery performance. Because at high SoC and at higher temperatures, the cathode undergoes degeneration. High temperatures have a larger impact on aging in LCO cells, followed by NMC, NCA, LMO cells, and to a lesser extent, LFP and LTO cells. This effect becomes even more pronounced at high discharge or charge rates and is further accelerated when high temperatures, high C-rates, and high ΔSoCs coincide [85,87,106].

Battery lifetime decreases also at low temperatures similar to high temperatures where significant deterioration in battery structure observed in both cases [103]. Decreased cycle life due to ambient conditions is one of the major issues that has prevented the widespread adoption of electric vehicles in cold climate regions. Therefore, the impact of low temperatures on battery aging and performance is noteworthy. Specifically, low temperatures can alter battery chemistry and result in the loss of active substances. Additionally, at low temperatures, the diffusion rate of Lithium-ion slows down, and the conductivity of the electrolyte weakens, leading to a reduction in capacity [67]. When temperatures drop below 20 ◦C, the rate at which lithium diffuses into the anode or electrolyte decreases [80,82]. Additionally, the intercalation potential of graphite material becomes more similar to that of metallic lithium, which can lead to the occurrence of metallic lithium plating. This is especially common when SoC and temperature are low, and the C-rates are high [80].

The factors that contribute to cycling aging are dependent on the usage mode of the battery. One of the most commonly cited factors in research is ΔSoC, which reflects the changes in the load state during a cycle. This factor primarily takes into account the amount of charge that the battery receives (or discharges) during a cycle. Studies have shown that high ΔSoC values lead to accelerated capacity loss, regardless of other conditions. This is mainly due to the degradation of the positive electrode and the development of SEI caused by high discharge or charge [90,91].

Studies have shown that the lowest cycling aging occurs at a SoC_{mean} of around 50%, which is within 40-60% ΔSoC. On the other hand, the highest cyclic aging occurs at a SoC_{mean} of 95%, which is within 90-100% ΔSoC.

Table 3. Overview of cycling aging studies reported in the literature.

Study	Chemistry	Capacity (Ah)	Cycle Numbers / EFC	Parameters			
				Temp. (°C)	ΔSoC (%)	DoD (%)	C-Rate (C)
Han et al. [73]	LTO+NMC, LMO and LFP	20, 35 and 10, 60 and 11, respectively.	1000	5 and 45	-	-	1.5
Preger et al. [93]	LFP, NCA and NMC	1.1, 3.2 and 3	2500-9000, 250-1500 and 200-2500,	15	40-60, 20-80, and 0-100	0-100, 20-80 and 40-60	0.5, 1, 2 and 3
Petit et al. [99]	NCA and LFP	7 and 2.3	4000	5-30	-	-	0.16-4C
Baghdadi et al. [76]	LMO+NMC and NCA	5.3 and 7	-	40, 45, and 50	20, 30 and 40	-	1 and 2
Wang et al. [42]	LMO+NMC	1.5	2000-5000	10, 22 34, and 46	-	10	0.5, 2, 3.5, 5 and 6.5
Wikner and Thiringer [90]	LMO+NMC	26	2000-10000	25 and 35	0-10, 0-30, 10-20, 20-30, 40-50, 60-70, 70-80 and 80-90	10, 20, 30, 40, 50, 60, 70, 80 and 90	1, 2 and 4
Cordoba-Arenas et al. [85]	LMO+NMC	15	-	10, 30 and 45	25, 35 and 45	-	0.33, 0.75 and 5C
Wu Yao et al. [98]	LCO+NCA	5	3000-6000	10, 25 and 40	50	-	1, 2 and 3
Yang et al. [74]	LFP	2.2	1000	25 and 40	-	75	3C
Wu et al. [80]	LFP	5	40-100	-10 and -20.	0-100%	-	0.3-0.5
Rauhala et al. [82]	LFP	2.3	-	-18, 0 and 25	-	-	1
Todeschini et al. [84]	LFP	2.3	4000-14000	55	0-10 and 0-30	-	2, 4 and 8
Wang et al. [95]	LFP	2.2	0-10000	0, 15, 45 and 60	-	10-90	0.5, 2, 6 and 10
Omar et al. [69]	LFP	2.3	1500-3000	-18, 0, 25 and 40	-	20, 40, 60, 80 and 100	1, 5, 10 and 15

(cont. on next page)

Table 3. (cont.).

Sarasketa-Zabala et al. [96]	LFP	2.3	2000-6000	30	50	5, 10, 30, 50, 60 and 100	1, 2 and 3.5
Groot et al. [97]	LFP	2.3	600-4800	23-53	60-100	60 and 90	1-4
Naumann et al. [94]	LFP	2.85	2000-14000	25 and 40	25, 50 and 75	-	0.2, 0.5 and 1
Hoog et al. [65]	NMC	20	3000	25, 35 and 45	35, 50, 65 and 80	20-100	0.33, 1 and 2
Burow et al. [81]	NMC	25	500	5 and 20	0-100	-	1
Gao et al. [89]	NMC	8	2800-3400	25	0–20, 20–40, 40–60, 60–80, 80–100% and 0–100	20	6
Saldana et al. [101]	NMC	63	1800	25 and 45	-	20, 40, 60 and 80	0.3786, 0.4812 and 0.6710
Gantenbein et al. [91]	NCA	2.6	4000	25	5–25, 25–45, 45–65, 65–85 and 75–95	20	1
Benavente-Araoz et al. [92]	NCA	2.5	700-1000	25	65–95, 35–65, 20–50, and 20–95	-	0.1
Saxena et al. [86]	LCO	1.5	800	25	0-100, 20-80, 40-60, 40-100 and 0-60	-	0.5 and 2
Barcellona and Piegari [100]	LCO	10	-	20-30	20-80	-	0.8, 2.5 and 5

The impact of SoC may vary depending on the different stages of lithiation of the graphite anode. When the graphite anode charges, it expands in volume, and when it discharges, it retracts. This expansion and retraction are more noticeable during the switching of lithiation stages. Cycling between these stages can lead to an increased particle fraction and the formation of new SEI. Also, in every SoC range, Li-on loss occurs due to the dominant aging mechanism [92].

At higher ΔSoC levels, LMO cells experience an accelerated aging process. In batteries featuring a graphite anode, Mn^{2+} ions may migrate towards the anode and undergo reduction on its surface, as the graphite anode has a low potential. These ions catalyze the thickening of the solid electrolyte interphase (SEI) film, which causes a reduction in battery capacity and an increase in resistance. As a result, during cycling, LMO cells experience a more significant increase in their capacity decay rates at elevated SoC levels and temperatures compared to other types of cells [73,90,107]. Studies on cycling aging have shown that NMC and NCA cells are more susceptible to SoC range cycling compared to LFP cells [89,91,93,94]. LTO chemistry is also more resistant to calendar aging than other battery chemistries when the state of charge is kept at medium to high levels [73]. LCO cells degrade rapidly at high SoCs and temperatures of 40-50°C, with SoC changes having the biggest impact for degradation.

One factor that affects the lifespan of a lithium-ion battery and its functionality is the rate of charge and discharge it undergoes over time. The main cause of aging from this factor is positive electrode degradation and the development of SEI due to high discharge or charge. Inferences regarding C-rate-dependent degradation can be interpreted from many studies with different chemistries. One type of battery, LFP cells, are known for their capacity to handle high amounts of power but also the literature shows that LMO cells have a longer life than LFP cells, which is consistent with the observed cycling trends [95]. The aging process of LMO cells is sped up when they are discharged to a lower potential at high rates. This happens because lithium ions gather on the surface of the LMO particles, and more lithium ions are added due to their faster diffusion rates in the electrolytes compared to LMO particles during discharge [42]. Li-on cells that use LTO anodes have the ability to sustain extremely high C rates with minimal degradation.

Because, since LTO does not change volume when charged or discharged, it is a zero-voltage material. This comes at the cost of lower energy density due to their higher potential. Additionally, studies have shown that NCA cells are more susceptible to aging

under high C-rates. However, when conducting cyclic aging tests, it is important to consider the impact of energy density on the C rate. If comparing cells with different energy densities but the same electrode surface area, it is possible to experience higher current densities for cells with higher energy density, potentially leading to an unfair comparison between different battery chemistries. After reviewing several studies, it was found that degradation rates exponentially increase when C rates exceed 2C. However, it was also discovered that LFP and NMC cells did not experience a significant increase in degradation when C -rates were below 2C and temperatures ranged from 30°C to 45°C. In one study [98], it was found that increasing the C-rate from 0.5C to 2C had little effect at 40°C but had a noticeable effect at 25°C, indicating that temperature affects C-rate. The authors suggested that the higher reaction rate and ion diffusion kinetics at these temperatures may decrease the stress caused by the increased C rate.

To properly explain how the C-rate affects battery performance, it is important to distinguish between temperatures above and below room temperature. When the temperature is lower, the conductivity of ions and the rate of intercalation decrease. On the other hand, a higher C-rate leads to faster diffusion kinetics and therefore higher current density. This means that at lower temperatures, the harmful effects of an increased C rate are accelerated, leading to more mechanical and kinetic stress on the electrodes and a greater polarization gradient. This can ultimately result in lithium plating. However, even at higher temperatures, the C-rate can still cause structural damage, such as crack propagation in the SEI layer, overloading of the cathode resulting from the increased polarization gradient, or exfoliation of graphite at the anode and cathode [26,102]. Overall, during cycling, temperature and C-rate are the most significant stress factors for all chemistries in both low and high-temperature domains. The most suitable cell chemistries for applications requiring high C-rates are LTO and NCA, followed by LFP, NMC and LCO cells [84,86,100,101].

In summary, cells with different chemistries for calendar and cyclic aging modes may exhibit divergent susceptibility to stressors affecting aging. Table 4 shows a qualitative comparison of the effects of stressors on different cell chemistries for both types of aging modes. LTO batteries seem to be the best option in this table, but they are not preferred too much in electric vehicles due to their low energy density and high weight.

Table 4. Effect of stress factors on aging for cell chemistries for both aging modes. (●●●●*:* highest impact, ●●●: high impact, ●●: medium impact, ●: low impact).

Parameter	Cell Chemistry						
	LFP	NMC	NCA	LMO	LCO	LTO	LMO+NMC
Energy Density (Wh/Kg)	●●●	●●●●	●●●●	●●	●●●	●	●●
Low SoC/ΔSoC	●	●	●	●	●	●●	●
Low C-rate	●	●	●	●	●	●	●
Low Temperature	●●	●●	●	●	●	●	●
Medium SoC/ΔSoC	●	●	●	●	●	●	●●
Medium C-rate	●	●●	●	●●	●	●	●●
Medium Temperature	●	●●	●	●	●●	●	●
High SoC/ΔSoC	●●	●●●	●●●●	●●●●	●●●●	●●	●●●
High C-rate	●●●	●●●	●●	●●	●●●	●	●●●
High Temperature	●●●	●●●●	●●●	●●●	●●●	●●	●●●●

CHAPTER 3

THEORETICAL BACKGROUND

Battery degradation in EVs is caused by a combination of factors. When batteries are repeatedly charged and discharged, they undergo chemical degradation, which leads to a gradual reduction in their capacity over time. Both very high and very low temperatures can speed up this process. Quick charging, deep discharging, and high charging rates can also contribute to faster deterioration. Even when they're not being used, batteries undergo calendar aging, which causes them to lose their overall capacity little by little. Both battery management systems (BMS) and manufacturing quality have a role to play in mitigating the effects of battery deterioration.

3.1. Battery Aging Modelling

As mentioned earlier, batteries can degrade over time due to various factors. To determine the battery's health over its lifetime, it is essential to comprehend and measure these processes accurately. In this reason, to gain a better understanding of the design and operational implications of performance degradation of Li-ion batteries, life prediction models have been developed. There are various methods of predicting lithium-ion battery wear and tear, which depend on the performance trait being observed (such as reduced capacity or increased resistance), the kind of battery life being evaluated (whether it is based on cycles or calendar), and the overall modeling method. As the battery ages, various characteristics such as resistance, capacity and power are predicted by these models. The degradation model for the application can be empirical, physics-based, or a combination of both. A vast range of model forms has been developed due to this. Some of these techniques employ electrochemical models that rely on theory to comprehend and predict the actual reactions that cause degradation within the battery. Other approaches utilize a more empirical method to model battery aging and establish connections between battery aging and specific variables by utilizing experimental data. Generally, the specific form of the model will depend on the technology used and stress factors monitored for degradation analysis [26,63,108].

3.1.1. Electrochemical Modelling

Electrochemical models are utilized to optimize the physical aspects of batteries and characterize the voltage, power and current parameters. Physical models can be used to determine battery aging by quantifying the impact of various factors on battery performance evolution. Battery aging can be predicted with the help of physical models that aim to measure the impact of various factors and thus provide a description of battery performance evolution. The aim of these approaches is to gain a clear understanding of the specific chemical and physical phenomena that occur during battery usage. The ultimate goal is to obtain a detailed description of battery performance and to use this information to optimize battery design and performance. Electrochemical models rely on the Butler-Volmer equations and porous electrode theory (Doyle and Newman 1995; Newman and Tiedemann 1975) as well as the single-particle model (SPM) to estimate the performance of a battery. While they are highly accurate, these models are complex to formulate and require the measurement and estimation of several electrochemical parameters to accurately describe the performance of the cell. Additionally, the solver may take hours to solve the non-linear differential equations with many unknown parameters. Furthermore, it is difficult to measure the physical parameters of the battery over time and use, as the battery usage and aging cause the parameters to change. Due to these reasons, electrochemical models are not extensively used for online estimation of battery aging.

In the context of battery management systems for vehicles, it is generally not practical to rely on PDE-based electrochemical models, as these models are computationally intensive and are mostly used in research settings. Therefore, attempting to model the battery pack using an electrochemical scheme would not be advantageous for long-duration simulations[8] .

3.1.2. Equivalent circuit based Modelling

Models based on electrical principles use equivalent circuit components to forecast how batteries will behave in terms of their terminal characteristics, such as voltage and current. However, the definition of equivalent circuit varies between studies and the parameters used to predict battery aging may include both internal battery

parameters and resistor aging parameters. The identification of these parameters can be achieved through direct measurements or more complex methods that involve equivalent circuit models. These methods require a diverse and large dataset, and testing is time-consuming. The equivalent circuit parameters differ with the battery's operating conditions such as temperature, SoC, and current, and also change as the battery ages. To accurately analyze the performance and aging of batteries, it is necessary to conduct an HPPC (hybrid pulse power characterization) test. This test helps to determine how the batteries respond to various operating conditions and how likely they are to deteriorate over time. By extrapolating degradation trends, predictions can be made about which battery components like electrolyte, anode, cathode, etc. are degrading and at what rate. However, since it is impossible to predict all possible deterioration events that may occur in the future, the predictions made through extrapolation are inherently inaccurate [108,109].

3.1.3. Semi-Empirical Modelling

There are different mathematical models in the literature for predicting battery calendar aging, based on empirical evidence. These models can be divided into two categories: empirical and semi-empirical.

Both electrochemical and empirical approaches have drawbacks. Electrochemical approaches are often too complex and theoretical to be practical. An empirical formula is a mathematical expression or curve that best fits observations or measurements. However, they require experimental data and are only valid for specific operating conditions. This can make it challenging to predict outcomes beyond the study range or designed experiment. The semi-empirical approach aims to combine the advantages of both approaches by using theoretical principles and experimental results to assign values to the fit parameters of the model. Semi-empirical models use a combination of theory and curve fitting. For instance, a theory predicts a linear relationship, and the best linear relationship is found from the available data, even if the best fit curve is non-linear[42,48]. Compared to electrochemical models, semi-empirical models are simpler, yet can be applied to a wider range of conditions than empirical models. This section aims to provide an in-depth analysis of both experimental and quasi-experimental studies. We will explore and elucidate the intricacies of these studies to ensure a comprehensive understanding of their methodologies.

3.1.3.1. Empirical/Semi-Empirical Modelling of Calendar Aging

A commonly used semi-empirical model, which follows the Arrhenius equation, has been extensively used in various studies to describe the deterioration of battery capacity while in storage. As a result of the influence of storage temperatures on physical reactions, battery SEI growth can be elucidated through the Arrhenius law. This approach correlates temperature with chemical reaction rate. Literature shows Arrhenius equation agrees with aging rates, especially for calendar aging [42]:

$$Q_{loss} = A.e^{-\frac{E_a}{RT}}.t^z \quad (1)$$

In this equation, A represents the exponential factor, E_a represents the activation energy, R is the gas constant, T is the absolute temperature and t represents time. SEI layer thickness inversely affects Li-ion consumption rate, which follows roughly the square root of time. Therefore, z is the power-law factor, and is typically assumed to be range 0.45-1.

Taking into account the correlation between temperature and SoC, the Arrhenius law can be formulated:

$$Q_{loss} = f(T, SoC, t) \quad (2)$$

According to Arrhenius' law, the degradation in calendar capacity can finally be expressed in a specific semi-empirical form as follows [43], [44], [45], [59], [96]:

$$Q_{loss} = A(SoC).e^{-\frac{E_a}{RT}}.t^z \quad (3)$$

Recognizing that the effects of storage SoC on parasitic chemical reactions can lead to degradation of battery capacity, studies have revealed both linear and exponential dependencies of the SoC. These models establish mathematical relationships between capacity loss, temperature, and SoC for the calendar life model. According to Sarasketa-Zabala et al. [47] calendar aging model, T refers to the storage temperature, t represents the storage time in days, and fitting parameters α_1, β_1, α_2, and β_2 are utilized. In their model, Hoog et al. combined both empirical and semi-empirical models. The Arrhenius law

establishes the correlation between temperature and calendar aging, whereas a linear empirical model is established for the SoC connection. The parameters *a, b, c* and d in the formula are fitting parameters.

Also, Eddahech et al. [49] modeled SoC dependence as a polynomial function, accounting for the interdependence of temperature and SoC through multiplication. The parameters a_{1-3}, b_{1-3}, *C, and D* in the formula are fitting parameters.

Both the exponential term A and the activation energy E_a in the equation are SoC dependence terms: So, the two parameters for calendar aging are expressed as a function of SoC: A(SoC) and E_a(SoC). Redondo-ıgleases et al. [55] selected a shape function f(t) = t z in their model, where the value of z remains constant regardless of T and SoC. The model was examined in this research using two different z values: 0.5 and 1. The general equation for the ageing model is given by Equation (8), where k represents the Boltzmann constant. The prediction error of the model is 4.5%.

In another study [48], a semi-empirical model that combines an exponential and a linear function following the Arrhenius law agrees well with measurements for all SoC and temperatures. It has been suggested that it reflects the aging process better than the commonly used square root dependence of time. The square root function tends to overestimate the decrease in capacity at the beginning of aging, and underestimate aging in the later period, especially when extrapolated. The Arrhenius model has three coefficients - α_C, β_C, *and* γ_C - which are adjusted separately for SoC and temperature. The activation energy E_a is the same for the exponential coefficients α_C and β_C, but different for γ_C, which defines the linear contribution.

In the literature, capacity loss models are typically presented as cumulative data extracted from experiments conducted under constant stress conditions (such as temperature and SoC). However, in real-world scenarios such as electric transportation, stress conditions vary over time. In this reason, a model that accounts for capacity decrease over time has been developed, unlike other semi-empirical models [45,58,59]:

$$\frac{dQ_{loss}}{dt} = k(T, SoC) \cdot \left(1 + \frac{Q_{loss}(t)}{C_{nom}}\right)^{-\alpha(T)} \quad (4)$$

k(T,SoC) represents the capacity fade evolution during storage concerning temperature and SoC. $Q_{loss}(t)/C_{nom}$ is the fractional capacity degradation at aging time *t*. In Grolleu et al. [45] model, the expression *ka* and *kb* represent how the rate of capacity

degradation changes with temperature and SoC when a battery is stored. Su et al. [58] describe the effect of temperature and SoC on the k parameter using a quadratic polynomial.

Naumann et al. [59]also developed a model for dynamic conditions that takes into account the decrease of capacity over time. After the aging model was developed, a differential form of aging models has been derived by differentiating the model with respect to time, to apply model equations with changing temperatures or SoCs over time. While K_{ref} represents the reference aging rates (temp. and SoC) for temperature, c_{Qloss} and d_{Qloss} parameters are curve-fitting parameters depending on the SoC obtained at the end of the aging study. These studies demonstrate that models can be developed with minimal errors under dynamic as well as static conditions (error < 4).

In their research, Ecker et al. [43] compare various empirical model equations and come to the conclusion that their measurement data has little to no linear component. As a result, they chose to use a semi-empirical model due to its low RMSE and smaller number of coefficients for capacity, ohmic, and polarization resistance. This model uses the parameters of temperature, aging period, and potential, which is related to the SoC of the cell:

$$\frac{L(T,V,t)}{L(T_0,V_0,t_0)} = 1 + B(T,V).c_a\,.t^{0.5} \tag{5}$$

The coefficient "c_a" is utilized to gauge the rate at which capacity declines under reference conditions T_0, t_0, and V_0. The value of L(T, V, t) provides an estimation of the resistance or capacitance at a particular time t with temperature T and voltage V. Furthermore, the effects of temperature and storage voltage are calculated according to an exponential dependence (6):

$$B(V,T) = C_v^{\frac{V-V_0}{\Delta V}}.C_T^{\frac{T-T_0}{\Delta T}} \tag{6}$$

The reference temperature and voltage are represented by T_0 and V_0 respectively. D_T and D_V have been set at 10°C and 0.1 V respectively, based on arbitrary values. The proposed law (6) utilizes c_T and c_V parameters, which are determined by analyzing the

results of accelerated calendar aging tests. It is assumed that the degradation rates are 1/2 dependent on time, based on this data.

Similarly, Schmalstieg et al. [53] also take a comparable approach, utilizing the Arrhenius function to account for temperature dependency of aging and a linear relationship to describe voltage dependency. However, they use a modified version of the square root with an exponent of 0.75 to account for time dependency.

The models discussed above are summarized in Table 3, highlighting their key elements. These different models vary in the stressors they consider, such as time, storage temperature and SoC, and in the outcomes of the aging type they examine. It should be noted that empirical and semi-empirical methods measure a battery's available capacity under reference conditions throughout its lifespan, eliminating variations in available capacity caused by different operating condition.

Table 5. Overview of Semi-Empirical/Empirical calendar aging models reported in the literature.

Source	**Model Cases**	**Initial Value (%)**	**Model Equation**	**Model parameters**	**Model Error**
Wang et al. [42]	SEM	Capacity Loss	$A.e^{-\frac{E_a}{RT}}t^{0.5}$	Temperature and time	5
Redondo-Iglesias et al. [55]	SEM	Capacity Loss	$A.e^{Bs.SoC}.e^{\frac{-E_a+Cs.SoC}{kT}}t^{z}$	Temperature, SoC and time	4.5
Sarasketa-Zabala et al. [47]	SEM	Capacity Loss	$\alpha_1.exp(\beta_1.T^{-1}).\exp(\beta_2.SoC).t^{0.5}$	Temperature, SoC and time	0.9
Eddahech et al. [49]	EM	Remaining Capacity	$(a_1.SoC + a_2.T + a_3.T.SoC).$ $e^{(b_1.SoC + b_2.T + b_3.T.SoC).t} + Ce^{Dt}$	Temperature, SoC and time	-
Werner et al. [48]	SEM	Remaining Capacity	$1 + \alpha_C\langle SoC,T\rangle.(\exp(-\beta_C\langle SoC,T\rangle.t) - 1) + \gamma_C\langle SoC,T\rangle.t$	Temperature, SoC and time	0.12-0.15

(cont. on next page)

Table 5. (cont.).

Hoog et al. [65]	SEM-EM	Capacity Loss	$A.e^{-\frac{E_a}{RT}}t^z$ / $(a_1.T^{a_2}.a_3.t^{b_1.T^{b_2}.b_3}.SoC^{c_1.T^{c_2}})$ + $(d_1.T^{d_2}.d_3.SoC.t)$	Temperature, SoC and time	5
Grolleu et al. [45]	SEM	Capacity Loss	$k_A.\exp\left\{-\frac{Ea_A}{R}\left(\frac{1}{T}-\frac{1}{T_{ref}}\right)\right\}.SoC +$ $k_B.\exp\left\{-\frac{Ea_B}{R}\left(\frac{1}{T}-\frac{1}{T_{ref}}\right)\right\}.\left(+\frac{1}{\frac{Q_{loss}(t)}{C_{nom}}}\right)^{-\propto(T)}$	Temperature, SoC and time	3-4
Su et al. [58]	SEM	Remaining Capacity	$a+b.\frac{T-52.5}{7.5}+c.\left(\frac{T-52.5}{7.5}\right)^2$ $+d.\frac{SoC-0.6}{0.2}+e.\left(\frac{SoC-0.6}{0.2}\right)^2+$ $f.\frac{T-52.5}{7.5}.\frac{SoC-0.6}{0.2}.\left(1+\frac{Q_{loss}(t)}{C_{nom}}\right)^{-\alpha_0.exp(\frac{\lambda}{T})}$	Temperature, SoC and time	3
Naumann et al. [59]	SEM	Capacity Loss	$k_{ref,Qloss}.\exp\left\{-\frac{Ea_{Qloss}}{R}\left(\frac{1}{T}-\frac{1}{T_{ref}}\right)\right\}.$ $(C_{Qloss}(SoC-0.5)^3+d_{Qloss}).\left(2\sqrt{t}\right)^{-1}$	Temperature, SoC and time	2.2
Ecker et al. [43]	SEM	Remaining Capacity	$1+C_a.C_v^{\frac{V-V_0}{\Delta V}}.C_T^{\frac{T-T_0}{\Delta T}}.\sqrt{t}$	Temperature, voltage and time	0.7-1
Schmalstieg et al. [53]	SEM	Remaining Capacity	$1-(C_{v1}.V-C_{v0}).10^6.exp\left(-\frac{C_T}{T}\right).t^{0.75}$	Temperature, voltage and time	1.2-1.7

3.1.3.2. Empirical/Semi-Empirical Modelling of Cycling Aging

Models based on cell aging studies, known as semi-empirical models, use limited data from cycled and stored cells under accelerated aging conditions. Cycle aging is more difficult to predict as it involves various independent variables such as temperature and current voltage. Moreover, these variables are linked to external conditions and battery usage. The primary factors taken into consideration are temperature, cycle number, SoC_{mean}, ΔSoC and C-rate. Cycling aging models are less uniform than calendar aging models and have varying structures and stressors considered. Generally, cyclic aging models utilize either the cumulative charge efficiency (Ah-throughput) or the total number of equivalent full cycles (EFC) to represent the battery cycle.

Cycle quantity is typically determined by scaling the EFC of the total charge efficiency (Q) with the battery capacity (C_{batt}) in Ah:

$$Q = \int_0^t |I(t')| dt' \quad (7)$$

$$EFC = \frac{Q}{2 * C_{batt}} \quad (8)$$

Here, I represents the charge-discharge current. Multiple definitions of C_{batt} exist, including nominal battery capacity at the beginning of life and present degraded battery capacity. The term "Ah-throughput" refers to the amount of Ah that the battery delivers over multiple cycles. Throughput is often modeled using a power-law relationship, similar to calendar aging (9). Additionally, throughput can also be associated with the number of cycles parameter (10):

$$Q = f(SoC, T, DoD, I) Ah^z \quad (9)$$

$$Q = f(SoC, T, DoD, I) N^z \quad (10)$$

Ah represents the total amount of energy delivered by the cell, N is the number of cycles performed, often expressed in terms of depth of discharge, and z is the power-law factor. Studies modeling the effect of throughput on cyclic aging often find an Ah^z relationship with $0.45 \leq z \leq 1$ and z is typically associated with the growth of the SEI layer.

Wang et al. [42] uncovered a power law correlation between battery capacity loss and charge throughput and developed a cycle life model based on it. The equation shows that capacity loss follows a power law relationship with time or load flow, while an Arrhenius correlation accounts for temperature effects. Also, it is widely accepted that the Arrhenius law applies to the effect of temperature on the reaction rate for most chemical processes for cycling aging, just as in calendar aging [53,61,65,95,110]. They created a battery life model that considers Ah throughput (time), C-rate, and temperature, which is a generalized model. Additionally, the study found that capacity fade is dependent on $Ah^{0.55}$, which is directly proportional to aging time. This parameter allows degradation to be correlated for different C-rates. In this equation, B represents the pre-exponential factor, E_a is the activation energy in J/mol, R stands for the gas constant, T represents the absolute temperature, and Ah is the Ah-throughput. According to the article, Ah-throughput can be defined using the following equation:

$$\text{Ah} = (\text{cycle number}) \times (\text{DoD}) \times (\text{full cell capacity}) \quad (11)$$

In their next study, Wang et al. [42] created a new life model by merging the calendar and cycling models. They developed an empirical cycle model based on the C-rate and temperature, which they combined with their semi-empirical calendar model. In the model, capacity degradation has an exponential relationship with C-rate and a linear relationship with time (or charge throughput). For temperature, the researchers obtained a highly effective empirical model that uses both an exponential and a quadratic polynomial relationship. The equation includes fitting parameters a, b, and c, which depend on temperature, and fitting parameter d, which depends on both temperature and c-rate. Additionally, parameter E depends only on c-rate.

In a study on the cycling aging model using Ah-throughput, Sarasketa-Zabala et al. [96] developed a semi-empirical model for dynamic conditions. They established mathematical relationships to connect DoD and charging efficiency in the cycle life model. First equation is used for DoD between 10% to 50%, while second equation is for all other DoD values. The cycling performance loss as a function of Ah-throughput differed depending on the DoD level ($Ah^{0.87}$ or $Ah^{0.65}$). The cycle aging model includes fitting parameters such as α_3, β_3, α_4, β_4, γ_1, γ_2, and γ_3, while the parameter k is a correction factor for dynamic operating conditions and equals 1 if the cyclic DoD is constant. However, the only challenge in applying this cycle life model is that SoC release during charge and discharge (DoD) is assumed to always occur around a mid-SoC of 50%.

The capacity degradation can be expressed as a function of either *Ah* or *n*, based on the one-to-one relationship between total ampere-hours throughput and total aging cycle. Unlike most studies in literature, instead of representing capacity degradation as a function of Ah-throughput, Todeschini et al. [84] used a power law fitting curve to express it as a function of *n*. The representation is as follows:

$$C_{f.i}(n) = a^i \cdot n^{b_i} \quad (12)$$

A model has been created to simulate the usage of low-charged batteries during the charging process. They uncovered that the most accurate curve fit was achieved with $z = 1.23$, using an exponential factor greater than 1 because of the battery's quick decline in charge. The variables α, β, and γ are fitting parameters used in the model.

A semi-empirical cyclic aging model has been developed by Cordoba-Arenas et al. [85], this research considered the amount of time that a vehicle spends in Charge-Depleting (*CD*) and Charge-Sustaining (*CS*) modes when assessing the capacity loss caused by cell cycling. The concept is defined by the following equation and ranges from 0 to 1:

$$Ratio = \frac{t_{CD}}{t_{CD}+t_{CS}} \tag{13}$$

The equation for capacity degradation relies on the temperature of the battery during active phases, its minimum SoC level, and the efficiency of Ah. The parameters α_c, β_c, and γ_c in the equation are used for fitting, while the power law factor z is set to 0.48. The battery's minimum SoC is determined by calculating the average SoC before each charging event.

In another study [94], it was aimed to create a unified aging model by superimposing calendar aging and cyclical aging model. In this study, a model representing pure cyclical aging was created in addition to the calendar aging model mentioned earlier. Similar to calendar aging models, they developed a model that only includes relevant impact parameters in the cyclical aging model. Therefore, they considered the impact of C-rate, DoC, and Ah yield on aging in their models. In the literature, DoC is also commonly referred to as depth of discharge (DoD or ΔDoD). One of the limitations of the model is that it does not account for the SoC stress factor in cyclic aging.

Omar et al. [69] proposed a new and intricate method for assessing the aging parameters of lithium batteries. The degradation of the batteries was modeled separately based on various factors such as charge-discharge current rates, operating temperatures, and discharge depths. These relationships were then integrated into MATLAB Simulink to create a general cycle life model under the suggested operating conditions. The researchers argued against the application of the Arrhenius law, as the battery exhibited nonlinear behavior throughout its cycle life. They instead used an empirical model with a 3rd-degree polynomial equation to explain the temperature and cycle life development. Additionally, the cycle life development for other factors (Charge-discharge rate and DoD) is defined as an exponential function. Equations 1, 2, 3, and 4 represent the life models associated with temperature, discharge, charge, and DoD, respectively. All parameters in the equations, except for stress factors, are fitting parameters. According to

the validation test, there is a maximum 5.4% error between the simulated and experimental results.

Saxena et al. [86] created a power law model that takes into account different SoC ranges to demonstrate how partial charge-discharge cycles can impact battery aging. The model shows that battery degradation is impacted not only by the average SoC, but also by the change in SoC (ΔSoC) during cycling. The model considers three different parameters at a constant temperature and C-rate: average SoC, ΔSoC, and equivalent full cycles. In the equation, the average SoC and ΔSoC are expressed as fractions instead of percentages, and the constants k_1, k_2, and k_3 are fitting parameters. The study also focused on the relationship between normalized discharge capacity (NDC) and capacity fade, as shown below:

$$\text{Normalized Discharge Capacity (\%)} = 100 - \text{Capacity Fade (\%)} \quad (14)$$

Most studies on cycling aging utilize the Arrhenius equation, as well as a power law relationship for efficiency or number of cycles, described in the models above. This form of modeling is often well suited to predicting aging due to cycling during post-processing computation. However, for online calculations over a shorter period of time or under rapidly changing operating conditions, the current age of the battery is often not taken into account in each new calculation. This situation was solved by Petit et al. [99] by varying the Arrhenius/power law over time. The study focused on temperature and current as stress factors for cycle aging. The semi-empirical model includes B_{cyc} as a pre-exponential factor in Ah^{1-zcyc}. This factor depends on the current, while a represents a coefficient for aging acceleration due to current, expressed in $Jmol^{-1}A^{-1}$. Additionally, z_{cyc} is an exponent constant that should be approximately 0.5 for a diffusion-limited process.

In studies based on Arrhenius and power law, aging of batteries is usually simulated by only considering degradation in the initial stages of battery life. However, as the battery ages, the rate of degradation tends to decrease. To account for this, Hoog et al. [65] created a polynomial equation based on the number of cycles, temperature and DoD, which models the point where the rate of degradation decreases. The impact of operational temperature is analyzed alongside the impact of DoD. This equation calculates the relative capacity degradation (RCD) percentage of a battery. The full equivalent cycle number is represented by x, and the DoD percentage is represented by y.

The ai and b_j parameters are used for fitting, while n and m represent the order of x and y. This polynomial model differs from other exponential models, as it considers the increasing rate of degradation during the later stages of battery life due to lithium plating.

The models discussed above are summarized in Table 6, highlighting their key elements. These different models vary in the stressors they consider, such as cycle time, temperature, SoC, and C-rate in the outcomes of the aging type they examine. It should be noted that empirical and semi-empirical methods measure a battery's available capacity under reference conditions throughout its lifespan, eliminating variations in available capacity caused by different operating conditions.

Table 6. Overview of Semi-Empirical/Empirical cycling aging models reported in the literature.

Source	Model Cases	Initial Value (%)	Model Equation	Model parameters	Model Error (RMSE)
Hoog et al. [65]	EM	Capacity loss	$\sum_{i=0,j=0}^{n,m} a_i x^i + b_i y^i$	DoD and EFC	-
Wang et al. [95]	SEM	Capacity loss	$B.exp\left(\frac{-E_a + 370.3 + C_{rate}}{R.T}\right) Ah^{0.55}$	Temperature, C-rate and Ah-throughput	-
Wang et al. [42]	EM	Capacity loss	$(a.T^2 + b.T + c).\exp[(d.T + e).I_{rate}].Ah$	Temperature, C-rate and Ah-throughput	5
Sarasketa-Zabala et al. [96]	SEM	Capacity loss	(**1**) $(\gamma_1.DoD^2 + \gamma_2.DoD + \gamma_3).k.Ah^{0.87}$ (**2**) $\left(\alpha_3.exp(\beta_3 DoD) + \alpha_4.exp(\beta_4 DoD)\right).k.Ah^{0.65}$	DoD and Ah-throughput	1.75
Cordoba-Arenas et al. [85]	SEM	Capacity loss	$(\alpha_c + \beta_c(Ratio)^{b_c} + \gamma_c.(SoC_{min} - 0.25)^{c_c}).e^{\frac{-Ea}{RT}}.Ah^z$	Temperature, DoD, SoC and Ah-throughput	0.0047
Saxena et al. [86]	SEM	Remaining capacity	$(k_1.\ SoC_{min}.(1 + k_2.\Delta SoC + k_3.\Delta SoC^2).(^{EFC}/_{100})^{0.453}$	SoC, ΔSoC and EFC	-
Naumann et al. [94]	SEM	Remaining capacity	$(a_{Qloss}.C - rate + b_{Qloss}).\left(c_{Qloss}(DoC - 0.6)^3 + d_{Qloss}\right).EFC^{z_{Qloss}}$	Current rate, DoC and EFC	0.98
Todeschini et al. [84]	EM	Remaining capacity	$(\alpha + \beta.\Delta SoC + \gamma.e^{C-rate}).n^{1.36}$	ΔSoC, C-rate and cycle number	0.24

(cont. on next page)

Table 6. (cont.).

Petit et al. [99]	SEM	Remaining capacity	$\frac{\lvert I\rvert}{3600} zB(I).exp \frac{-E_a+\alpha\lvert I\rvert}{RT}.\left(\frac{Q_{loss}}{B(I)exp\frac{-E_a+\alpha\lvert I\rvert}{RT}}\right)^{1-\frac{1}{z}}$	Current, Temperature and Ah-throughp ut	5
Omar et al. [69]	SEM	Remaining capacity	$(\mathbf{1})\ CL(T) = a.T^3 - b.T^2 + c.T + d$ $(\mathbf{2})\ CL(I_d) = e.e^{(f.I_d)} + g.e^{(h.I_d)}$ $(\mathbf{3})\ CL(I_{ch}) = m.e^{(n.I_{ch})} + o.e^{(p.I_{ch})}$ $(\mathbf{4})\ CL(DoD) = i.e^{(j.DoD)} + k.e^{(l.DoD)}$	Temperature, C-rate and DoD	5.4

CHAPTER 4

METHOD AND VALIDATION

Chapter 3.1.2 highlights the existence of a plethora of empirical and semi-empirical models for calendar aging, which have been extensively studied and documented in the literature. These models provide a valuable framework for understanding the aging behavior of batteries and predicting their performance over time. By analyzing the fundamental mechanisms that drive the aging process and incorporating relevant main factors, such as time, temperature and SoC, these models offer insights into the complex nature of calendar aging and the factors that influence it.

To model battery aging, a variable that reflects battery degradation must be selected, such as cell impedance or the decrease in capacity over time. In this study, the capacity decay development, which is a crucial parameter in electric vehicle (EV) applications, is chosen for modeling. Equation (15) is a general example of the Q_{Loss} aging model as a function of time (t), temperature (T), and SoC, where the aging factors (T, SoC) are separated from time [111]:

$$Q_{loss}(T, SoC, t) = C_A.(T, SoC).f(t) \quad (15)$$

This equation implies that the evolution of Q_{loss} for each cell follows the identical shape (f(t)), regardless of the value of T and SoC. Typically, researchers choose f(t) to be a power of time (t^z) [112], an exponential function [113], or a time functions combination [43]. The traditional approach to aging modeling involves expressing the capacity aging (CA) in an Arrhenius expression [112,114]. The pre-exponential factor (A) and activation energy (E_a) of the Arrhenius law may vary with other aging factors. For calendar aging, it is possible to express these two parameters as a function of SoC: A = A(SoC), E_a= E_a(SoC) [55].

Arrhenius law-based SEM-type models, which are based on physical reactions, are commonly used in literature. Therefore, in this study, we focus on investigating Arrhenius law-based SEMs that consider the effects of battery storage SOC, temperature, and storage time on battery capacity loss Q_{loss}.

Given that the structure of a regression model is flexible, many semi-empirical models have been reported in the literature. Three of these models detailed above were selected for detailed analysis based on the following criteria:

• The capability to apply to various aging conditions;

• Stress factors which determine the rate of aging (operating conditions);

• Applicability to various chemistries;

In this chapter, we explain the aging models and equations to be used for the experiments. First, we describe the mathematical solution methods of the models. Two methods were considered: Linear Regression Least Squares and Genetic Algorithm (GA). When a linear relationship was observed between variables, the least squares method was used to examine and draw inferences about how the variables affect each other. The procedures for identifying all model parameters using the linear regression method were conducted within the MATLAB program. When there is no linear relationship between variables, model parameters were found using the genetic algorithm. In the following section, each of these models in the literature is explained, and validation studies are conducted. Finally, to contribute to the literature with comprehensive and different models, four different calendar aging models are generated and clarified. All of these models will be compared on the different experimental sets that will be explained later.

4.1. Linear Regression Least Squares Method

Least squares is a method for implementing linear regression. To apply this method, it is necessary to bring the model into linear state-space form. Linearization is the process of taking the gradient of a nonlinear function with respect to all variables and creating a linear approximation at that point. An example of exponential model can be given as follows (16):

$$f(x) = y_i = b_2 \exp(b_1 x_i) \tag{16}$$

Where the b_2 and b_1 model parameters. Then, by taking the logarithm of both sides, the equation can be formed into a linearized form such that (17):

$$\ln(y_i) = \ln(b_2) + b_1 x_i \qquad for\ i = 1, \dots, n \tag{17}$$

The exponential function can be transformed into a linear fitting problem for easier handling. The open form of the above equation can be represented as follows, where i=1,…,n:

$$\begin{aligned} \ln(y_1) &= \ln(b_1) + b_2 x_1 \\ \ln(y_2) &= \ln(b_1) + b_2 x_2 \\ &\vdots \\ \ln(y_n) &= \ln(b_1) + b_2 x_n \end{aligned} \tag{18}$$

The above simple linear regression equation can be expressed in matrix notation as:

$$\begin{bmatrix} 1 & x_1 \\ 1 & x_2 \\ \vdots & \vdots \\ 1 & x_n \end{bmatrix} \begin{bmatrix} b_1 \\ b_2 \end{bmatrix} = \begin{bmatrix} y_1 \\ y_2 \\ \vdots \\ y_n \end{bmatrix} \tag{19}$$

A x Y

In matrix notation this model can be written as:

$$Ax = Y \tag{20}$$

Where the Y=ln(f(x)), x is the column vector that includes the model parameters b_1 and b_2, and A includes the corresponding matrix where the terms are known. After that, by taking the pseudo-inverse of the A the model parameters can be found as following:

$$x = (A^T A)^{-1} A^T y \tag{21}$$

After the coefficients of the functions of the exponential model are found, y_i can be estimated for any x_i respectively using Equation (16).

The least-squares estimate minimizes the sum of the squares of the errors, also known as the mean-squared error (MSE):

$$\text{MSE} = \frac{1}{n} \sum_{i=1}^{n} \left(Y_i - \hat{Y}_i\right)^2 \tag{22}$$

The corresponding predicted value for Y_i is denoted as $\widehat{Y}_1$, where Y_i represents the ith observed value. The total number of observations is denoted as n.

4.2. Genetic Algorithm (GA)

Genetic Algorithm performs a permutation-based optimization and is a non-linear function that searches under convergence criteria over probabilities. It is a search and optimization method that works similarly to the evolutionary process observed in nature. Genetic Algorithm is explained in the literature as follows: GA is a powerful evolutionary strategy inspired by the basic principles of biological evolution. Genetic algorithms imitate the evolutionary process in a computer environment to solve problems. In genetic algorithm terminology, a solution set that represents many possible solutions to the problem is called a population or population. Populations consist of sequences of numbers called vectors, chromosomes, or individuals. GA mechanisms create individuals in the population in the evolutionary process. Each element within the individual is called a gene. A gene is a representation of a model parameter (or decision variable) that is optimized, using bits that consist of 0s and 1s [115].

The first step for a researcher is correctly defining the variable type and problem being addressed and writing code accordingly. Then, the fitness function, one of the inputs of the Algorithm, is defined and the objective function that needs to be optimized is this function. Chromosomes in a population are evaluated based on fitness function.

To determine the fitness of each chromosome, the following method can be applied:

$$F(C_i) = \frac{f(C_i)}{\sum f(C_i)} \tag{23}$$

Where C_i represents chromosome *i; F(C_i)* is the percentage of variables in the pool that corresponds to the fitness value of chromosome *i*; and *f(C_i)* is the value of the objective function evaluated for chromosome *i.* The resulting fitness values determine which chromosomes are fit for reproduction and can mate with others who also have high fitness scores. These chromosomes produce new chromosomes called children at the end of the crossover process. As a result of chromosomes being subjected to the fitness function process, the fitness value is determined, which evaluates how close the solution is to the optimal solution. The Genetic Algorithm, with an initial population created,

works with three evolution operators. These are selection, crossover and mutation operators. In general, each of these operators is applied to every chromosome of the population that will be formed in the new generation [116].

The selection process is selecting parent individuals to create new individuals, depending on the fitness values of individuals in the population. The crossover operator, which is used after the selection phase, refers to the mutual replacement of certain parts of the chromosomes of the parent individuals, thus creating individuals with new features. Mutation involves altering a gene within any of the chromosomes of a newly formed individual, potentially occurring based on the likelihood of mutation. Illustrated in Figure 3, the value initially at 153 undergoes modifications through crossover and mutation, eventually culminating in a final value of 249. This process spans across diverse solution domains[117,118] .

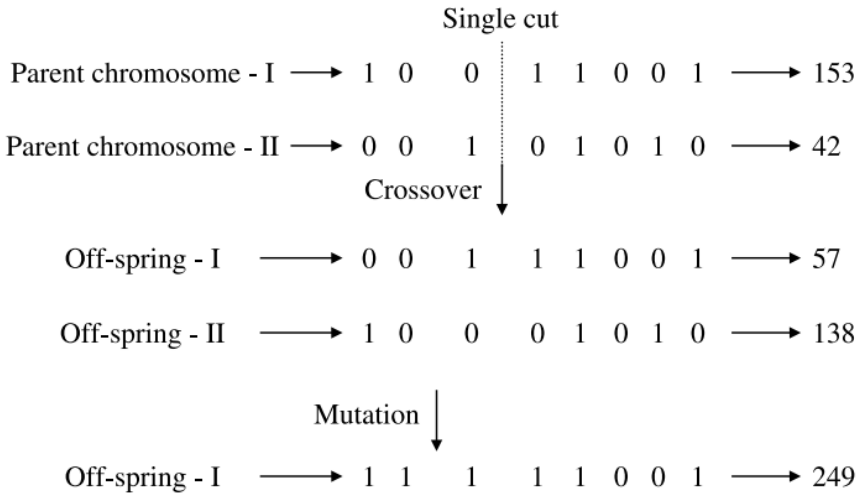

Figure 3. Example for GA process [117,118].

Finally, convergence criteria must be met, and the problem must be solved with optimal cost. GA conducts a global search, not a local one, to solve the problem. There are various methods to finalize the genetic algorithm process. These methods: When the desired solution is found during the operation of the Algorithm when the total number of iterations defined at the beginning of the GA is reached, or when the fitness value remains constant, the solution represented by the best individual found is presented as the most appropriate solution found for the problem. If many factors affect the problem, using a Genetic Algorithm in the solution is recommended in the literature [119]. A diagram describing the process of the genetic algorithm is shown in Figure 4.

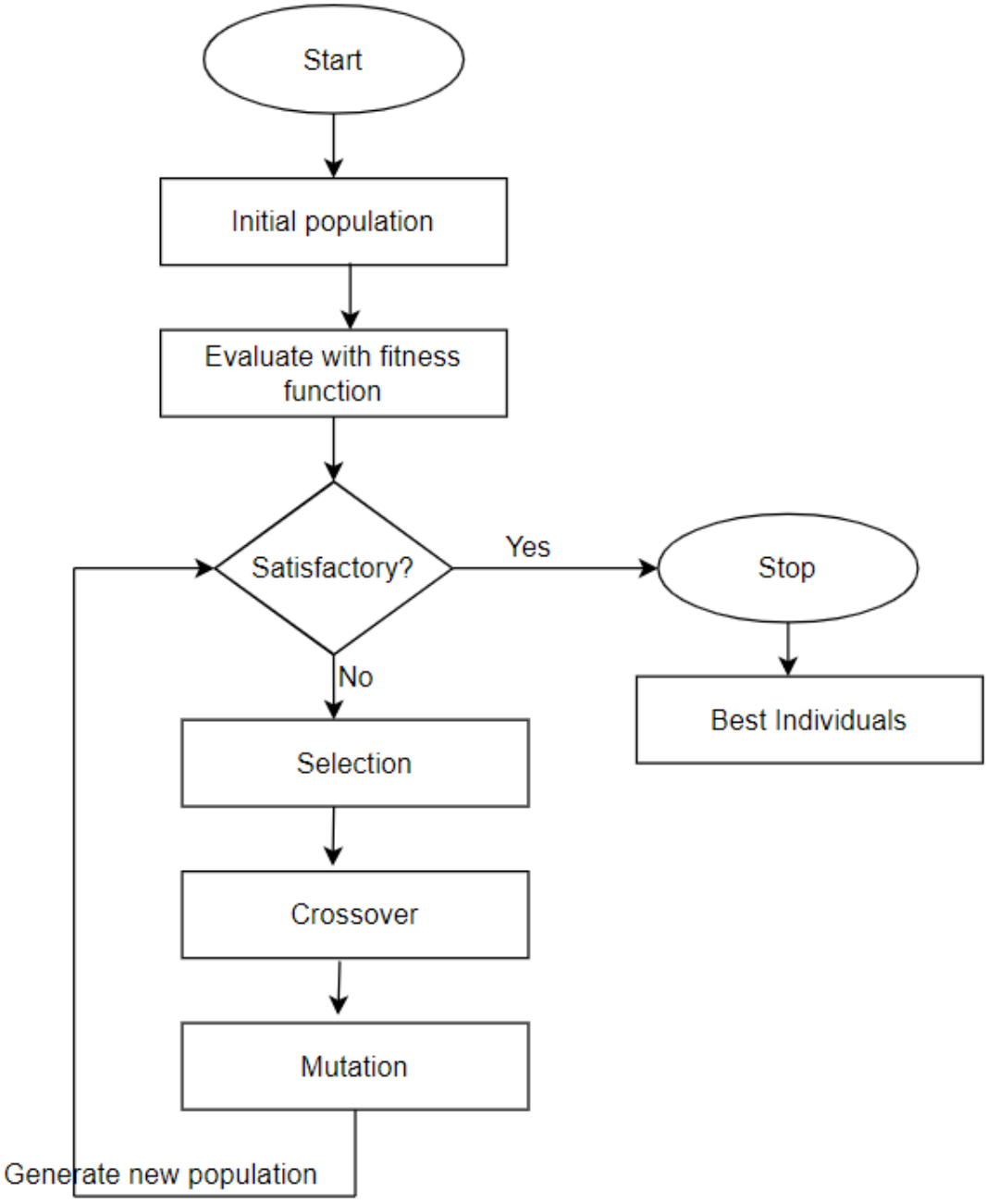

Figure 4. Process of Genetic Algorithm [118].

It is important to note that the GA model has the ability to generate varying values for its model parameters with each run. This is due to the fact that random initial values are assigned to each model parameter, in addition to the major operations of cross-over and mutation. The search process in GA involves limiting the range of each parameter for each model during every iteration. These limitations will be changed according to a theory or the functions to which it is connected and repeated until the correct result is reached. For this study, we used the trial version of the GA solver, which was developed for Microsoft Excel by Palisade Corporation, known as EVOLVER [120]. Using the Recipe Solving Method, the algorithm aims to optimize an objective function while adhering to predefined constraints. By minimizing the mean square error objective function (MSE), the optimal parameter values were determined. In all the studies shown below, in which genetic algorithm was used to find the optimal parameter, the MSE function was used.

The program has a dialog box for setting parameters and parameters limits and is shown in Figure 5. The initial values assigned for each model parameter of the GA model are taken from the analytical solutions and it should be noted that the GA model may produce different values for the model parameters in each run due to the main crossover and mutation operations. During the GA search process, the range of t parameters in each model was limited to [0.45, 1] and the fitting parameters related to temperature were limited to values ranging between [minus,0] in each iteration.

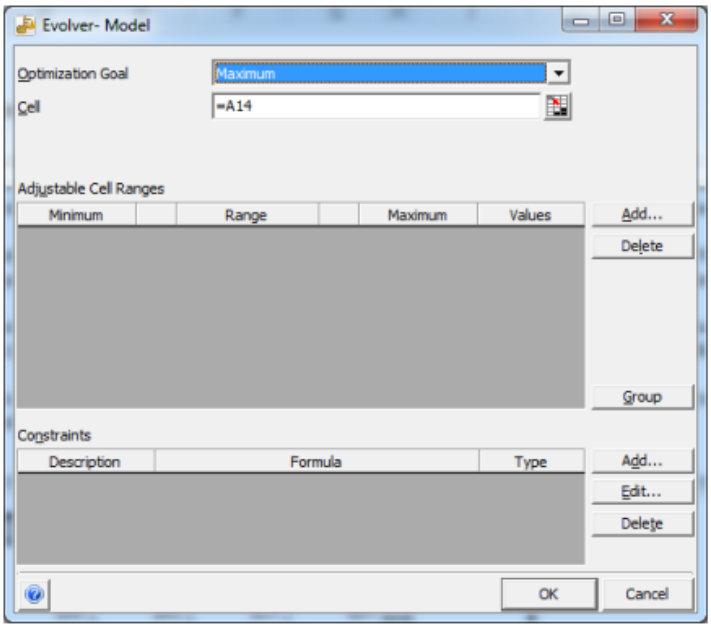

Figure 5. Evolver Model dialog box.

Convergence criteria for model parameters were set to: if 20000 trials have passed and the target cell value has not improved by more than 0.01%, the evolution will stop ($10^{-2} > Error_{n-1} - Error_n$). Convergence criteria adjustments are made in the Evolver optimization settings box shown in Figure 6.

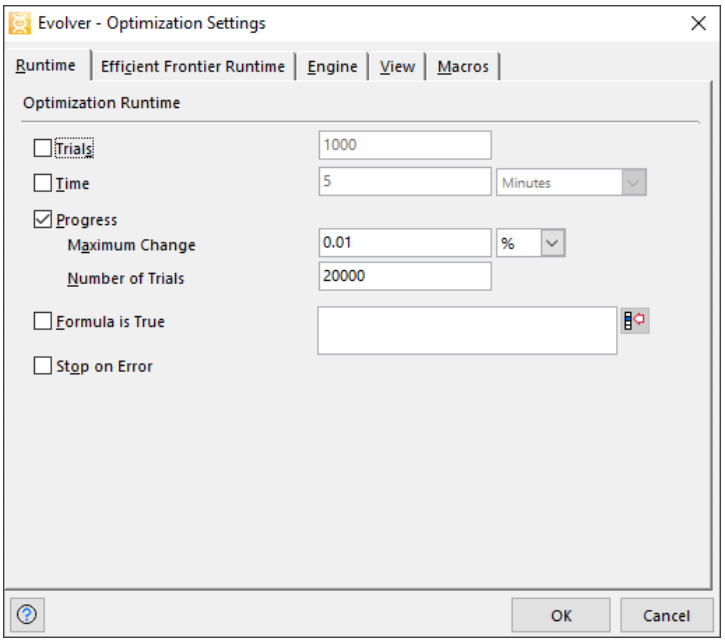

Figure 6. Optimization settings box.

4.3. Validation

Validation studies of these three selected models are included in the following subheadings. All data were taken from the main article for validation studies, and verification processes were carried out without modification.

4.3.1. Model – 1

The paper by E. Sarasketa-Zabala et al. [47] presents a study on how the capacity of 2.3 Ah LFP Lithium-ion batteries is affected by different states of charge (30%, 70%, 90%) and temperatures (30°C, 40°C, 50°C). They analyzed five static calendar aging conditions to model the dominant aging phenomenon, which is the SEI and the resulting loss of active lithium. The data used to model the calendar aging was obtained from experiments that lasted 300-400 days.

Based on the experimental data, the study concluded that exponential methods are more suitable for analyzing the effects of parasitic chemical reactions on capacity loss and voltage and the final version of the equation is given below (24):

$$Q_{loss,\%} = \alpha_1 . \exp\ (\beta_1 . T^{-1}) . \exp(\beta_2 . SoC) .\ t^{0.5} \tag{24}$$

The equation contains unknown parameters such as α_1, β_1, and β_2, while T, SoC, and t are known values obtained experimentally. To find the parameters in the equation, mathematical transformations were performed. Equation (24) can be converted into a linear regression function, and Equation (25) illustrates the transformed form:

$$\ln(\ Q_{loss,\%}) = \ln\ (\alpha_1) + (\beta_1 . T^{-1}) + (\beta_2 . SoC) + 0.5\ln t \tag{25}$$

Since z is taken as constant, the equation is transformed into the following form:

$$\ln(\ Q_{loss,\%}) - 0.5\ln t = \ln\ (\alpha_1) + (\beta_1 . T^{-1}) + (\beta_2 . SoC) \tag{26}$$

For each experiment, there is a corresponding set of Q_{loss}, T, SoC, and t values. The z coefficient on T is taken as a constant value of 0.5. Thus, the total experimental data can be converted into matrix form as shown below:

$$\begin{bmatrix} 1 & \frac{1}{T_1} & SoC_1 \\ 1 & \frac{1}{T_2} & SoC_2 \\ \vdots & \vdots & \vdots \\ 1 & \frac{1}{T_n} & SoC_n \end{bmatrix} \begin{bmatrix} \alpha_0 \\ \beta_1 \\ \beta_2 \end{bmatrix} = \begin{bmatrix} \ln(Q_{loss,1}) - 0.5\ln t_1 \\ \ln(Q_{loss,2}) - 0.5\ln t_2 \\ \vdots \\ \ln(Q_{loss,n}) - 0.5\ln t_n \end{bmatrix} \tag{27}$$

In order to simplify the equation (27), the matrix A and Y were assigned the following values:

$$A = \begin{bmatrix} 1 & \frac{1}{T_1} & SoC_1 \\ 1 & \frac{1}{T_2} & SoC_2 \\ \vdots & \vdots & \vdots \\ 1 & \frac{1}{T_n} & SoC_n \end{bmatrix} \quad Y = \begin{bmatrix} \ln(Q_{loss,1}) \\ \ln(Q_{loss,2}) \\ \vdots \\ \ln(Q_{loss,n}) \end{bmatrix} \tag{28}$$

Equation (29) represents the least squares estimates of the unknown number. A^T is the transpose matrix of A, while A^{-1} is the inverse matrix of A:

$$\begin{bmatrix} \alpha_0 \\ \beta_1 \\ \beta_2 \end{bmatrix} = (A^T A)^{-1} A^T Y \tag{29}$$

The fitting parameters, α_0, β_1, and β_2, were determined from the experimental data. Analytical optimal values of model parameters were obtained using 55 measured data sets. Equation (29) was solved using MATLAB's inner language "inv" and "transpose" to calculate the transport and inverse matrices. The fitting parameters found during the verification process were compared with those in the article and are shown in Table 7.

Table 7. Model parameters for Sarasketa-Zabala et al. Model and current model [47].

Model	**α_1**	**β_1**	**β_2**
Sarasketa-Zabala et al. Model	265.10^3	-4148	0.01
Current Model	268.10^3	-4243	0.0092

Figure 7 displays the experimental results (markers) for capacity fading under aging conditions and the estimates resulting from the model (dashed lines) constructed using Equation (24).

The model estimates have a root-mean-square error of 0.87% for the calendar capacity fade. The accuracy of the model for estimating calendar aging was high for 40°C and 70% state of charge (SoC) conditions (RMSE: 0.16). Furthermore, the model accuracy was observed to be high in data for 70% SoC and various temperatures (30, 40 and 50°C) (RMSE: 0.32).

These results imply that calendar aging is strongly related to temperature. The model has a very accurate goodness of fit with the experimental results, making it possible to predict calendar aging in most cases under high-temperature conditions. However,

when tested under 40°C and 90% SoC storage conditions, the model output had the lowest accuracy (RMSE: 1.42).

According to the article by Sarasketa-Zabala et al., the RMSE value was found to be 1. This indicates a reduction in model error, with a 13% improvement in model error compared to the RMSE value we obtained during validation (0.87).

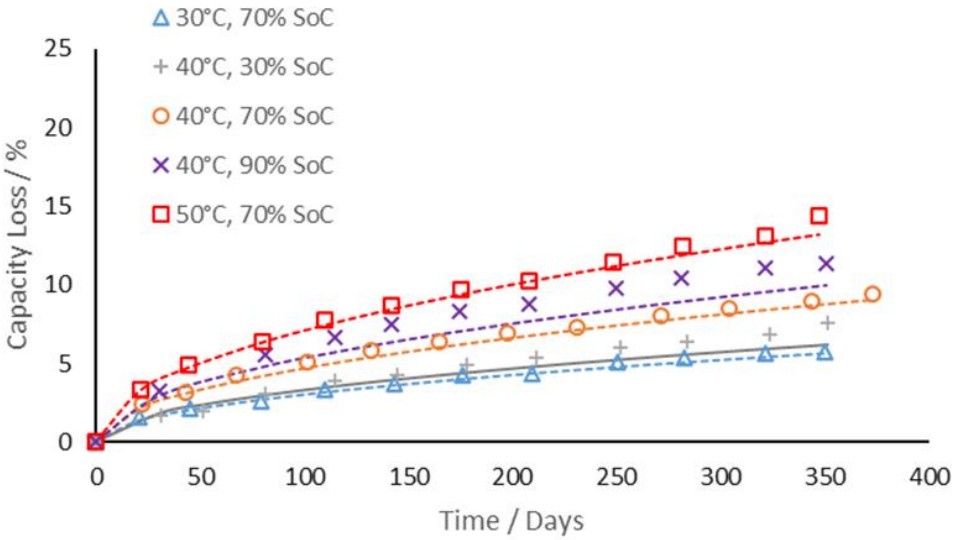

Figure 7. Capacity loss during storage at different temperatures (30°C, 40°C, 50°C) and SoCs (30%, 70%, 90%) taken from test results and model.

4.3.2. Model – 2

Redondo-Iglesias et al. [42] have developed a calendar model that can predict the lifespan of lithium-ion batteries. The researchers conducted tests on LFP batteries with a capacity of 2.3 Ah at various temperatures (30°C, 45°C, and 60°C) and SoCs (30%, 65% and 100%) over a period of 500-800 days.

The chosen time-dependent shape function in this study's model is t^z, where z is a fixed value independent of T and SoC. The model has been analyzed with two different values of z, namely 0.5 and 1. Only the z:1 value will be used in this validation study. This is because when z:1 is taken, it provides a much better model prediction than 0.5. Equation (30) represents the final equation of the ageing model, where k denotes the Boltzmann constant:

$$Q_{loss,\%} = A_0 . \exp\ (B_s . SoC) . \exp\left(\frac{-E_{a0}+C_s . SoC}{k.T}\right) . \ t^1 \qquad (30)$$

It is demonstrated that log(A) and E_a are linearly dependent on SoC. Therefore, a linear regression can be conducted to determine the parameters A0, Bs, Ea0, and Cs:

$$ln(Q_{loss,\%}) = \ln A_0 + B_s.SoC + \left(\frac{-E_{a0}}{k.T}\right) + \left(\frac{C_s.SoC}{k.T}\right) + 1\ln t \tag{31}$$

Since z is taken as constant, the equation is transformed into the following form:

$$ln(Q_{loss,\%}) - 1\ln t = \ln A_0 + B_s.SoC + \left(\frac{-E_{a0}}{k.T}\right) + \left(\frac{C_s.SoC}{k.T}\right) \tag{32}$$

The total experimental data can be converted into matrix form as shown below Eqn. (33):

$$\begin{bmatrix} 1 & SoC_1 & -\frac{1}{kT_1} & \frac{SoC_1}{-kT_1} \\ 1 & SoC_2 & -\frac{1}{kT_2} & \frac{SoC_2}{-kT_2} \\ \vdots & \vdots & \vdots & \vdots \\ 1 & SoC_n & -\frac{1}{kT_n} & \frac{SoC_n}{-kT_n} \end{bmatrix} \begin{bmatrix} A_0 \\ B_s \\ Ea_0 \\ C_s \end{bmatrix} = \begin{bmatrix} \ln(\mathrm{Q_{loss,1}}) - 1\ln t_1 \\ \ln(\mathrm{Q_{loss,2}}) - 1\ln t_2 \\ \vdots \\ \ln(\mathrm{Q_{loss,n}}) - 1\ln t_n \end{bmatrix} \tag{33}$$

In order to simplify the equation (33), the matrix A and Y were assigned the following values (33):

$$A = \begin{bmatrix} 1 & SoC_1 & -\frac{1}{kT_1} & \frac{SoC_1}{-kT_1} \\ 1 & SoC_2 & -\frac{1}{kT_2} & \frac{SoC_2}{-kT_2} \\ \vdots & \vdots & \vdots & \vdots \\ 1 & SoC_n & -\frac{1}{kT_n} & \frac{SoC_n}{-kT_n} \end{bmatrix} \quad Y = \begin{bmatrix} \ln(\mathrm{Q_{loss,1}}) - 1\ln t_1 \\ \ln(\mathrm{Q_{loss,2}}) - 1\ln t_2 \\ \vdots \\ \ln(\mathrm{Q_{loss,n}}) - 1\ln t_n \end{bmatrix} \tag{34}$$

Equation (35) represents the least squares estimates of the unknown number. A^T is the transport matrix of A, while A^{-1} is the inverse matrix of A:

$$\begin{bmatrix} A_0 \\ B_s \\ Ea_0 \\ C_s \end{bmatrix} = (A^T A)^{-1} A^T Y \tag{35}$$

The fitting parameters, A_0, B_s, Ea_0 and Cs were determined from the experimental data. Analytical optimal values of model parameters were obtained using 160 measured data sets. Equation (35) was solved using MATLAB's inner language "inv" and "transpose" to calculate the transport and inverse matrices. The fitting parameters found during the validation process were compared with those in the article and are shown in Table 9.

Table 8. Model parameters for Redondo-Iglesias et al. Model and current model [42].

Model	**A_0 (p.u./day^z)**	**B_s**	**E_{a0} (eV)**	**C_s**
Redondo-Iglesias et al. Model	$3.22.10^{11}$	$-6.16.10^{-2}$	0.969	$-4.52.10^{-3}$
Current Model	$2.83.10^{9}$	-9.10^{-2}	0.8321	$-2.7.10^{-3}$

Figure 8 displays experimental results (markers) for capacity degradation under aging conditions and predictions obtained from a model built using Equation (30) (dashed lines). To enable easy comparison, all capacity measurements and simulations are relative to initial capacity (p.u.).

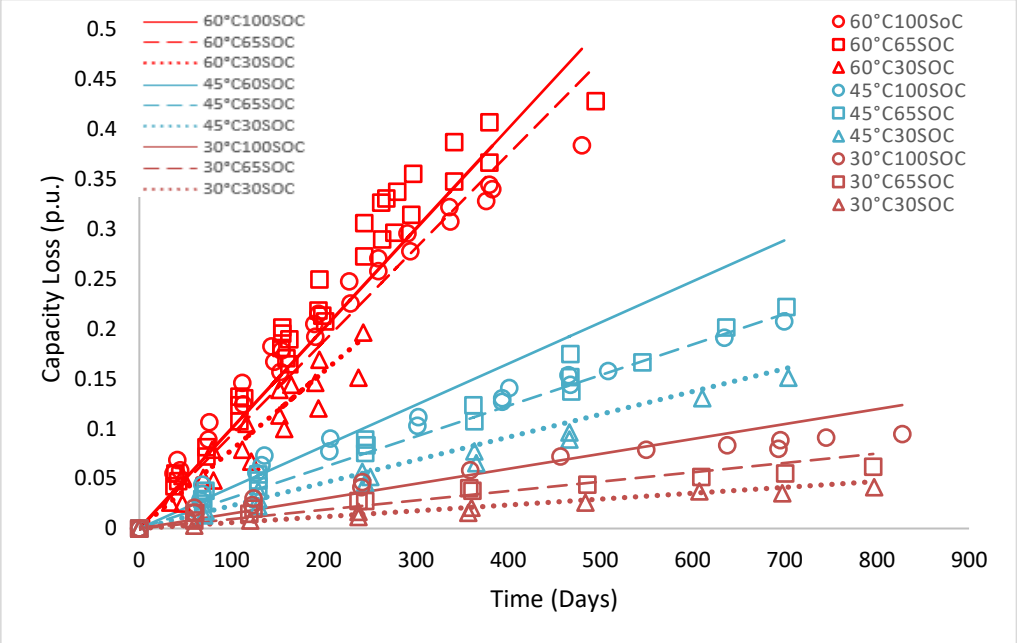

Figure 8. Capacity loss during storage at different temperatures (30°C, 45°C, 60°C) and SoCs (30%, 65%, 100%) taken from test results and model.

After examining the model's predictions, it was seen that the reduction in calendar capacity for the entire experimental setup has a root mean square error of 2.75.

The model generally fits well with experimental results, enabling the prediction of calendar aging in different temperature and SoC conditions in most cases. The model's accuracy for predicting calendar aging was high (RMSE: 0.37) for 30°C and 30% SoC conditions. Additionally, it was observed that the model accuracy was at its highest values in the data for various SoC values at 30°C. At 60°C and 30 SoC, the model was compatible with other temperatures (RMSE: 0.82). However, the accuracy of the model output was the lowest (RMSE: 4.43) when tested under storage conditions of 60°C and 65% SoC. This may be because the experimental data degrades more rapidly at 65% SoC, surpassing even the degradation rates seen at 100% SoC.

According to the article by Redondo et al., the model error value was found to be 4.8%. This indicates a reduction in model error, with a 33.3% improvement in model error compared to the error value we obtained during validation.

4.3.3. Model – 3

Schmalstieg et al. [53] developed a cycling and calendar aging model to study the aging of lithium-ion batteries. The researchers conducted tests on 2.05 Ah NMC batteries for a duration of 160-500 days, at different temperatures (35°C, 40°C, and 50°C) and SoC levels ranging from 0% to 100% to study the calendar aging model.

Due to the cell's OCV dependence on SoC and OCV dependence on anode potential, it should be noted that for calendar aging, voltage, SoC, and anode potential capture identical phenomena. This means that the calendar aging model is capable of simulating Voltage or SoC in the same direction for any load profile. Therefore, the authors also showed that the model can be written as functions dependent on SoC and T instead of voltage.

After testing the effect of various SoC values at a constant temperature of 50°C on the capacity's aging factor, it was observed that the aging factor displays a linear trend across the full range of SoC. Therefore, it can be defined as follows (36):

$$\alpha(SoC) = a_1 SoC + a_2 \quad (36)$$

This function was selected to model the relationship between the aging factor and SoC, using fitting parameters a_1 and a_2. In this study, the dependence function of the SoC differs from the exponential function studies mentioned above.

It was observed that the time dependence of the experimental data did not match the linear and square root functions well. However, the superimposed linear and square root functions matched the data well. Therefore, to get accurate aging parameters, the function with $t^{0.75}$ was used:

$$Q(T, SoC, t) = a(SoC, T).t^{0.75} \quad (37)$$

For a mathematical model of calendar aging, the dependencies on SoC and temperature need to be combined. The equation in its final form is as follows (38):

$$Q(T, SoC, t) = (a_1 SoC + a_2).exp\left(\frac{E_a}{T}\right).t^{0.75} \quad (38)$$

The equation (37) includes unknown parameters like a_1, a_2, and E_a, whereas T, SoC, and t are known values that are obtained via experimentation. However, it is not possible to convert Equation (37) into a linear regression function as the SoC-dependent function side becomes nonlinear during the conversion process. For this reason, a numerical optimization algorithm based on GA was used to solve the problem. This method and the numerical solution program are explained in more detail in the following subheading. The fitting parameters found during the validation process are shown in Table 9.

Table 9. Model parameters for current model.

Model	**a_1**	**a_2**	**E_a**
Current Model	$2.5.10^6$	$6.9.10^4$	$-6.6.10^3$

Figure 9 displays the experimental results (markers) for capacity fading under aging conditions and the estimates resulting from the model (dashed lines) constructed using Equation (37). Figure (a) shows the results at a constant 50% SoC and at different temperatures, while Figure (b) shows the results at a constant 50°C constant temperature

and different SoC values. Here C_{act}/C_{int} is the ratio of the actual value in capacity to the initial value.

The model estimates have a root-mean-square error of 1.11% for the calendar capacity fade. The accuracy of the model for estimating calendar aging was high for 50°C and 50% SoC conditions (RMSE: 0.46).

These results imply that calendar aging is strongly related to temperature. The model has a very accurate fit with the experimental results, making it possible to predict calendar aging in most cases under high-temperature different SoCs conditions. However, when tested under 50°C and 30% SoC storage conditions, the model output had the lowest accuracy (RMSE: 1.55).

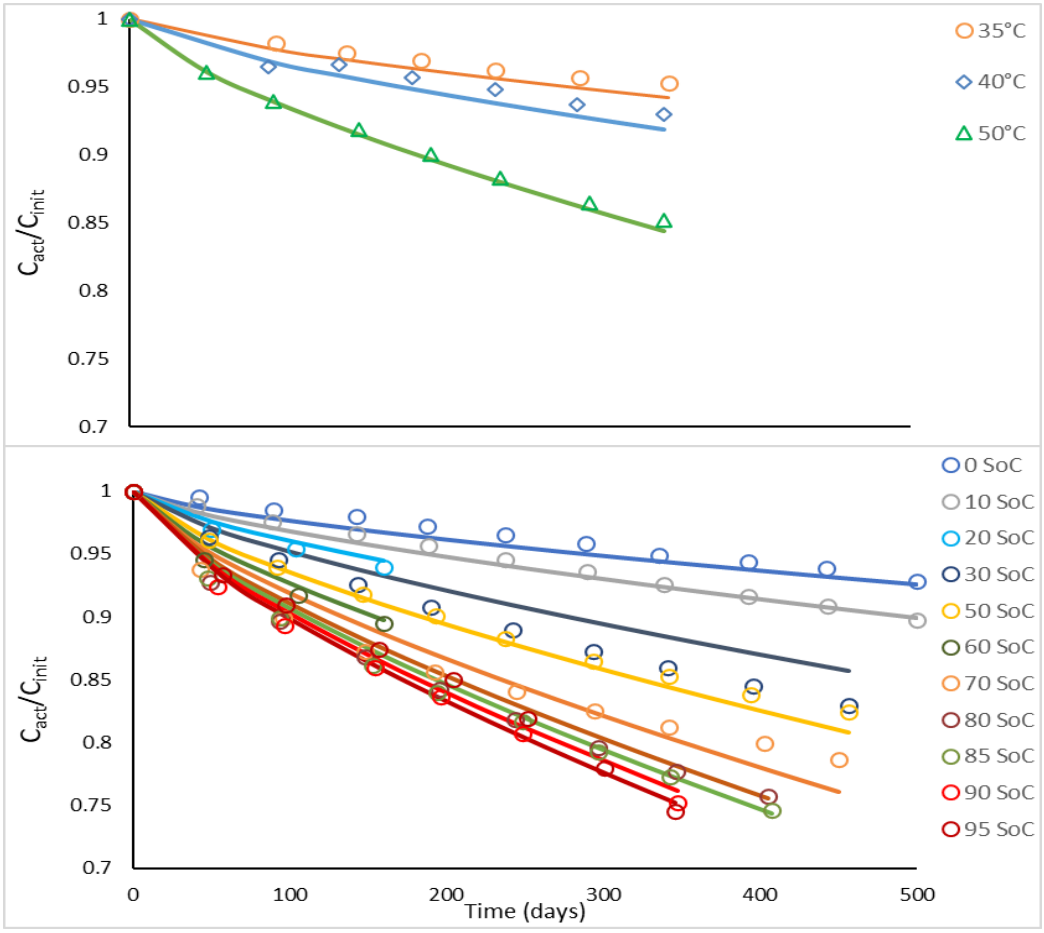

Figure 9. Capacity loss during storage at different temperatures (30°C, 40°C, 50°C) and SoCs (0%, 10%, 20%, 30%, 50%, 60%, 70%, 80%, 85%, 90%, 95%) taken from test results and model.

4.5. Developed Models

In order to contribute to the literature, we propose four different Semi-Empirical Models (SEM) for calendar aging. The models include both temperature and SoC stress factors.

It is evident from the equations that the coefficient of t over z is considered a variable in these models. The reason behind this is that, as mentioned in the literature, the z coefficient varies based on experimental sets. Therefore, since the models taken from the literature (Sarasketa-Zabala et al., Redondo et al. and Schmalstieg et al.) will be used in different data sets, the z coefficient was taken as a variable in these models as well. Additionally, the linear regression matrices of these models were updated to include the z coefficient and the equations were modified accordingly.

For an overview of all model equations to be used in this study, they are summarized in Table 10 below. The equations are given with the parameter numbers corresponding to the model. In order to compare the models, the literature's equation parameters were rearranged. In the models by Redondo-igleases et al. and Schmalstieg et al., the E_a/R function is represented with a single parameter, as E_a and R remain constant parameters throughout the model.

While the fitting parameters of Models 4, 5 and 6 were found by linear regression, the parameters of Model 7 were found by the GA method. The steps to find the fitting parameters using the regression method for Models 4, 5 and 6 are shown below, respectively.

The equation of Model-3 is transformed into a linear regression function:

$$\ln(Q_{loss}) = lnc_1 + (c_2.SoC^2 + c_3.SoC + c_4) + \left(\frac{c_5.SoC}{T}\right).c_6 lnt \qquad (39)$$

The total experimental data can be converted into matrix form as shown below Eqn. (40):

$$\begin{bmatrix} 1 & {SoC_1}^2 & SoC_1 & 1 & \frac{SoC_1}{T_1} & lnt \\ 1 & {SoC_2}^2 & SoC_2 & 1 & \frac{SoC_2}{T_2} & lnt \\ \vdots & \vdots & \vdots & \vdots & \vdots & \vdots \\ 1 & {SoC_n}^2 & SoC_n & 1 & \frac{SoC_n}{T_n} & lnt \end{bmatrix} \begin{bmatrix} c_1 \\ c_2 \\ c_3 \\ c_4 \\ c_5 \\ c_6 \end{bmatrix} = \begin{bmatrix} \ln(Q_{loss,1}) \\ \ln(Q_{loss,2}) \\ \vdots \\ \ln(Q_{loss,n}) \end{bmatrix} \quad (40)$$

In order to simplify the equation (40), the matrix A and Y were assigned the following values:

$$A = \begin{bmatrix} 1 & {SoC_1}^2 & SoC_1 & 1 & \frac{SoC_1}{T_1} & lnt \\ 1 & {SoC_2}^2 & SoC_2 & 1 & \frac{SoC_2}{T_2} & lnt \\ \vdots & \vdots & \vdots & \vdots & \vdots & \vdots \\ 1 & {SoC_n}^2 & SoC_n & 1 & \frac{SoC_n}{T_n} & lnt \end{bmatrix} Y = \begin{bmatrix} \ln(Q_{loss,1}) \\ \ln(Q_{loss,2}) \\ \vdots \\ \ln(Q_{loss,n}) \end{bmatrix} \quad (41)$$

Equation (42) represents the least squares estimates of the unknown number. A^T is the transport matrix of A, while A^{-1} is the inverse matrix of A.

$$\begin{bmatrix} c_1 \\ c_2 \\ c_3 \\ c_4 \\ c_5 \\ c_6 \end{bmatrix} = (A^T A)^{-1} A^T Y \quad (42)$$

<u>The equation of Model-4 is transformed into a linear regression function:</u>

$$\ln(Q_{loss}) = lnd_1 + (d_2.SoC + d_3) + \left(\frac{d_4}{T}\right).d_5 lnt \quad (43)$$

The total experimental data can be converted into matrix algebra form as shown below Eqn. (43):

$$\begin{bmatrix} 1 & SoC_1 & 1 & \frac{1}{T_1} & lnt \\ 1 & SoC_2 & 1 & \frac{1}{T_2} & lnt \\ \vdots & \vdots & \vdots & \vdots & \vdots \\ 1 & SoC_n & 1 & \frac{1}{T_n} & lnt \end{bmatrix} \begin{bmatrix} d_1 \\ d_2 \\ d_3 \\ d_4 \\ d_5 \end{bmatrix} = \begin{bmatrix} \ln(Q_{loss,1}) \\ \ln(Q_{loss,2}) \\ \vdots \\ \ln(Q_{loss,n}) \end{bmatrix} \quad (44)$$

The operations described in Equations 41 and 42 in Model 4 were respectively applied in this model.

The equation of Model-5 is transformed into a linear regression function:

$$\ln(Q_{loss}) = lne_1 + (e_2.SoC + e_3) + \left(\frac{e_4.SoC}{T}\right).e_5 lnt \tag{45}$$

The total experimental data can be converted into matrix form as shown below Eqn. (46):

$$\begin{bmatrix} 1 & SoC_1 & 1 & \frac{SoC_1}{T_1} & lnt \\ 1 & SoC_2 & 1 & \frac{SoC_2}{T_2} & lnt \\ \vdots & \vdots & \vdots & \vdots & \vdots \\ 1 & SoC_n & 1 & \frac{SoC_n}{T_n} & lnt \end{bmatrix} \begin{bmatrix} e_1 \\ e_2 \\ e_3 \\ e_4 \\ e_5 \end{bmatrix} = \begin{bmatrix} \ln(Q_{loss,1}) \\ \ln(Q_{loss,2}) \\ \vdots \\ \ln(Q_{loss,n}) \end{bmatrix} \tag{46}$$

The operations described in Equations 41 and 42 in Model 3 were respectively applied in this model.

Table 10. Overview of all model equations.

Model	Equation	Parameters
Sarasketa-Zabala et al. SEM-1	$a_1.\exp(a_3.SoC).\exp\left(\frac{a_2}{T}\right).\ t^{a_4}$	4
Redondo-Iglesias et al. SEM-2	$b_1.\exp\ (b_2.SoC).\exp\left(\frac{b_3+b_4SoC}{T}\right).\ t^{b_5}$	5
SEM-3	$c_1.\exp(c_2.SoC^2+c_3.SoC+c_4).\exp\left(\frac{c_5}{T}\right).t^{c_6}$	6
SEM-4	$d_1.\exp(\ d_2.SoC+d_3).\exp\left(\frac{d_4}{T}\right).t^{d_5}$	5
SEM-5	$e_1.\exp(\ e_2.SoC+e_3).\exp\left(\frac{e_4.SoC}{T}\right).t^{e_5}$	5
Schmalstieg et al. SEM-6	$(f_1SoC+\ f_2).exp\left(\frac{f_3}{T}\right).t^{f_4}$	4
SEM -7	$(g_1SoC^2+SoCg_2+g_3).exp\left(\frac{g_4}{T}\right).t^{g_5}$	5

CHAPTER 5

AGING DATA AVAILABLE IN LITERATURE

In this section, the details and working conditions of a total of 7 experimental sets, including 6 different experimental sets taken from the literature and our own experimental set (Helios Project), are explained. Empirical aging models are dependent on a regression fitted to aging data, as was covered in the preceding chapter. In order for the model to be useful in different scenarios, the aging data used for calibration should encompass a range of operating conditions, including temperature and SoC, particularly in the case of calendar aging.

This section discusses six experimental sets taken from studies in literature. While selecting the experimental sets, attention was paid to using different battery chemistries. A total of 4 different battery chemistries were selected: 2 NMC, 1 LFP, 1 NCA and 1 LMO/NMC. Generally, the purpose here is to examine the behavior of aging models in different battery chemistries.

The selection of these datasets was based on the criteria specified for the purpose of detailed analysis:

- Availability of data
- Range of operating conditions
- Usage profile/target application
- Cell chemistries

In addition to the experimental sets in the literature, the calendar aging experiment set we carried out on NMC batteries within the scope of the HORIZON-HELIOS2022 project is explained in detail.

For each of these datasets, the testing parameters, cells utilized, and testing time are described in detail in the following section. The subsequent section presents a crucial comparison of these datasets.

5.1. Schmitt 2017 NMC Dataset

Sony Energy Devices Corporation's US18650V3 high-energy cylindrical commercial 18650 cells were put through testing [121]. The nominal capacity, as stated by the manufacturer, is 2.15 Ah when the discharge current rate is 0.2C. These cells' specifics are listed in Table 11.

Table 11. Schmitt 2017 NMC Dataset – cell specifications.

Manufacturer	Sony
Cell Chemistry	NMC
Model	US18650V3
Nominal Capacity (Ah)	2.15
Voltage Range (V)	3.5-4.2

Cells were kept in climate chambers under carefully monitored settings for the duration of calendar aging studies. The cells were kept in storage for around 30 days, and then they were put in a temperature chamber set at 20°C until thermodynamic equilibrium was attained. After conducting electrochemical characterization, the SoC was reset. The combinations of temperatures and SoC tested during storage are shown in Table 12.

Table 12. Test matrix of storage conditions. Tested combinations of ambient temperature and SoC are marked by an ' ✓'.

SoC/T	0 °C	20 °C	45 °C
25 %		✓	
50 %	✓	✓	✓
75 %		✓	
100 %	✓	✓	✓

Each test was performed with three cells to see statistical effects. After the characterization procedure, cells were adjusted to a defined SoC. Since the characterization ended at 50% SoC, no SoC correction was needed for cells stored at this SoC at three temperatures. For storage conditions at 100% SoC, cells were fully charged using CCCV (constant current constant voltage) charging at 1C. To adjust other storage

SoC levels, cells were charged with CCCV and then CC (constant current) discharged with 1C. The cells were disconnected from the battery test system and stored at defined ambient temperatures T for approximately 30 days. The results shown in this study are based on approximately 470 days of observed aging.

To observe statistical effects, three cells were used for each test. After the characterization process, the cells were adjusted to a specific SoC. As the characterization ended at 50% SoC, cells stored at this level did not require any SoC correction at three different temperatures. For cells held at this level, no SoC correction was needed at three different temperatures because the characterization concluded at 50% SoC. Using CCCV charging at 1°C, batteries were completely charged for storage conditions at 100% SoC. After that, the cells were disconnected from the battery test system and stored at specific ambient temperatures T, approximately for 30 days. The experimental results are shown in Figure 10 below.

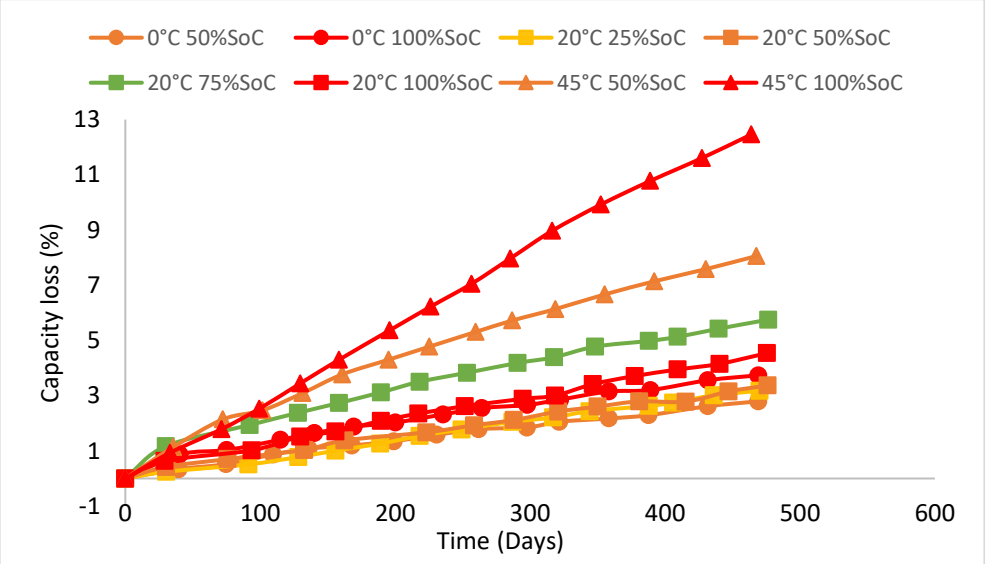

Figure 10. NMC-1 Experimental results for each storage condition.

5.2. Dane 2017 NMC Dataset

The Dane 2017 [122] dataset measured the impact of calendar aging on the capacity of NMC cells. This data is the data of the aging study conducted for NMC cells from the European project on battery materials and mechanisms called MAT4BAT. Calendar

aging tests were performed on 18 state-of-the-art Li-ion cells (NMC/Graphite, 16 Ah). The specifications of the battery are shown in Table 13.

Table 13. Dane 2017 dataset – cell specifications.

Manufacturer	Kokam
Cell Chemistry	NMC
Model	SLPB78205130H
Nominal Capacity (Ah)	16
Voltage Range (V)	2.7-4.2

The aging mode was examined under 9 different operating conditions, including 3 different SOCs (50%, 90% and 100%)) and 3 different ambient temperatures (5°C, 25°C and 45°C). This means that 2 cells were used for each operating condition. The duration of the experiment ranged from 120 to 540 days.

This study involves creating an extensive experimental plan for aging, both in terms of calendar and cycling. Additionally, it includes performing periodic electrical tests at a temperature of 25°C, regardless of the aging conditions.

The Extended Check-Up (ECU) includes two capacity tests at 1C-1C, a Dynamic Stress Test (DST) discharge, pulses at 1C – 30s according to 3 SoC, and for some experimenters, additional Electrochemical Impedance Measurements. The experimental results are shown in Figure 11 below.

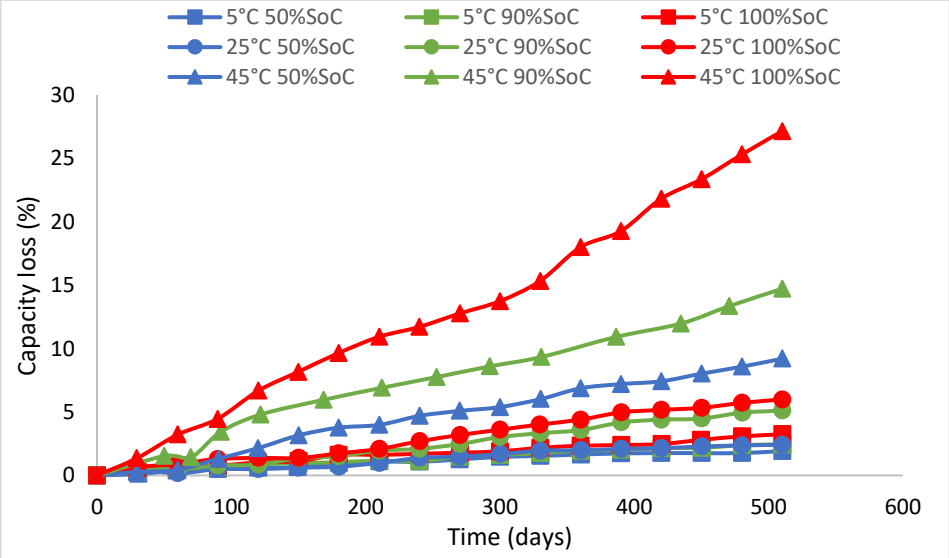

Figure 11. NMC-2 Experimental results for each storage condition.

5.3. Sun 2018 LFP Dataset

The Sun 2018 [123] dataset used 3 Ah 26650 LFP cells to measure the decrease in capacity caused by calendar aging. The manufacturer's datasheet in Table 14 shows the parameter values of the cells.

Table 14. Sun 2018 dataset – cell specifications.

Manufacturer	Sony
Cell Chemistry	LFP
Model	US26650FTC1
Nominal Capacity (Ah)	2.85
Voltage Range (V)	2-3.65

The experiments were carried out at 25°C, 40°C, and 60°C for all cells. The cells were stored at 0%, 50%, and 100% SOC for each temperature condition. The maximum continuous charging current used in this aging study was 1C. To reduce the effect of parameter variation from cell to cell and possible deviations in aging behavior, 3 cells were used for each operating condition. This also helped to reduce the danger of premature cell failure.

All cells were stored at approximately 8°C with a storage SoC of 50% to minimize inevitable calendar aging. An initial extended check-up was performed with all selected cells at the beginning of the calendar aging study. The capacity of the 27 selected cells showed a slight decrease of about 0.5-1.2%, with an average of 0.8%. After this and subsequent check-ups, each cell was loaded into the corresponding storage SoC as defined by the test matrix through Ah counting relative to the actual capacity measured at the full discharge step of the previous capacity measurement. All cells were then stored at the temperature defined in the experimental design. This entire experimental procedure took approximately 900 days. The experimental results are shown in Figure 12 below.

The graph clearly illustrates a significant capacity reduction of 60% to 100% at different SoC. As anticipated, batteries operating at lower temperatures and lower SOCs, such as 25 degrees and 0%SoC, exhibited a lesser capacity decrease compared to other temperature conditions.

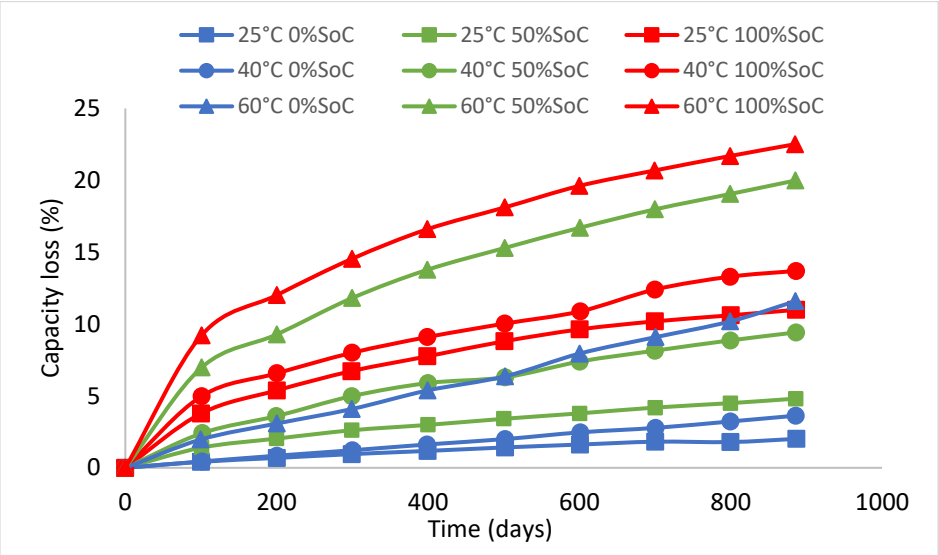

Figure 12. LFP Experimental results for each storage condition.

5.4. Baghdadi 2020 LMO/NMC Dataset

The Baghdadi 2016 [76] dataset conducted extensive testing to simulate the batteries in an EV. They used Li-on batteries based on LGChem's cathode NMC/LMO. Table 14 summarizes the fundamental characteristics of batteries and their respective charging procedures. The dataset is a subset of dataset from SIMCAL and SIMSTOCK projects commissioned by National Research Agency and French ADEME [77,124]. The study examined unused batteries initially stored at low temperatures (<10°C) and medium SoC. Before checking their initial performance, the batteries underwent a preconditioning process that involved six complete charge/discharge cycles to eliminate any suspect cells. Both calendar and power cycling tests were performed on both technologies, and three cells were tested for each aging condition to ensure reproducibility and for postmortem analysis.

Table 15. Baghdadi 2020 dataset – cell specifications.

Manufacturer	LGChem
Cell Chemistry	NMC/LMO
Nominal Capacity (Ah)	7
Voltage Range (V)	2.3-4

The aging test environment was controlled using climate chambers. The temperature was controlled within 1C for the calendar aging test. The test matrix of aging conditions under calendar aging and the corresponding symbols are presented in Table 2. The battery technology was aged under nine different conditions, including three different temperatures (30, 45, and 60°C) and three different SoCs (30, 65, and 100%). After each performance check, the target SOC was determined by ampere-hour counting after fully charging the battery using the relevant protocol. The batteries were then discharged under a 1C current at 25°C for a specific time of 1 hour multiplied by 100-SoC/100. The experimental results are shown in Figure 13 below.

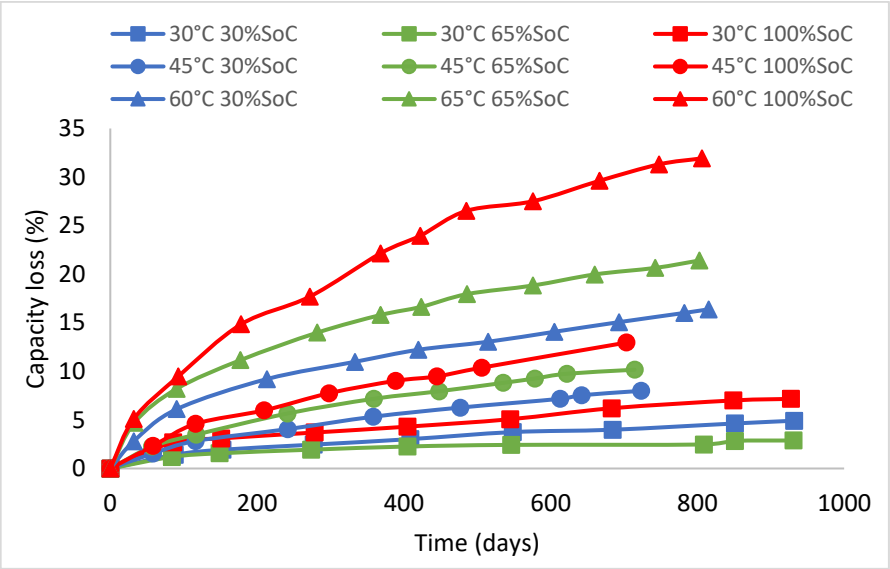

Figure 13. LMO/NMC Experimental results for each storage condition.

5.5. Keil 2016 NCA Dataset

Keil 2016 [125] dataset measured the effects of calendar aging on capacity for Li-ion cells. The test battery is an 18650 NCA Li-ion, the same cell in the battery pack found in the Tesla EVs. Tested battery cell specifications are shown in Table 15.

The study examined eight storage levels ranging from completely empty to fully charged, and four different temperatures 10 °C, 25 °C, 40 °C, 55 °C were analyzed. However, the study only showed experimental results for low 14%, medium 50%, and high 90% SoC charge values for different temperatures. Therefore, this study examined 12 combinations of storage SoC and storage temperature. The temperatures were defined

in uniform intervals of 15°C, while the storage SoCs were defined arbitrarily between fully charged and fully discharged states.

Table 16. Keil Dataset- Tested cell specifications.

Manufacturer	Panasonic
Cell Chemistry	NCA
Model	NCR1860PD
Nominal Capacity (Ah)	2.8
Voltage Range (V)	2.5-4.2

For each of the four temperatures, eight cells with different SoCs were stored in the corresponding thermal chamber. The aging process was checked periodically throughout the entire testing period and evaluated at 25°C. The control procedure included voltage ramps for cyclic voltammetry, CCCV charging and discharging for capacitance measurements, and pulses at 50% SoC to monitor changes in internal resistances. Finally, each cell was brought back to its own storage level. These experiments continued for a period of approximately 700 days. The experimental results are shown in Figure 14 below.

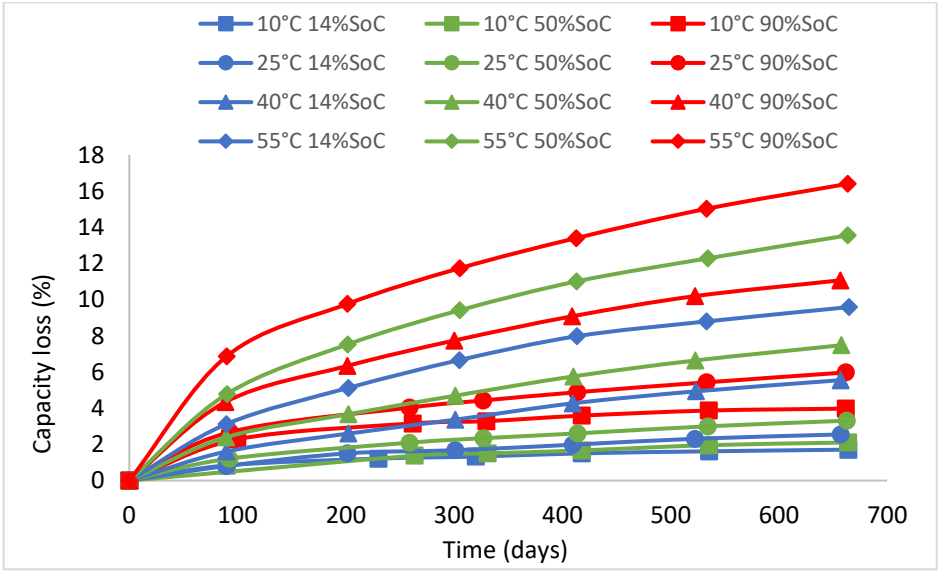

Figure 14. NCA Experimental results for each storage condition.

5.6. HORIZON-HELIOS 2022 NMC Dataset

Under the scope of the HORIZON 2022- HELIOS project, aging tests were carried out on Farasis NMC cells. Battery specifications shared by the manufacturer are given in Table 16.

Table 17. Farasis cell specifications.

Manufacturer	Faras is
Cell Chemistry	811 NMC
Model	P73
Nominal Capacity (Ah)	73
Voltage Range (V)	2.75-4.2
Nominal Voltage	3.6

As the calendar ages, batteries are stored in different states of charge and temperatures. To ensure accurate results, the tests were conducted in climate chambers. The cells were isolated during storage and examined for a duration of 1 year.

For the project, a test matrix was developed to study the impact of temperature and SoC on the internal resistance and capacity of the batteries. The test matrix included 19 tests per cell, and the recommended temperature and SoC values were determined using a design of experiments (DoE) approach. The distribution of the 19 tests and the recommended temperature and SoC values are presented in Table 17.

Table 18. Helios Test matrix of storage conditions.

Temperature	SoC values (%)				
25 °C	5%	37%	65%	80%	93%**
40 °C	0%	50%***	75%	100%**	
60 °C	0%	25%	50%	75%	100%

** represents that it will be repeated 2 times, *** represents that it will be repeated 4 times.

The test procedure is briefly mentioned in order to have information about the tests. Capacity tests are conducted to measure the energy content and capacity of a cell at different C-rates and temperatures. The data obtained from these tests is considered as the basic information for modeling the cells. These tests are also known as discharge performance tests. They are divided into three parts: Part A, Part B, and Part C. In Part A, the capacity test procedure is carried out only at 25°C, where the cell is discharged until the lower cut-off voltage is reached. Then the cell is charged with CC-CV until the current drops to C/3. In Part B, the same steps are repeated for other test temperatures in addition to Part A. Part C is the capacity testing procedure for only one fresh cell, which should be performed at 25°C, 40°C, and 60°C.

Pulse tests (pulse power characterization tests) were performed to estimate the power capacity of the cells during charging and discharging processes. Testing is usually performed under different SoC, temperature and current rates. Pulse tests were performed immediately after capacity tests. The tests were divided into three parts: A, B and C. In Pulse A, the battery cells were fully charged at 25°C to cut-off voltage and then at constant voltage until the current dropped below C/10. Immediately afterward, the cell was discharged with a constant current up to the first test SoC level. In Part B, the mid-aging impact test procedure was repeated with the same procedure at 40°C and 60°C. Part C, the Impact test procedure for fresh cells, is similar to part A except that it is applied at all three temperatures 25°C, 40°C and 60°C.

Since the project is ongoing, tests are still performed under the storage conditions given in Table 17. For this reason, in this study, analyses were made considering the data obtained so far. The analyses available so far are shown in two separate graphs below, 25°C degrees and 60°C. The experimental results are shown in Figure 15 below. Figure 15 a) shows the experimental results at different SoC values at 25°C, figure 15 b) shows the experimental results at different SoC values at 60°C.

Calendar aging tests were conducted on Farasis NMC batteries spanning 240 to 360 days. These tests involved 4 different States of Charge (SoCs) at temperatures of 25 and 60 degrees Celsius. The results for the 40-degree test have not yet been initiated and thus were not included in the analysis. It's evident that cells exposed to 60 degrees age more rapidly than those at 25 degrees. Consistent with literature findings, an increase in State of Charge values correlates with a higher aging rate in these batteries.

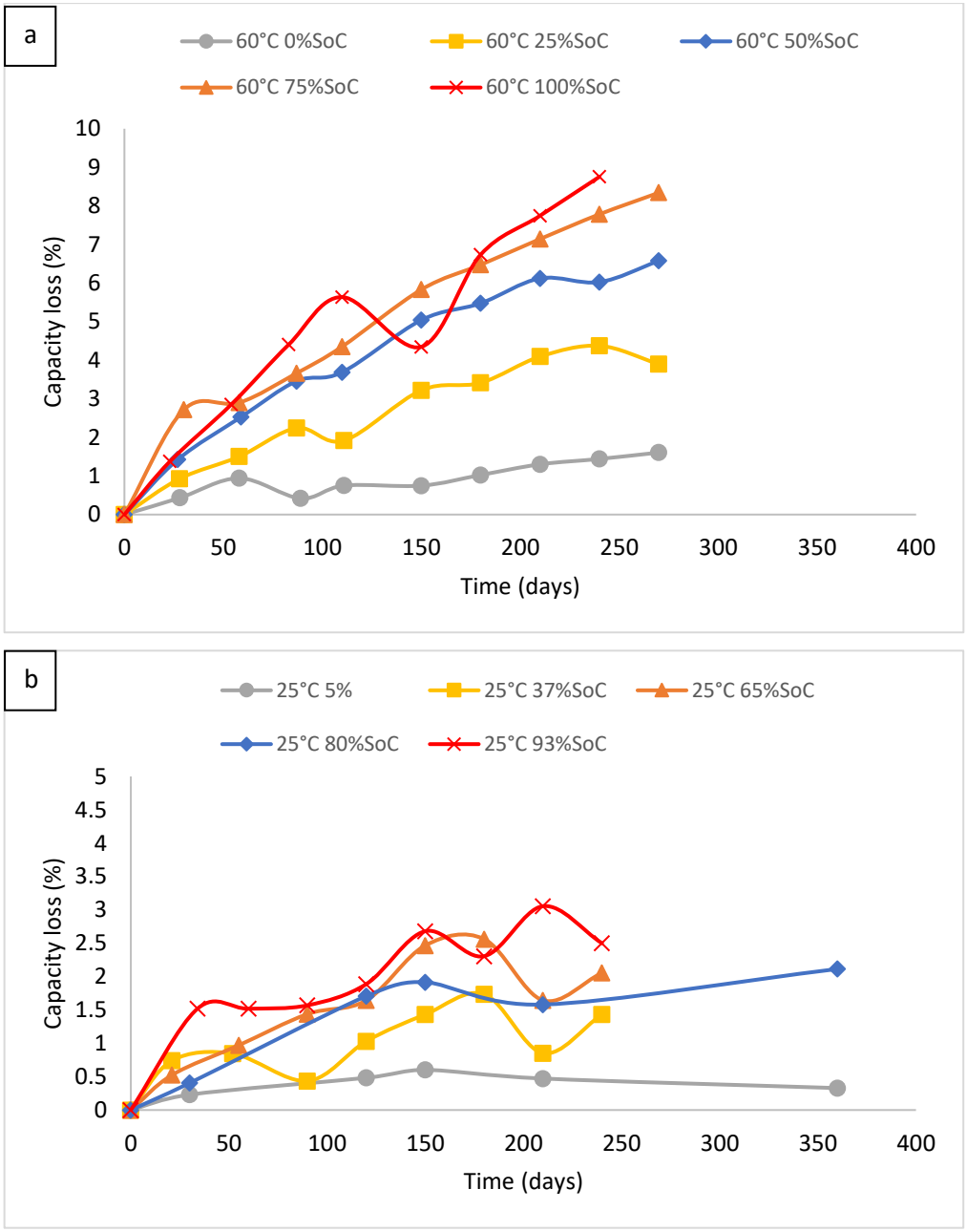

Figure 15. Helios Farasis NMC experimental results for each storage condition. a) for 25°C and b) for 60°C.

CHAPTER 6

RESULTS AND DISCUSSION

Under this heading, you can find the outputs of 5 SEMs calculated with linear regression and 7 SEMs calculated with Genetic Algorithm. For each dataset used in the study, we examined the compatibility of these different SEMs with the dataset. Moreover, we compared the corresponding quantitative measurements for the entire model-dataset fit.

This evaluation study utilizes three quantitative metrics to evaluate the prediction capabilities of various aging models. The initial metric, mean-absolute-error (MAE), quantifies the average prediction error of the models and is defined in Equation (47).

$$MAE = \frac{1}{n} \sum_{i=1}^{N} |y_i - \hat{y}_i| \tag{47}$$

where *y* represents the measured capacity values and b*y* represents the capacity values predicted by the utilized model. These definitions are also adopted for the following metrics. The second metric, root-mean-squared-error (RMSE), which also represents the average model prediction error. It differs in that it involves squaring the errors before averaging, assigning greater significance to larger errors. The RMSE metric emphasizes the points with large deviations between predicted and measured values as:

$$RMSE = \sqrt{\frac{1}{n} \sum_{i=1}^{N} |y_i - \hat{y}_i|^2} \tag{48}$$

The last metric, mean-absolute-percentage-error (MAPE), is a variation of the MAE metric. In Equation (49), MAPE not only evaluates the errors between predicted and actual values but also incorporates the ratio between these errors and the actual values themselves. This means that MAPE accounts for the relative magnitude of errors in relation to the true values:

$$MAPE = \frac{100\%}{N} \sum_{i=1}^{N} \frac{|y_i - \hat{y}_i|}{y_i} \tag{49}$$

6.1. NMC-1 Dataset

The model parameters obtained through various methods for the NMC-1 dataset are presented. Additionally, the models' MAE, RMSE, and MAPE values were compared.

6.1.1. Linear Regression Solution

Table 18 shows the parameter identification results obtained after performing linear regression calculations for every 5 SEMs based on all aging data in ' NMC-1 Dataset'. According to the fit results for all SEMs as shown in Figure 16, the SEM is capable of providing a long-term capacity degradation trend with a generalized exponential form.

Table 18. NMC-1 model parameters are based on an analytical solution for each SEM.

Model Cases	Fitting Parameter					
SEM-1	a_1 = 24.781	a_2 = -2071.3	a_3 = 0.0084	a_4 = 0.7829		
SEM-2	b_1 = 255.5	b_2 = -0.0226	b_3 = 9.1183	b_4 = -2755	b_5 = 0.7820	
SEM-3	c_1 = 3.385	c_2 = -0.0002	c_3 = 0.0353	c_4 = 1.2196	c_5 = -2069	c_6 =0.78
SEM-4	d_1 = 4.978	d_2 = 0.0084	d_3 = 1.6051	d_4 = -2071	d_5 = 0.7829	
SEM-5	e_1 = 0.145	e_2 = 0.0901	e_3 = -1.924	e_4 = 23.943	e_5 = 0.7823	

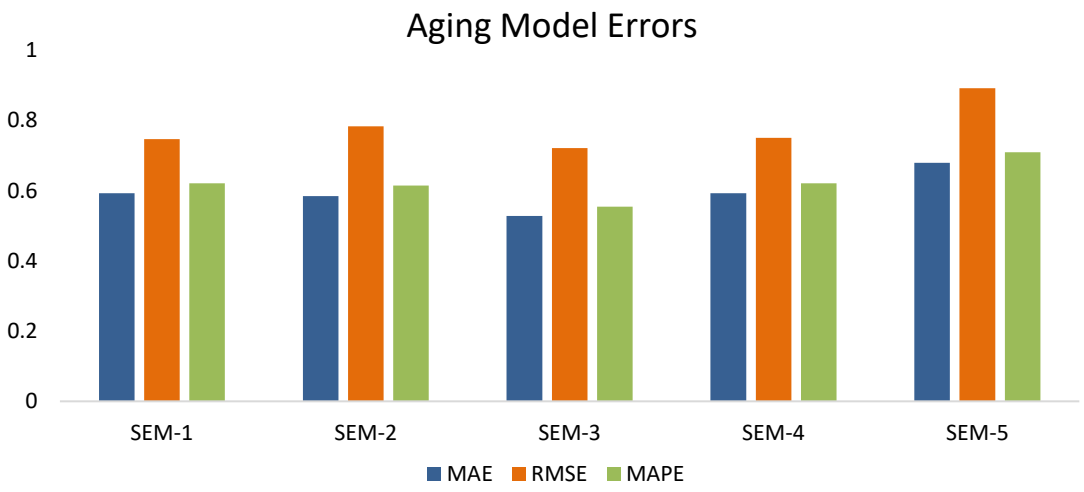

Figure 16. Performance indicators for each NMC-1 dataset modeling with analytical solution.

In general, for the NMC-1 dataset, SEM 3 provides more effective prediction results than other SEMs, with an RMSE of 0.7205. SEM 5 provides fitting results with a 23% higher RMSE than the best-fitting model. On the other hand, SEM 1 gives the closest model fit after SEM 3, with an RMSE of 0.7464. This is 3% less than SEM 3.

6.1.2. GA Solution

Table 19 shows the parameter identification results obtained after performing Genetic Algorithm for every 5 SEMs based on all aging data in 'NMC-1 Dataset'. Figure 17 shows the corresponding quantitative measurements for each model fitting.

Table 19. NMC-1 model parameters based on a GA solution for each SEM.

Model Cases	Fitting Parameter					
SEM-1	a_1 = 154.03	a_2 = -2668.7	a_3 = 0.0070	a_4 = 0.83		
SEM-2	b_1 = 9133.3	b_2 = -0.0438	b_3 = 15.611	b_4 = -3937	b_5 = 0.84	
SEM-3	c_1 = 21.599	c_2 = -0.0002	c_3 = 0.0353	c_4 = 0.9321	c_5 = -2670	c_6 = 0.85
SEM-4	d_1 = 20.324	d_2 = 0.0071	d_3 = 1.9962	d_4 = -2635	d_5 = 0.81	
SEM-5	e_1 = 17.331	e_2 = 0.0923	e_3 = -6.7447	e_4 = -25.63	e_5 = 0.84	
SEM-6	f_1 = 10.308	f_2 = 681.77	f_3 = -2621.8	f_4 = 0.52		
SEM-7	g_1 = -0.536	g_2 = 98.386	g_3 = -655.28	g_4 = -3252	g_5 = 0.72	

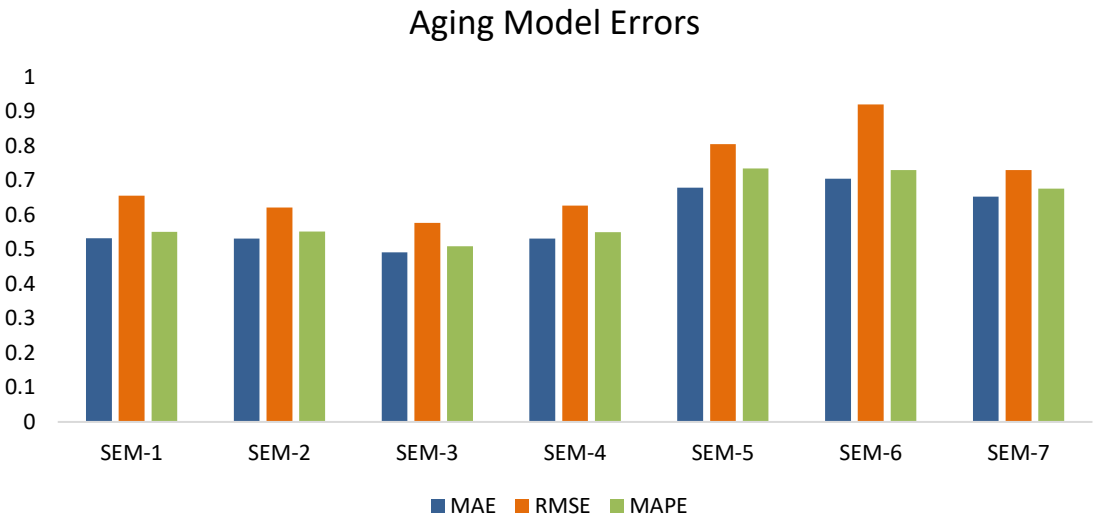

Figure 17. Performance indicators for each NMC dataset modeling with GA.

With the GA solution, SEM 3 provides more effective prediction results than other SEMs, with an RMSE of 0.5763. SEM 6 provides fitting results with a 52% higher RMSE than the best-fitting model. An average of 15% improvement was seen in the RMSEs of models analyzed with GA instead of linear regression.

6.2. NMC-2 Dataset

The model parameters obtained through various methods for the NMC-2 dataset are presented. Additionally, the models' MAE, RMSE, and MAPE values were compared.

6.2.1. Linear Regression Solution

Table 20 shows the parameter identification results obtained after performing linear regression calculations for every 5 SEMs based on all aging data in 'NMC-2 Dataset'.

Table 20. NMC-2 model parameters based on an analytical solution for each SEM.

Model Cases	Fitting Parameter					
SEM-1	a_1 = 682.51	a_2 = -3501	a_3 = 0.02	a_4 = 0.92		
SEM-2	b_1 = 0.89	b_2 = 0.10	b_3 = -24.78	b_4 = -1528	b_5 = 0.92	
SEM-3	c_1 = 76.632	c_2 = -0.0004	c_3 = 0.0512	c_4 = 4.3386	c_5 = -3481	c_6 = 0.92
SEM-4	d_1 = 26.124	d_2 = 0.0152	d_3 = 3.262	d_4 = -3501	d_5 = 0.92	
SEM-5	e_1 = 0.0719	e_2 = 0.1587	e_3 = -2.631	e_4 = -42.636	e_5 = 0.92	

Figure 18 shows the corresponding quantitative measurements for each model fitting. In general, for the NMC-2 dataset, SEM 5 provides more effective prediction results than other SEMs, with an RMSE of 1.681. SEM 5 provides fitting results with a 25% higher RMSE than the best-fitting model. On the other hand, SEM 1 gives the closest model fit after SEM 2, with an RMSE of 1.8018.

Figure 18. Performance indicators for each NMC-2 dataset modeling with analytical solution.

6.2.2. GA Solution

Table 21 shows the parameter identification results obtained after performing Genetic Algorithm for every 5 SEMs based on all aging data in 'NMC-2'. Figure 19 shows the corresponding quantitative measurements for all model cases.

Table 21. NMC-2 model parameters based on a GA solution for each SEM.

Model Cases	Fitting Parameter					
SEM-1	a_1 = 23043	a_2 = -4838.9	a_3 = 0.0214	a_4 = 1.00		
SEM-2	b_1 = 28.331	b_2 = 0.0999	b_3 = -25.63	b_4 = -2564	b_5 = 0.96	
SEM-3	c_1 = 104.72	c_2 = 0.0005	c_3 = -0.0596	c_4 = 9.8766	c_5 = -5425	c_6 = 1.0
SEM-4	d_1 = 873.99	d_2 = 0.0203	d_3 = 6.7396	d_4 = -5897	d_5 = 1.00	
SEM-5	e_1 = 0.1748	e_2 = 0.1780	e_3 = -3.6303	e_4 = -49.173	e_5 = 1.00	
SEM-6	f_1 = 9305.4	f_2 = -412	f_3 = -5347.1	f_4 = 1.00		
SEM-7	g_1 = 148.05	g_2 = 10002	g_3 = 11205	g_4 = -5637	g_5 = 1.00	

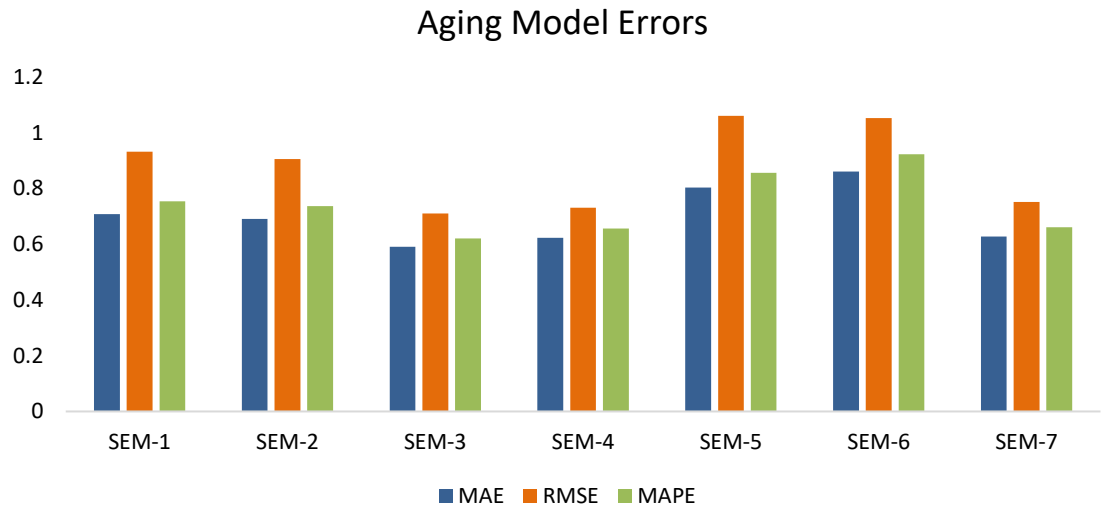

Figure 19. Performance indicators for each NMC-2 dataset modeling with GA.

SEM 3 provides more effective prediction results with the GA solution than other SEMs, with an RMSE of 0.7099. Then, the closest fit result gives SEM 4 with 0.7313 RMSE. SEM 6 provides fitting results with a 49% higher RMSE than the best-fitting model. An average of 46% improvement was seen in the RMSEs of models analyzed with GA instead of linear regression.

6.3. LFP Dataset

The model parameters obtained through various methods for the LFP dataset are presented. Additionally, the models' MAE, RMSE, and MAPE values were compared.

6.3.1. Linear Regression

Table 22 shows the parameter identification results obtained after performing linear regression calculations for every 5 SEMs based on all aging data in 'LFP Dataset'. According to the fit results for all SEMs as shown in Table 22, the SEM is capable of providing a long-term capacity degradation trend with a generalized exponential form. Figure 20 shows the corresponding quantitative measurements for all model cases.

Table 22. LFP model parameters based on an analytical solution for each SEM.

Model Cases	Fitting Parameter					
SEM-1	a_1 = 6486.2	a_2 = -3650	a_3 = 0.0156	a_4 = 0.62		
SEM-2	b_1 = 303670	b_2 = -0.060	b_3 = 23.998	b_4 = -4858.6	b_5 = 0.62	
SEM-3	c_1 = 776.78	c_2 = -0.0001	c_3 = 0.0260	c_4 = 4.34102	c_5 = -3650	c_6 = 0.62
SEM-4	d_1 = 80.540	d_2 = 0.0156	d_3 = 4.3887	d_4 = -3600.6	d_5 = 0.62	
SEM-5	e_1 = 0.2408	e_2 = 0.1260	e_3 = -1.423	e_4 = -34.688	e_5 = 0.62	

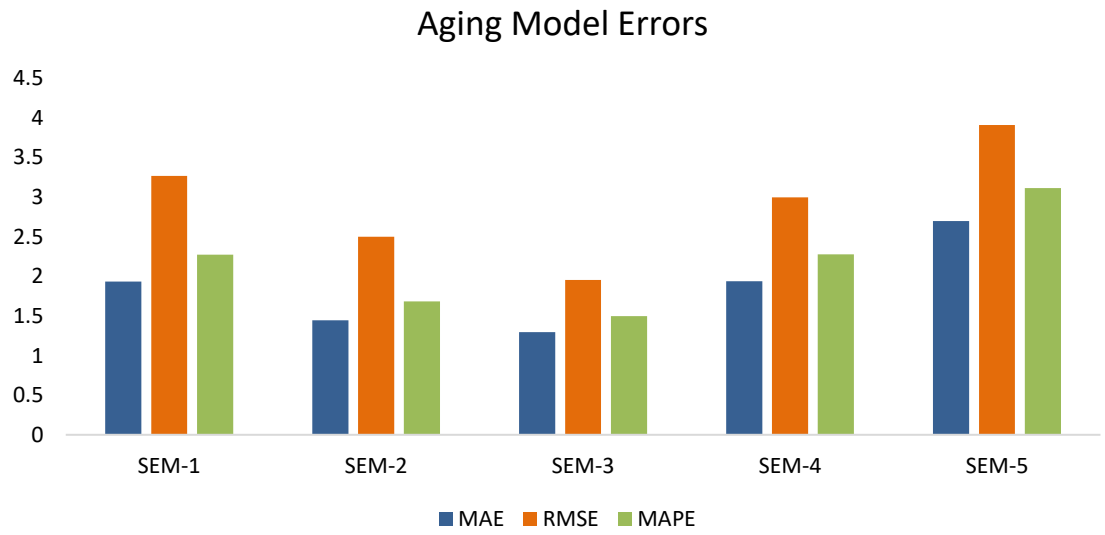

Figure 20. Performance indicators for each LFP dataset modeling with analytical solution.

In general, for the LFP dataset, SEM 3 provides more effective prediction results than other SEMs, with an RMSE of 1.9533. SEM 5 provides fitting results with a 100% higher RMSE than the best-fitting model.

6.3.2. GA Solution

Table 23 shows the parameter identification results obtained after performing Genetic Algorithm for every 7 SEMs based on all aging data in 'LFP Dataset'. Figure 21 shows the corresponding quantitative measurements for all model cases.

Table 23. LFP model parameters are based on a GA solution for each SEM.

Model Cases	Fitting Parameter					
SEM-1	a_1 = 2435	a_2 = -3056.9	a_3 = 0.0090	a_4 = 0.55		
SEM-2	b_1 = 3445	b_2 = -0.0035	b_3 = 4.1232	b_4 = -3171	b_5 = 0.55	
SEM-3	c_1 = 73.19	c_2 = -0.0001	c_3 = -0.0222	c_4 = 4.4416	c_5 = -3290	c_6 = 0.48
SEM-4	d_1 = 72.95	d_2 = 0.0089	d_3 = 4.7091	d_4 = -3299	d_5 = 0.47	
SEM-5	e_1 = 0.254	e_2 = 0.1084	e_3 = -0.077	e_4 = -31.55	e_5 = 0.49	
SEM-6	f_1 = 56.10	f_2 = 3066.8	f_3 = -3058.0	f_4 = 0.49		
SEM-7	g_1 = -0.451	g_2 = 122.76	g_3 = 3819.0	g_4 = -3143	g_5 = 0.48	

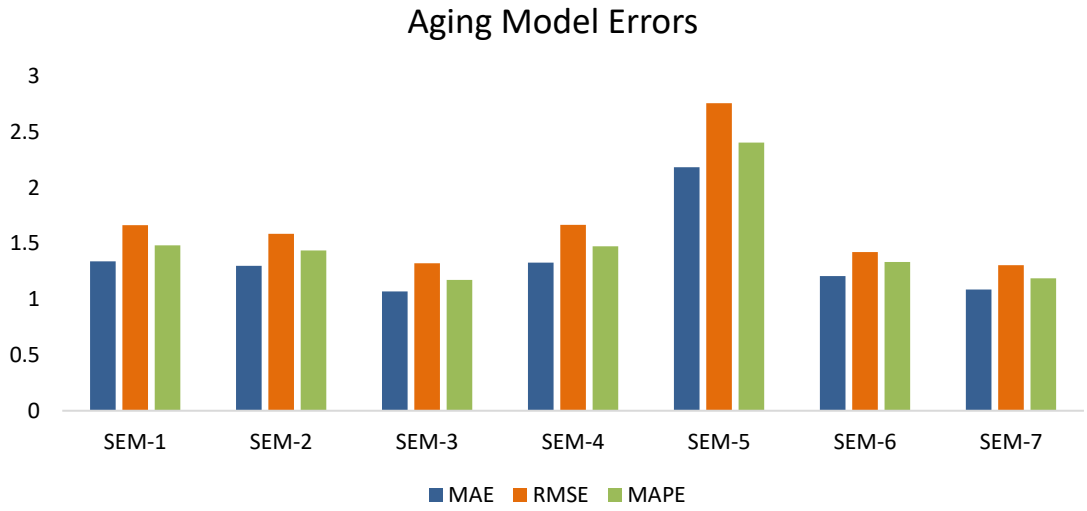

Figure 21. Performance indicators for each LFP dataset modeling with GA.

SEM 7 provides more effective prediction results with the GA solution than other SEMs, with an RMSE of 1.3062. Then, the closest fit result gives SEM 3 with 1.3224 RMSE. An average of 35% improvement was seen in the RMSEs of models analyzed with GA instead of linear regression.

6.4. LMO/NMC Dataset

The model parameters obtained through various methods for the LMO/NMC dataset are presented. Additionally, the models' MAE, RMSE, and MAPE values were compared.

6.4.1. Linear Regression Solution

Table 24 shows the parameter identification results obtained after performing linear regression calculations for every 5 SEMs based on all aging data in 'LMO/NMC Dataset'. Figure 22 shows the corresponding quantitative measurements for all model cases.

Table 24. LMO/NMC model parameters are based on an analytical solution for each SEM.

Model Cases	Fitting Parameter					
SEM-1	a_1 = 6x10^6	a_2 = -5498	a_3 = 0.0075	a_4 = 0.53		
SEM-2	b_1 = 73592	b_2 = 0.0398	b_3 = -10.3	b_4 = -4823	b_5 = 0.53	
SEM-3	c_1 = 3057	c_2 = 0.0001	c_3 = -0.008	c_4 = 8.0253	c_5 = -5503	c_6 = 0.53
SEM-4	d_1 = 2472	d_2 = 0.0075	d_3 = 7.813	d_4 = -5498	d_5 = 0.53	
SEM-5	e_1 = 0.4557	e_2 = 0.2338	e_3 = -0.785	e_4 = -72.16	e_5 = 0.52	

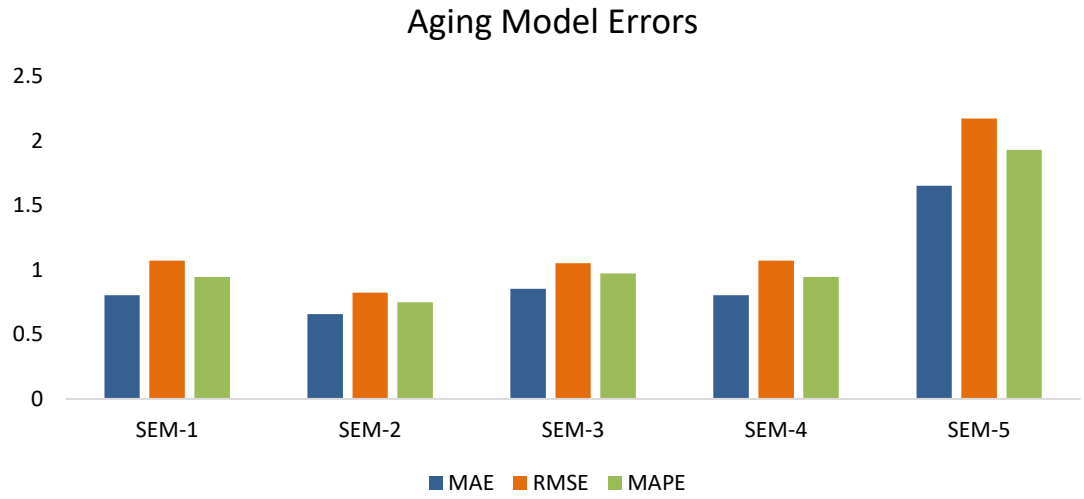

Figure 22. Performance indicators for each LMO/NMC dataset modeling with analytical solution.

In general, for the LMO/NMC dataset, SEM 2 provides more effective prediction results than other SEMs, with an RMSE of 0.8237. Then, the closest fit result gives SEM 3 with 1.0532 RMSE.

6.4.2. GA Solution

Table 25 shows the parameter identification results obtained after performing Genetic Algorithm for every 7 SEMs based on all aging data in 'LMO/NMC Dataset'. Figure 23 shows the corresponding quantitative measurements for all model cases.

Table 25. LMO/NMC model parameters are based on a GA solution for each SEM.

Model Cases	Fitting Parameter					
SEM-1	$a_1 = 6x10^{\wedge 6}$	$a_2 = -5556.7$	$a_3 = 0.0095$	$a_4 = 0.53$		
SEM-2	$b_1 = 85590$	$b_2 = 0.0125$	$b_3 = -8.754$	$b_4 = -3623$	$b_5 = 0.53$	
SEM-3	$c_1 = 3598.3$	$c_2 = 0.0001$	$c_3 = -0.0069$	$c_4 = 8.3881$	$c_5 = -5667$	$c_6 = 0.51$
SEM-4	$d_1 = 2080.5$	$d_2 = 0.0094$	$d_3 = 8.5173$	$d_4 = -5682$	$d_5 = 0.51$	
SEM-5	$e_1 = 0.4549$	$e_2 = 0.2349$	$e_3 = -0.3604$	$e_4 = -74.20$	$e_5 = 0.52$	
SEM-6	$f_1 = 0.4214$	$f_2 = 249.33$	$f_3 = -1694.0$	$f_4 = 0.8210$		
SEM-7	$g_1 = 1251.1$	$g_2 = 1237.2$	$g_3 = 1153.3$	$g_4 = -5648$	$g_5 = 0.51$	

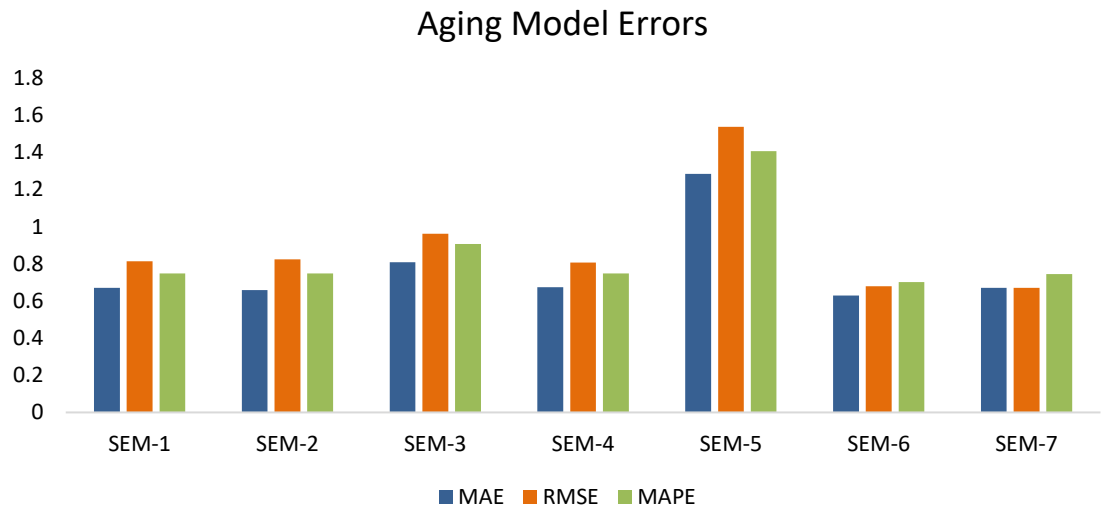

Figure 23. Performance indicators for each LMO/NMC dataset modeling with GA.

SEM 7 provides more effective prediction results with the GA solution than other SEMs, with an RMSE of 0.6714. Then, the closest fit result gives SEM 6 with 0.6796 RMSE. An average of 25% improvement was seen in the RMSEs of models analyzed with GA instead of linear regression.

6.5. NCA Dataset

The model parameters obtained through various methods for the NCA dataset are presented. Additionally, the models' MAE, RMSE, and MAPE values were compared.

6.5.1. Linear Regression Solution

Table 26 shows the parameter identification results obtained after performing linear regression calculations for every 5 SEMs based on all aging data in 'NCA Dataset. Figure 24 shows the corresponding quantitative measurements for all model cases.

Table 26. NCA model parameters are based on an analytical solution for each SEM.

Model Cases	Fitting Parameter					
SEM-1	$a_1 = 5719.9$	$a_2 = -3185.7$	$a_3 = 0.0084$	$a_4 = 0.48$		
SEM-2	$b_1 = 9530.0$	$b_2 = -0.0015$	$b_3 = 3.0720$	$b_4 = -3340$	$b_5 = 0.48$	
SEM-3	$c_1 = 86.307$	$c_2 = 0.0001$	$c_3 = -0.0065$	$c_4 = 4.4579$	$c_5 = -3202$	$c_6 = 0.49$
SEM-4	$d_1 = 75.630$	$d_2 = 0.0084$	$d_3 = 4.3259$	$d_4 = -3185$	$d_5 = 0.48$	
SEM-5	$e_1 = 0.4234$	$e_2 = 0.1535$	$e_3 = -0.859$	$e_4 = -44.20$	$e_5 = 0.47$	

Figure 24. Performance indicators for each NCA dataset modeling with analytical solution.

6.5.2. GA Solution

Table 27 shows the parameter identification results obtained after performing Genetic Algorithm for every 7 SEMs based on all aging data in 'NCA Dataset'.

Table 27. NCA model parameters are based on a GA solution for each SEM.

Model Cases	Fitting Parameter					
SEM-1	$a_1 = 3629.0$	$a_2 = -3061.3$	$a_3 = 0.0762$	$a_4 = 0.51$		
SEM-2	$b_1 = 9874.6$	$b_2 = 0.0017$	$b_3 = 1.9870$	$b_4 = -3340.7$	$b_5 = 0.49$	
SEM-3	$c_1 = 97.964$	$c_2 = 0.0001$	$c_3 = -0.0048$	$c_4 = 4.5272$	$c_5 = -3235$	$c_6 = 0.48$
SEM-4	$d_1 = 63.945$	$d_2 = 0.0076$	$d_3 = 4.8253$	$d_4 = -3271.0$	$d_5 = 0.48$	
SEM-5	$e_1 = 0.3537$	$e_2 = 0.1487$	$e_3 = -0.275$	$e_4 = -44.552$	$e_5 = 0.48$	
SEM-6	$f_1 = 53.227$	$f_2 = 4219.4$	$f_3 = -3154.1$	$f_4 = 0.52$		
SEM-7	$g_1 = 0.4928$	$g_2 = 47.962$	$g_3 = 8980.1$	$g_4 = -3291.4$	$g_5 = 0.48$	

According to the fit results for all SEMs as shown in Table 27, the SEM is capable of providing a long-term capacity degradation trend with a generalized exponential form. Figure 25 shows the corresponding quantitative measurements for all model cases.

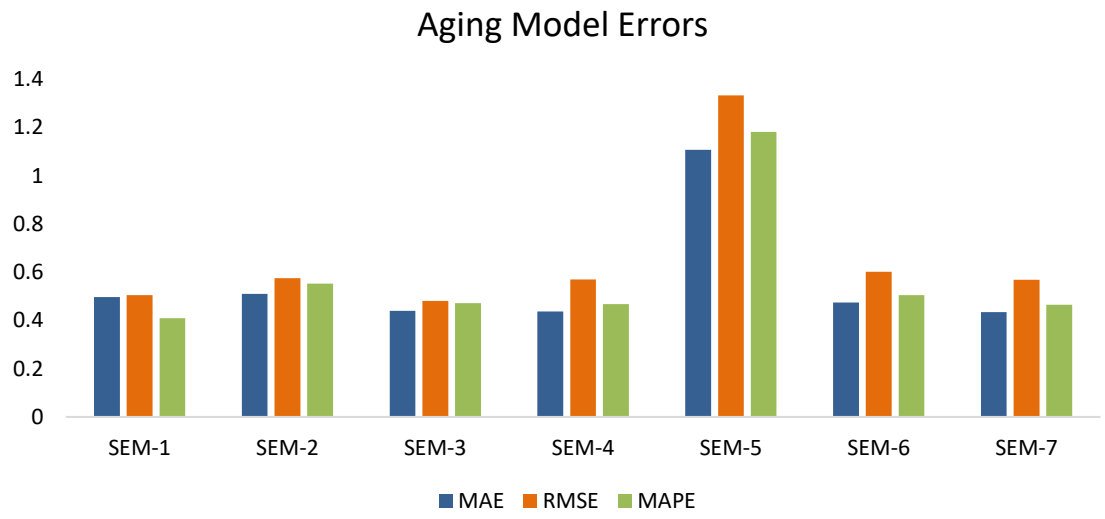

Figure 25. Performance indicators for each NCA dataset modeling with GA.

SEM 3 provides more effective prediction results with the GA solution than other SEMs, with an RMSE of 0.4810. Then, the closest fit result gives SEM 1 with 0.5043 RMSE. An average of 21% improvement was seen in the RMSEs of models analyzed with GA instead of linear regression.

6.6. HORIZON-HELIOS 2022 NMC Dataset

In order to measure the capacity of the data set in our Helios project to predict future capacity loss data, calculations were made by dividing the total data into two: 70% training data and 30% prediction data. So, approximately 70% of each case was used to calculate model parameters. The objective here is to assess the models' capacity to predict future data. Under the heading 6.1.1, the prediction results covering 30% of the data set are shown, and in 6.1.2, the estimated values for the total data set are shown. Table 28 shows the ten different experimental cases in the experiment set.

Table 28. Storage conditions for each case.

T (°C)	SoC (%)	Case Number
25	5	Case-1
	37	Case-2
	65	Case-3
	80	Case-4
	93	Case-5
60	0	Case-6
	25	Case-7
	50	Case-8
	75	Case-9
	100	Case-10

6.6.1. Prediction Results

70% of the experimental data obtained from NMC batteries within the scope of the Helios project was used to determine the model parameters. The analysis results of the model parameters using Linear Regression are shown under the heading specified in

6.6.1.1, and the analysis results using the Genetic Algorithm are shown under the heading 6.6.1.2..

6.6.1.1. Linear Regression

Table 29 displays the parameter identification results obtained from performing linear regression calculations for every 5 SEMs, based on 70% of the aging data in the 'Helios dataset.

Table 29. Helios NMC model parameters based on an analytical solution for each SEM.

Model Cases	Fitting Parameter					
SEM-1	a_1 = 220.41	a_2 = -2634.4	a_3 = 0.0163	a_4 = 0.58		
SEM-2	b_1 = 87.655	b_2 = 0.0331	b_3 = -5.3776	b_4 = -2340.4	b_5 = 0.58	
SEM-3	c_1 = 16.092	c_2 = -0.0002	c_3 = 0.0427	c_4 = 2.7783	c_5 = -2803.2	c_6 = 0.58
SEM-4	d_1 = 14.846	d_2 = 0.0163	d_3 = 2.6977	d_4 = -2634.4	d_5 = 0.58	
SEM-5	e_1 = 0.2375	e_2 = 0.1324	e_3 = -1.4234	e_4 = -37.224	e_5 = 0.59	

Figure 26 displays the model error results obtained from performing linear regression calculations for every 5 SEMs based on all prediction aging datasets in the 'HORIZON dataset'.

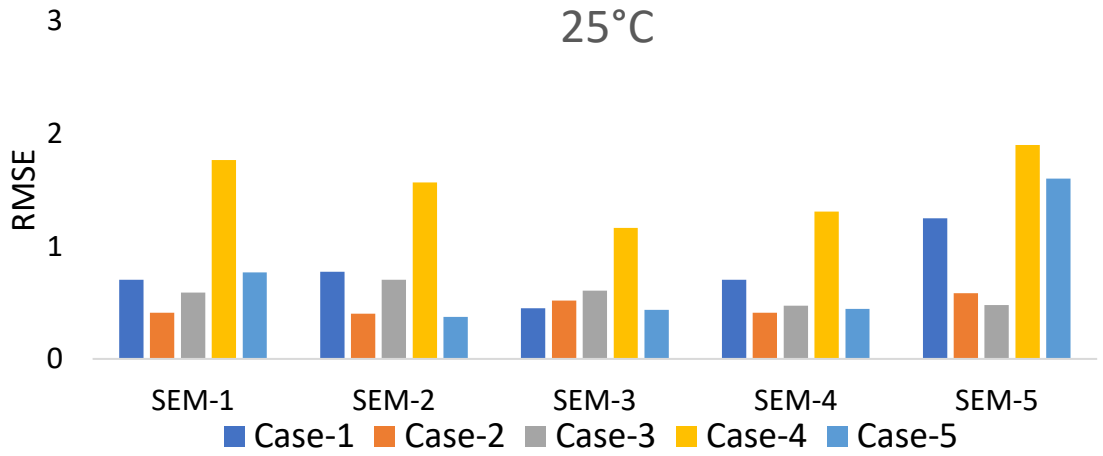

Figure 26. Performance indicators for each Helios NMC prediction case modeling with analytical solution.

(cont. on the next page.)

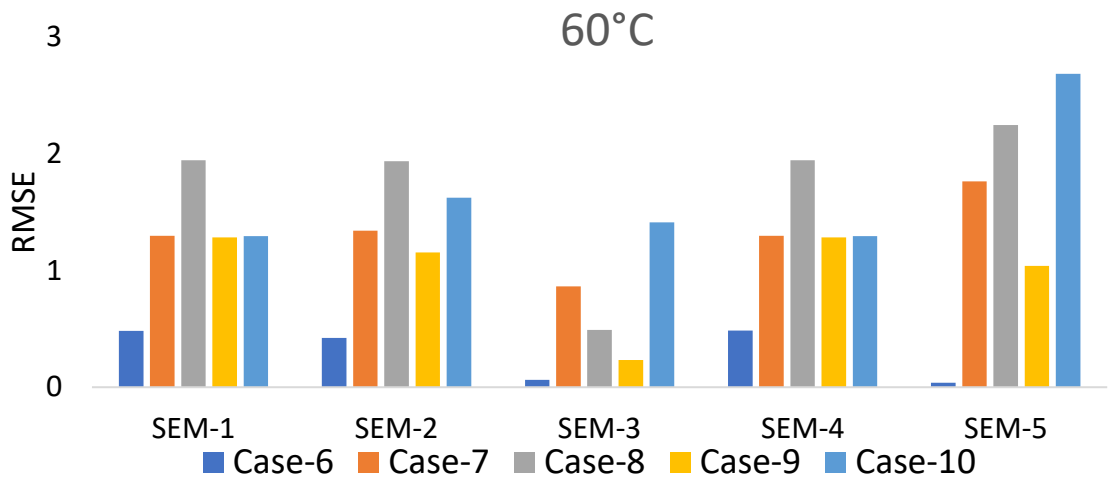

Figure 26. (cont.)

In Case 6, SEM 5 provides the best fit results with an RMSE of 0.038. SEM 3 offers the most effective prediction results for Case 9 and Case 1, with corresponding RMSEs of 0.232 and 0.451. Overall, SEM 3 (RMSE: 0.51) and SEM 1 (RMSE: 0.92) outperform their counterparts in terms of prediction results.

6.6.1.2. GA Solution

Table 30 displays the parameter identification results obtained from performing Genetic algorithm for every 7 SEMs, based on 70% of the aging data in the 'Helios dataset.

Table 30. Helios NMC model parameters based on a GA solution for each SEM.

Model Cases	Fitting Parameter					
SEM-1	a_1 = 132.05	a_2 = -2301.0	a_3 = 0.0111	a_4 = 0.56		
SEM-2	b_1 = 6.1890	b_2 = 0.0571	b_3 = -16.162	b_4 = -1124.7	b_5 = 0.57	
SEM-3	c_1 = 14.824	c_2 = -0.0002	c_3 = 0.0448	c_4 = 2.5821	c_5 = -2665.2	c_6 = 0.56
SEM-4	d_1 = 49.947	d_2 = 0.0112	d_3 = 2.1937	d_4 = -2702	d_5 = 0.56	
SEM-5	e_1 = 0.2596	e_2 = 0.1121	e_3 = -1.622	e_4 = -28.22	e_5 = 0.56	
SEM-6	f_1 = 303.93	f_2 = 8981.9	f_3 = -3975.9	f_4 = 0.65		
SEM-7	g_1 = -23.10	g_2 = 4568.9	g_3 = 32639	g_4 = -4534	g_5 = 0.59	

Figure 27 shows the model error results obtained after performing Genetic Algorithm for every 7 SEMs based on all prediction aging data in 'HORIZON dataset'.

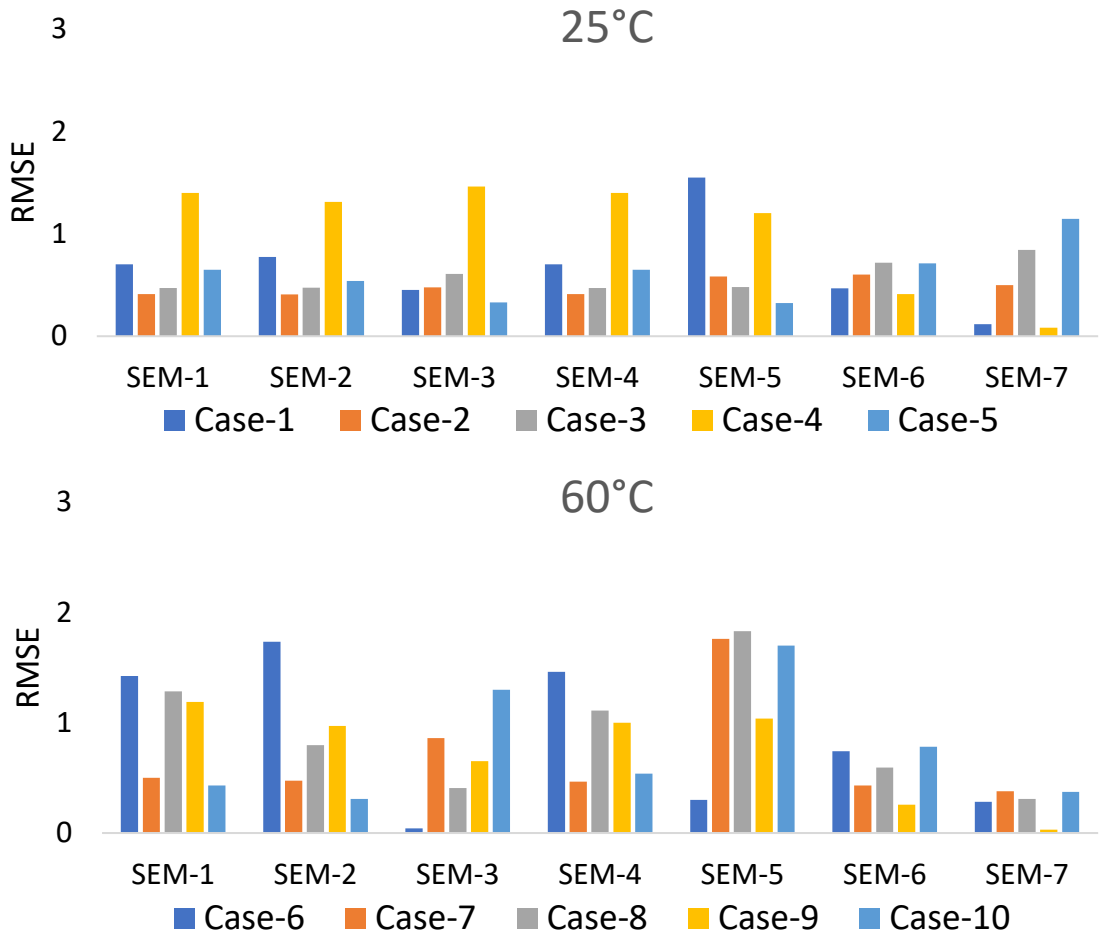

Figure 27. Performance indicators for each Helios NMC prediction case modeling with analytical solution.

In Case 9, SEM-7 provides the best fit results with an RMSE of 0.031. For Case 6, SEM 3 provides the best fit results with an RMSE of 0.042. For Case 2, SEM 2 provides the best fit results with an RMSE of 0.402. On the other hand, SEM 2 gives the most accurate result for Case 5, with an RMSE of 0.334. Overall, SEM 3 (RMSE: 0.39) and SEM 1 (RMSE: 0.82) outperform their counterparts in terms of total results.

6.6.2. Total Results

In this section, the compatibility between the aging models found using 70% of the experimental data and the entire experimental data set is examined.

6.6.2.1. Linear Regression Solution

Figure 28 shows the model RMSE results obtained after performing linear regression calculations for every 5 SEMs based on all aging data in 'HORIZON dataset'.

SEM 3 provides the most effective prediction results for Case 6 and Case 1; corresponding RMSEs of 0.214 and 0.218. For Case 4, SEM 5 provides the best fit results, with RMSEs that are 23.4% lower than the worst fit cases. On the other hand, SEM 4 gives the most accurate result for Case 2, with an RMSE of 0.340, which is 22.5% less than SEM 5. It is important to note that different SEMs will yield different training results for a given storage situation. Overall, SEM 1 (RMSE: 0.35) and SEM 3 (RMSE: 0.86) outperform their counterparts in terms of total results.

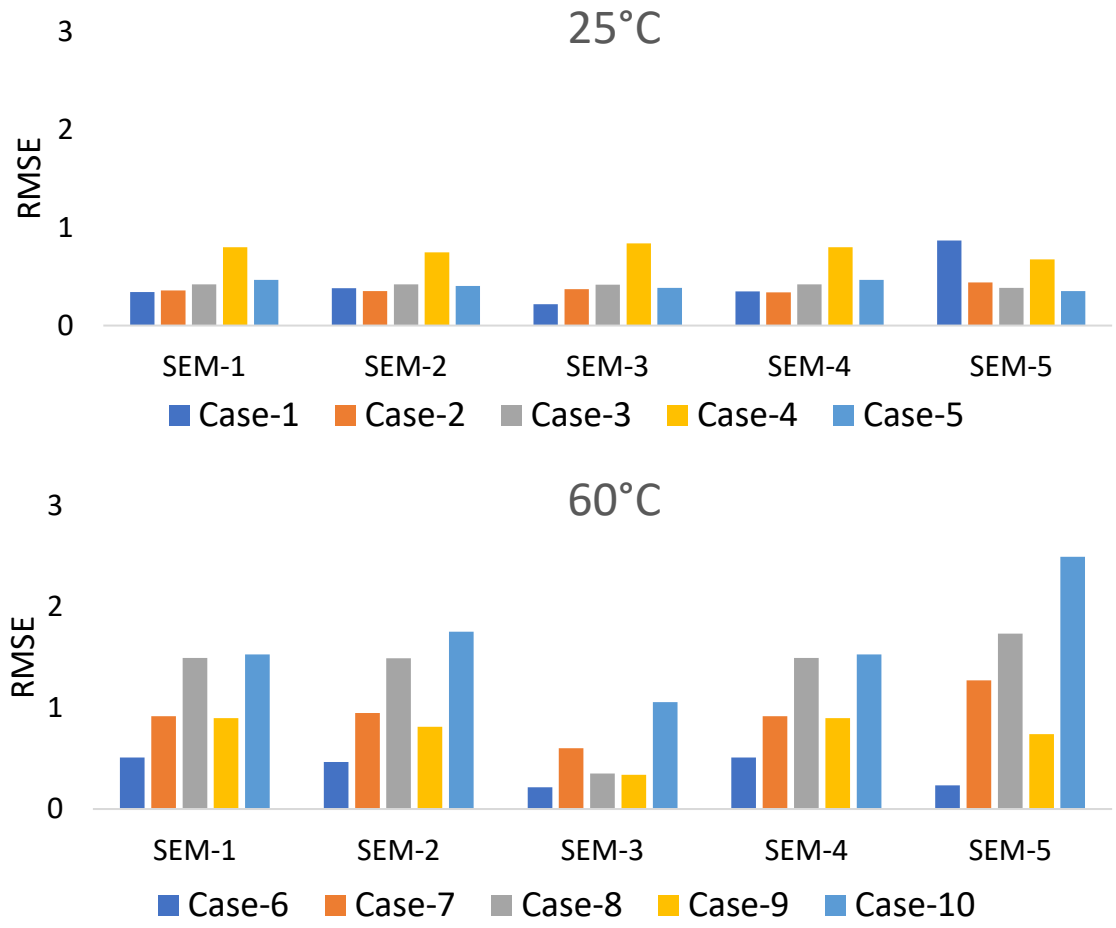

Figure 28. Performance indicators for each Helios NMC case modeling with analytical solution.

6.6.2.2. GA Solution

Figure 29 shows the model RMSE results obtained after performing Genetic Algorithm for every 7 SEMs based on all aging data in 'HORIZON dataset'.

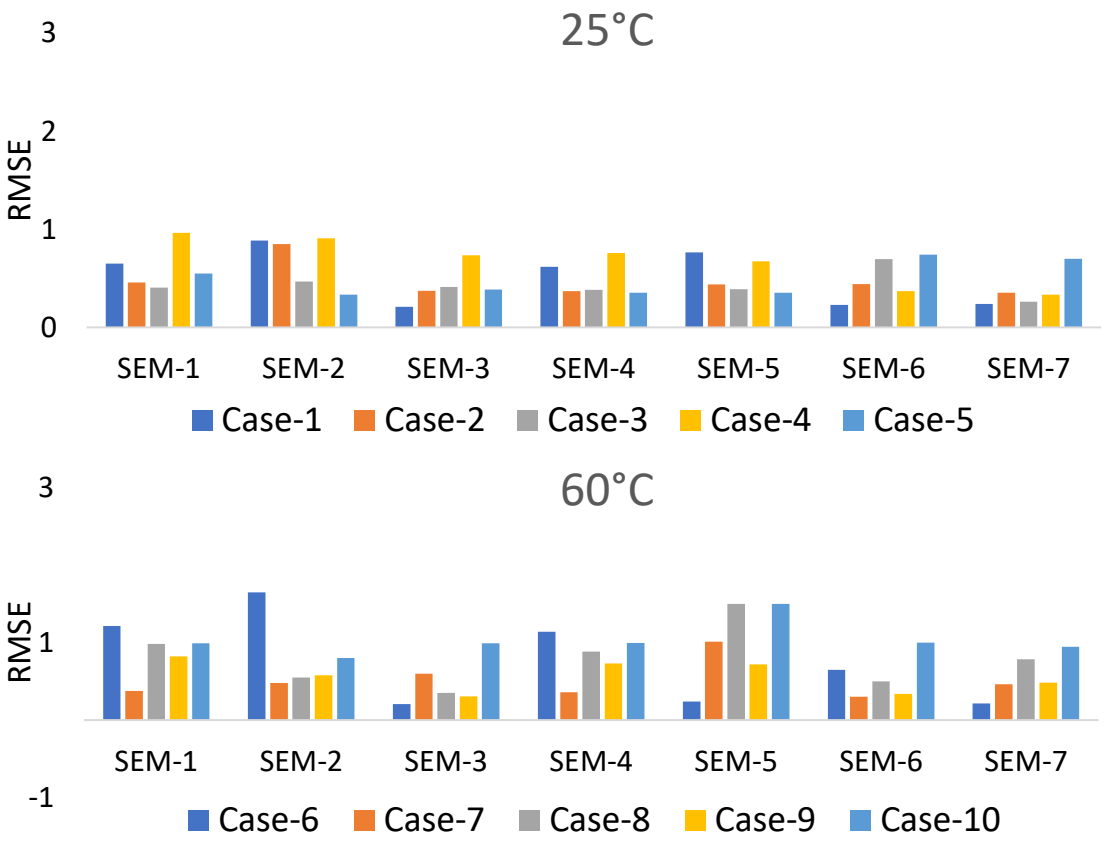

Figure 29. Performance indicators for each Helios NMC case modeling with GA.

Quantitatively, SEM 3 offers the most effective prediction results for Case 6 and Case 1, with corresponding RMSEs of 0.205 and 0.209, which are almost half of the RMSEs obtained using the other three SEMs. For Case 4, SEM 4 provides the best fit results, with RMSEs that are 60.2% lower than the worst fit cases. On the other hand, SEM 2 gives the most accurate result for Case 5, with an RMSE of 0.334. It is important to note that different SEMs will yield different training results for a given storage situation. Overall, SEM 3 (RMSE: 0.18) and SEM 1 (RMSE: 0.62) outperform their counterparts in terms of total results.

CHAPTER 7

CONCLUSION

Adaptation of EVs could be achieved by enhancing the feasibility of batteries where lifetime is an essential contributor. The lifespan of batteries decreases over time, which affects the mileage in the lifetime of operation and is primarily caused by complex and multiple side reactions. This study delves into the behavior and semi-empirical modeling of Li-ion aging, emphasizing the impact and interdependence of various operational stress factors. The study concludes that it is challenging to generalize aging behavior under operational conditions since many stress factors contribute to battery aging, rather than a single factor. Therefore, when creating empirical and semi-empirical aging models for batteries, it is essential to consider the relationships between stress factors and the limitations of the models. The literature shows that there is no perfect aging prediction model but should be decided based on application and relative variables and estimation algorithms should be based on the target application. Key findings of the study are summarized below:

• This study examined aging models for various battery types, focusing on calendar, and cycling aging. The findings were summarized in separate tables for each aging type. The articles reviewed revealed that model prediction errors were lower in calendar aging models than in bicycle aging models. Additionally, the literature showed quite satisfactory prediction accuracy for calendar aging.

• Temperature and SoC are the most critical factors that affect aging mechanisms in batteries. Increased chemical activity caused by high temperatures and degradation mechanisms such as lithium loss accelerate battery degradation. Also, battery performance can be negatively impacted by low temperatures, which increase battery aging. Lithium plating is the main degradation mechanism at low temperatures, unlike high temperatures. Although there is no linear relation between SoC and battery capacity, the battery capacity tends to decrease more quickly at high SoC values.

• One of the most critical aging mechanisms for cycling and calendar aging is SEI growth. During idle conditions, there is a strong correlation between the SEI layer growth and the anode potential, with a higher SoC leading to increased growth. However, other

kinetic effects during cycling can accelerate aging at low SoC. Aging induced by SoC can take various forms, such as exponential or linear, depending on the operating conditions.

• Another stress factor that occurs during cycle aging is the charge and discharge rate to which the battery is exposed. High rates of charge or discharge can lead to the development of SEI and degradation in the positive electrode. Additionally, it has been observed that there exists a strong relationship between the C rate and temperature: as the temperature rises, the impact of the C ratio decreases. In other words, as temperature increases, the negative effects of the C ratio intensify. Some models fail to consider this aspect, which can be attributed to the fact that testing is often conducted under accelerated conditions.

• Various studies have investigated the impact of temperature, state of SoC, and C-rate stress factors on battery aging for different chemistries, including LFP, NMC, NCA, LMO, LCO, LTO, and LMO+NMC. Among these, Li-ions with LTO and LFP cell chemistries show greater resistance to battery degradation compared to other chemistries.

• The Arrhenius model is useful for understanding how temperature affects calendar aging. However, it's important to consider that different aging processes occur at temperatures above and below room temperature during cycling. Therefore, when creating models for cyclic aging below room temperature, these differences must be taken into account.

• In general, calendar aging models represent battery storage time using a time-dependent exponential z coefficient. The aging behavior, which is primarily affected by the passivation properties of the SEI layer, is most commonly modeled using a t^z relationship, where $0.45 \leq z \leq 1$. By taking z as a variable instead of the t over z coefficient, which is assumed constant in literature, model compatibility with different data sets can be improved.

• In calendar aging modeling, it has been observed that most of the models in the literature can be solved by linear regression. However, in order for the equations to be solved using linear regression, they must be linearized. As a result of this linearization, the error is minimized by considering the natural logarithm of the Q_{loss} parameter instead of Q_{loss} itself. Therefore, when analyzing modeling studies, it is a better approach to use numerical solutions.

• As seen from 5 different analytical SEMs of 6 different experimental sets, the model error increases as the temperature increases. This error increase is caused by the 1/T dependence of temperature in the models.

• Based on evaluations in studies using a fixed set of defined parameters, SEMs can obtain satisfactory calendar aging estimates for a given storage situation. Model-3, 4, and 5 were able to predict capacity loss with low errors. In particular, Model-3 had the lowest RMSE in most experimental sets. While model errors are generally close to each other, Redondo-Iglesias et al. model and Model 7 have lower errors, similar to Model-3.

• As can be seen from the data in the Helios project, if the same parameters are still used in other different storage conditions, the prediction performance will inevitably decrease. This situation can be corrected in two ways: by improving the qualities of the relevant weathering tests and by further improving the adaptability of the SEM.

• The aging trend of a battery capacity generally shows an initial rapid deterioration followed by a relatively more linear deterioration. This is mainly due to the phenomenon of 'anode bulge', which represents the presence of excess anode electrode area compared to the cathode-electrode area. It can be seen that the exponential form in the Arrhenius-based SEM matches well with the rapid initial capacity decay.

REFERENCES

(1) Han, X.; Lu, L.; Zheng, Y.; Feng, X.; Li, Z.; Li, J.; Ouyang, M. A Review on the Key Issues of the Lithium Ion Battery Degradation among the Whole Life Cycle. *eTransportation* **2019**, *1*, 100005. https://doi.org/10.1016/J.ETRAN.2019.100005.

(2) Xiong, R.; Li, L.; Tian, J. Towards a Smarter Battery Management System: A Critical Review on Battery State of Health Monitoring Methods. *J Power Sources* **2018**, *405*, 18–29. https://doi.org/10.1016/J.JPOWSOUR.2018.10.019.

(3) Sun, X.; Li, Z.; Wang, X.; Li, C. Technology Development of Electric Vehicles: A Review. *Energies 2020, Vol. 13, Page 90* **2019**, *13* (1), 90. https://doi.org/10.3390/EN13010090.

(4) Kumar, R. R.; Alok, K. Adoption of Electric Vehicle: A Literature Review and Prospects for Sustainability. *J Clean Prod* **2020**, *253*, 119911. https://doi.org/10.1016/J.JCLEPRO.2019.119911.

(5) Sehil, K.; Alamri, B.; Alqarni, M.; Sallama, A.; Darwish, M. Empirical Analysis of High Voltage Battery Pack Cells for Electric Racing Vehicles. *Energies (Basel)* **2021**, *14* (6). https://doi.org/10.3390/EN14061556.

(6) Ovshinsky, S. R.; Fetcenko, M. A.; Ross, J. A Nickel Metal Hydride Battery for Electric Vehicles. *Science (1979)* **1993**, *260* (5105), 176–181. https://doi.org/10.1126/SCIENCE.260.5105.176.

(7) Badeda, J.; Huck, M.; Sauer, D. U.; Kabzinski, J.; Wirth, J. Basics of Lead-Acid Battery Modelling and Simulation. *Lead-Acid Batteries for Future Automobiles* **2017**, 463–507. https://doi.org/10.1016/B978-0-444-63700-0.00016-7.

(8) Zhang, C.; Li, K.; McLoone, S.; Yang, Z. Battery Modelling Methods for Electric Vehicles - A Review. *2014 European Control Conference, ECC 2014* **2014**, 2673–2678. https://doi.org/10.1109/ECC.2014.6862541.

(9) Hannan, M. A.; Hoque, M. M.; Hussain, A.; Yusof, Y.; Ker, P. J. State-of-the-Art and Energy Management System of Lithium-Ion Batteries in Electric Vehicle Applications: Issues and Recommendations. *IEEE Access* **2018**, *6*, 19362–19378. https://doi.org/10.1109/ACCESS.2018.2817655.

(10) Chen, W.; Liang, J.; Yang, Z.; Li, G. A Review of Lithium-Ion Battery for Electric Vehicle Applications and Beyond. *Energy Procedia* **2019**, *158*, 4363–4368. https://doi.org/10.1016/J.EGYPRO.2019.01.783.

(11) Stan, A. I.; Swierczynski, M.; Stroe, D. I.; Teodorescu, R.; Andreasen, S. J. Lithium Ion Battery Chemistries from Renewable Energy Storage to Automotive and Back-up Power Applications - An Overview. *2014 International Conference on Optimization of Electrical and Electronic Equipment, OPTIM 2014* **2014**, 713–720. https://doi.org/10.1109/OPTIM.2014.6850936.

(12) Chen, X.; Shen, W.; Vo, T. T.; Cao, Z.; Kapoor, A. An Overview of Lithium-Ion Batteries for Electric Vehicles. *10th International Power and Energy Conference, IPEC 2012* **2012**, 230–235. https://doi.org/10.1109/ASSCC.2012.6523269.

(13) Xiong, R.; Pan, Y.; Shen, W.; Li, H.; Sun, F. Lithium-Ion Battery Aging Mechanisms and Diagnosis Method for Automotive Applications: Recent Advances and Perspectives. *Renewable and Sustainable Energy Reviews* **2020**, *131*, 110048. https://doi.org/10.1016/J.RSER.2020.110048.

(14) Waldmann, T.; Wilka, M.; Kasper, M.; Fleischhammer, M.; Wohlfahrt-Mehrens, M. Temperature Dependent Ageing Mechanisms in Lithium-Ion Batteries – A Post-Mortem Study. *J Power Sources* **2014**, *262*, 129–135. https://doi.org/10.1016/J.JPOWSOUR.2014.03.112.

(15) Guha, A.; Patra, A. State of Health Estimation of Lithium-Ion Batteries Using Capacity Fade and Internal Resistance Growth Models. *IEEE Transactions on Transportation Electrification* **2017**, *4* (1), 135–146. https://doi.org/10.1109/TTE.2017.2776558.

(16) Han, X.; Ouyang, M.; Lu, L.; Li, J.; Zheng, Y.; Li, Z. A Comparative Study of Commercial Lithium Ion Battery Cycle Life in Electrical Vehicle: Aging Mechanism Identification. *J Power Sources* **2014**, *251*, 38–54. https://doi.org/10.1016/J.JPOWSOUR.2013.11.029.

(17) Jaguemont, J.; Boulon, L.; Venet, P.; Dube, Y.; Sari, A. Lithium-Ion Battery Aging Experiments at Subzero Temperatures and Model Development for Capacity Fade Estimation. *IEEE Trans Veh Technol* **2016**, *65* (6), 4328–4343. https://doi.org/10.1109/TVT.2015.2473841.

(18) Barré, A.; Deguilhem, B.; Grolleau, S.; Gérard, M.; Suard, F.; Riu, D.; Grolleau, S. A Review on Lithium-Ion Battery Ageing Mechanisms and Estimations for Automotive Applications *J Power Sources* **2013**, 680–689. https://doi.org/10.1016/j.jpowsour.2013.05.040ï.

(19) Palacín, M. R. Understanding Ageing in Li-Ion Batteries: A Chemical Issue. *undefined* **2018**, *47* (13), 4924–4933. https://doi.org/10.1039/C7CS00889A.

(20) Li, D.; Danilov, D.; Gao, L.; Yang, Y.; Notten, P. H. L. Degradation Mechanisms of C6/LiFePO4 Batteries: Experimental Analyses of Cycling-Induced Aging. *Electrochim Acta* **2016**, *210*, 445–455. https://doi.org/10.1016/J.ELECTACTA.2016.05.091.

(21) Li, D.; Danilov, D. L.; Xie, J.; Raijmakers, L.; Gao, L.; Yang, Y.; Notten, P. H. L. Degradation Mechanisms of C6/LiFePO4 Batteries: Experimental Analyses of Calendar Aging. *Electrochim Acta* **2016**, *190*, 1124–1133. https://doi.org/10.1016/J.ELECTACTA.2015.12.161.

(22) Safari, M.; Delacourt, C. Aging of a Commercial Graphite/LiFePO4 Cell. *J Electrochem Soc* **2011**, *158* (10), A1123. https://doi.org/10.1149/1.3614529/XML.

(23) Christensen, J.; Newman, J. A Mathematical Model for the Lithium-Ion Negative Electrode Solid Electrolyte Interphase. In *Proceedings - Electrochemical Society*; 2003; Vol. 20, pp 85–94. https://doi.org/10.1149/1.1804812.

(24) Peled, E.; Menkin, S. Review—SEI: Past, Present and Future. *J Electrochem Soc* **2017**, *164* (7), A1703–A1719. https://doi.org/10.1149/2.1441707JES.

(25) Liu, Q.; Du, C.; Shen, B.; Zuo, P.; Cheng, X.; Ma, Y.; Yin, G.; Gao, Y. Understanding Undesirable Anode Lithium Plating Issues in Lithium-Ion Batteries. *RSC Adv* **2016**, *6* (91), 88683–88700. https://doi.org/10.1039/C6RA19482F.

(26) Birkl, C. R.; Roberts, M. R.; McTurk, E.; Bruce, P. G.; Howey, D. A. Degradation Diagnostics for Lithium Ion Cells. *J Power Sources* **2017**, *341*, 373–386. https://doi.org/10.1016/J.JPOWSOUR.2016.12.011.

(27) Zhang, J.; Zhang, L.; Sun, F.; Wang, Z. An Overview on Thermal Safety Issues of Lithium-Ion Batteries for Electric Vehicle Application. *IEEE Access* **2018**, *6*, 23848–23863. https://doi.org/10.1109/ACCESS.2018.2824838.

(28) Manzetti, S.; Mariasiu, F. Electric Vehicle Battery Technologies: From Present State to Future Systems. *Renewable and Sustainable Energy Reviews* **2015**, *51*, 1004–1012. https://doi.org/10.1016/J.RSER.2015.07.010.

(29) Ecker, M.; Gerschler, J. B.; Vogel, J.; Käbitz, S.; Hust, F.; Dechent, P.; Sauer, D. U. Development of a Lifetime Prediction Model for Lithium-Ion Batteries Based on Extended Accelerated Aging Test Data. *J Power Sources* **2012**, *215*, 248–257. https://doi.org/10.1016/J.JPOWSOUR.2012.05.012.

(30) Hentunen, A.; Lehmuspelto, T.; Suomela, J. Time-Domain Parameter Extraction Method for Thévenin-Equivalent Circuit Battery Models. *IEEE Transactions on Energy Conversion* **2014**, *29* (3), 558–566. https://doi.org/10.1109/TEC.2014.2318205.

(31) Groot, J.; Chalmers tekniska högskola. Division of Electric Power Engineering. State-of-Health Estimation of Li-Ion Batteries: Ageing Models. **2014**.

(32) Vetter, J.; Novák, P.; Wagner, M. R.; Veit, C.; Möller, K. C.; Besenhard, J. O.; Winter, M.; Wohlfahrt-Mehrens, M.; Vogler, C.; Hammouche, A. Ageing Mechanisms in Lithium-Ion Batteries. *J Power Sources* **2005**, *147* (1–2), 269–281. https://doi.org/10.1016/J.JPOWSOUR.2005.01.006.

(33) Olabi, A. G.; Maghrabie, H. M.; Adhari, O. H. K.; Sayed, E. T.; Yousef, B. A. A.; Salameh, T.; Kamil, M.; Abdelkareem, M. A. Battery Thermal Management Systems: Recent Progress and Challenges. *International Journal of Thermofluids* **2022**, *15*. https://doi.org/10.1016/J.IJFT.2022.100171.

(34) Krupp, A.; Beckmann, R.; Diekmann, T.; Ferg, E.; Schuldt, F.; Agert, C. Calendar Aging Model for Lithium-Ion Batteries Considering the Influence of Cell Characterization. *J Energy Storage* **2022**, *45*, 103506. https://doi.org/10.1016/J.EST.2021.103506.

(35) Eddahech, A.; Briat, O.; Vinassa, J. M. Performance Comparison of Four Lithium–Ion Battery Technologies under Calendar Aging. *Energy (Oxford)* **2015**, *84*, 542–550. https://doi.org/10.1016/J.ENERGY.2015.03.019.

(36) Stiaszny, B.; Ziegler, J. C.; Krauß, E. E.; Zhang, M.; Schmidt, J. P.; Ivers-Tiffée, E. Electrochemical Characterization and Post-Mortem Analysis of Aged LiMn2O4–NMC/Graphite Lithium Ion Batteries Part II: Calendar Aging. *J Power Sources* **2014**, *258*, 61–75. https://doi.org/10.1016/J.JPOWSOUR.2014.02.019.

(37) McBrayer, J. D.; Rodrigues, M. T. F.; Schulze, M. C.; Abraham, D. P.; Apblett, C. A.; Bloom, I.; Carroll, G. M.; Colclasure, A. M.; Fang, C.; Harrison, K. L.; Liu, G.; Minteer, S. D.; Neale, N. R.; Veith, G. M.; Johnson, C. S.; Vaughey, J. T.; Burrell, A. K.; Cunningham, B. Calendar Aging of Silicon-Containing Batteries. *Nature Energy 2021 6:9* **2021**, *6* (9), 866–872. https://doi.org/10.1038/s41560-021-00883-w.

(38) Lammer, M.; Königseder, A.; Gluschitz, P.; Hacker, V. Influence of Aging on the Heat and Gas Emissions from Commercial Lithium Ion Cells in Case of Thermal Failure. *Journal of Electrochemical Science and Engineering* **2018**, *8* (1), 101–110. https://doi.org/10.5599/JESE.476.

(39) Deichmann, E.; Torres-Castro, L.; Lamb, J.; Karulkar, M.; Ivanov, S.; Grosso, C.; Gray, L.; Langendorf, J.; Garzon, F. Investigating the Effects of Lithium Deposition on the Abuse Response of Lithium-Ion Batteries. *J Electrochem Soc* **2020**, *167* (9), 090552. https://doi.org/10.1149/1945-7111/AB9941.

(40) Barré, A.; Deguilhem, B.; Grolleau, S.; Gérard, M.; Suard, F.; Riu, D. A Review on Lithium-Ion Battery Ageing Mechanisms and Estimations for Automotive Applications. *J Power Sources* **2013**, *241*, 680–689. https://doi.org/10.1016/J.JPOWSOUR.2013.05.040.

(41) Liu, X.; Wu, Z.; Stoliarov, S. I.; Denlinger, M.; Masias, A.; Snyder, K. Heat Release during Thermally-Induced Failure of a Lithium Ion Battery: Impact of Cathode Composition. *Fire Saf J* **2016**, *85*, 10–22. https://doi.org/10.1016/j.firesaf.2016.08.001.

(42) Wang, J.; Purewal, J.; Liu, P.; Hicks-Garner, J.; Soukazian, S.; Sherman, E.; Sorenson, A.; Vu, L.; Tataria, H.; Verbrugge, M. W. Degradation of Lithium Ion Batteries Employing Graphite Negatives and Nickel-Cobalt-Manganese Oxide + Spinel Manganese Oxide Positives: Part 1, Aging Mechanisms and Life Estimation. *J Power Sources* **2014**, *269*, 937–948. https://doi.org/10.1016/j.jpowsour.2014.07.030.

(43) Ecker, M.; Gerschler, J. B.; Vogel, J.; Käbitz, S.; Hust, F.; Dechent, P.; Sauer, D. U. Development of a Lifetime Prediction Model for Lithium-Ion Batteries Based on Extended Accelerated Aging Test Data. *J Power Sources* **2012**, *215*, 248–257. https://doi.org/10.1016/j.jpowsour.2012.05.012.

(44) Omar, N.; Firouz, Y.; Timmermans, J. M.; Monem, M. A.; Gualous, H.; Coosemans, T.; Van Den Bossche, P.; Van Mierlo, J. Lithium Iron Phosphate - Assessment of Calendar Life and Change of Battery Parameters. *2014 IEEE Vehicle Power and Propulsion Conference, VPPC 2014* **2014**. https://doi.org/10.1109/VPPC.2014.7007095.

(45) Grolleau, S.; Delaille, A.; Gualous, H.; Gyan, P.; Revel, R.; Bernard, J.; Redondo-Iglesias, E.; Peter, J. Calendar Aging of Commercial Graphite/LiFePO4 Cell – Predicting Capacity Fade under Time Dependent Storage Conditions. *J Power Sources* **2014**, *255*, 450–458. https://doi.org/10.1016/J.JPOWSOUR.2013.11.098.

(46) Kassem, M.; Bernard, J.; Revel, R.; Pélissier, S.; Duclaud, F.; Delacourt, C. Calendar Aging of a Graphite/LiFePO4 Cell. *J Power Sources* **2012**, *208*, 296–305. https://doi.org/10.1016/J.JPOWSOUR.2012.02.068.

(47) Sarasketa-Zabala, E.; Gandiaga, I.; Rodriguez-Martinez, L. M.; Villarreal, I. Calendar Ageing Analysis of a LiFePO4/Graphite Cell with Dynamic Model Validations: Towards Realistic Lifetime Predictions. *J Power Sources* **2014**, *272*, 45–57. https://doi.org/10.1016/J.JPOWSOUR.2014.08.051.

(48) Werner, D.; Paarmann, S.; Wetzel, T. Calendar Aging of Li-Ion Cells—Experimental Investigation and Empirical Correlation. *Batteries* **2021**, *7* (2). https://doi.org/10.3390/batteries7020028.

(49) Eddahech, A.; Briat, O.; Vinassa, J. M. Performance Comparison of Four Lithium–Ion Battery Technologies under Calendar Aging. *Energy* **2015**, *84*, 542–550. https://doi.org/10.1016/J.ENERGY.2015.03.019.

(50) Geisbauer, C.; Wöhrl, K.; Koch, D.; Wilhelm, G.; Schneider, G.; Schweiger, H. G. Comparative Study on the Calendar Aging Behavior of Six Different Lithium-ion Cell Chemistries in Terms of Parameter Variation. *Energies (Basel)* **2021**, *14* (11), 3358. https://doi.org/10.3390/EN14113358/S1.

(51) Jaguemont, J.; Boulon, L.; Venet, P.; Dube, Y.; Sari, A. Low Temperature Aging Tests for Lithium-Ion Batteries. *IEEE International Symposium on Industrial Electronics* **2015**, *2015-September*, 1284–1289. https://doi.org/10.1109/ISIE.2015.7281657.

(52) Maures, M.; Zhang, Y.; Martin, C.; Delétage, J. Y.; Vinassa, J. M.; Briat, O. Impact of Temperature on Calendar Ageing of Lithium-Ion Battery Using Incremental Capacity Analysis. *Microelectronics Reliability* **2019**, *100–101*, 113364. https://doi.org/10.1016/J.MICROREL.2019.06.056.

(53) Schmalstieg, J.; Käbitz, S.; Ecker, M.; Sauer, D. U. A Holistic Aging Model for Li(NiMnCo)O2 Based 18650 Lithium-Ion Batteries. *J Power Sources* **2014**, *257*, 325–334. https://doi.org/10.1016/J.JPOWSOUR.2014.02.012.

(54) Zheng, Y.; He, Y. B.; Qian, K.; Li, B.; Wang, X.; Li, J.; Miao, C.; Kang, F. Effects of State of Charge on the Degradation of LiFePO4/Graphite Batteries during Accelerated Storage Test. *J Alloys Compd* **2015**, *639*, 406–414. https://doi.org/10.1016/J.JALLCOM.2015.03.169.

(55) Redondo-Iglesias, E.; Venet, P.; Pelissier, S. Eyring Acceleration Model for Predicting Calendar Ageing of Lithium-Ion Batteries *J Energy Storage* **2017**, *13*, 176–183. https://doi.org/10.1016/j.est.2017.06.009ï.

(56) Dai, H.; Zhang, X.; Gu, W.; Wei, X.; Sun, Z. A Semi-Empirical Capacity Degradation Model of Ev Li-Ion Batteries Based on Eyring Equation. *2013 9th IEEE Vehicle Power and Propulsion Conference, IEEE VPPC 2013* **2013**, 36–40. https://doi.org/10.1109/VPPC.2013.6671660.

(57) Redondo-Iglesias, E.; Venet, P.; Pélissier, S. Influence of the Non-Conservation of SoC Value during Calendar Ageing Tests on Modelling the Capacity Loss of Batteries. *2015 10th International Conference on Ecological Vehicles and Renewable Energies, EVER 2015* **2015**. https://doi.org/10.1109/EVER.2015.7112987.

(58) Su, L.; Zhang, J.; Huang, J.; Ge, H.; Li, Z.; Xie, F.; Liaw, B. Y. Path Dependence of Lithium Ion Cells Aging under Storage Conditions. *J Power Sources* **2016**, *315*, 35–46. https://doi.org/10.1016/J.JPOWSOUR.2016.03.043.

(59) Naumann, M.; Schimpe, M.; Keil, P.; Hesse, H. C.; Jossen, A. Analysis and Modeling of Calendar Aging of a Commercial LiFePO4/Graphite Cell. *J Energy Storage* **2018**, *17*, 153–169. https://doi.org/10.1016/J.EST.2018.01.019.

(60) Keil, P.; Wilhelm, J.; Schuster, S. Calendar Aging of Lithium-Ion Batteries You May Also like Insights on Calendar Aging of Lithium-Ion Batteries from Differential Voltage Analysis and Coulometry. *J Electrochem Soc* **2016**. https://doi.org/10.1149/2.0411609jes.

(61) Xu, B.; Oudalov, A.; Ulbig, A.; Andersson, G.; Kirschen, D. S. Modeling of Lithium-Ion Battery Degradation for Cell Life Assessment. *IEEE Trans Smart Grid* **2018**, *9* (2), 1131–1140. https://doi.org/10.1109/TSG.2016.2578950.

(62) Montaru, M.; Fiette, S.; Koné, J. L.; Bultel, Y. Calendar Ageing Model of Li-Ion Battery Combining Physics-Based and Empirical Approaches. *J Energy Storage* **2022**, *51*, 104544. https://doi.org/10.1016/J.EST.2022.104544.

(63) Dubarry, M.; Truchot, C.; Liaw, B. Y. Synthesize Battery Degradation Modes via a Diagnostic and Prognostic Model. *J Power Sources* **2012**, *219*, 204–216. https://doi.org/10.1016/J.JPOWSOUR.2012.07.016.

(64) Ma, Z.; Wang, Z.; Xiong, R.; Jiang, J. A Mechanism Identification Model Based State-of-Health Diagnosis of Lithium-Ion Batteries for Energy Storage Applications. *J Clean Prod* **2018**, *193*, 379–390. https://doi.org/10.1016/J.JCLEPRO.2018.05.074.

(65) de Hoog, J.; Timmermans, J. M.; Ioan-Stroe, D.; Swierczynski, M.; Jaguemont, J.; Goutam, S.; Omar, N.; Van Mierlo, J.; Van Den Bossche, P. Combined Cycling and Calendar Capacity Fade Modeling of a Nickel-Manganese-Cobalt Oxide Cell with Real-Life Profile Validation. *Appl Energy* **2017**, *200*, 47–61. https://doi.org/10.1016/j.apenergy.2017.05.018.

(66) Krupp, A.; Beckmann, R.; Diekmann, T.; Ferg, E.; Schuldt, F.; Agert, C. Calendar Aging Model for Lithium-Ion Batteries Considering the Influence of Cell Characterization. *J Energy Storage* **2022**, *45*. https://doi.org/10.1016/j.est.2021.103506.

(67) Jaguemont, J.; Boulon, L.; Dubé, Y. A Comprehensive Review of Lithium-Ion Batteries Used in Hybrid and Electric Vehicles at Cold Temperatures. *Appl Energy* **2016**, *164*, 99–114. https://doi.org/10.1016/J.APENERGY.2015.11.034.

(68) Zheng, Y.; Ouyang, M.; Lu, L.; Li, J. Understanding Aging Mechanisms in Lithium-Ion Battery Packs: From Cell Capacity Loss to Pack Capacity Evolution. *J Power Sources* **2015**, *278*, 287–295. https://doi.org/10.1016/J.JPOWSOUR.2014.12.105.

(69) Omar, N.; Monem, M. A.; Firouz, Y.; Salminen, J.; Smekens, J.; Hegazy, O.; Gaulous, H.; Mulder, G.; Van den Bossche, P.; Coosemans, T.; Van Mierlo, J. Lithium Iron Phosphate Based Battery - Assessment of the Aging Parameters and Development of Cycle Life Model. *Appl Energy* **2014**, *113*, 1575–1585. https://doi.org/10.1016/j.apenergy.2013.09.003.

(70) Pan, B.; Dong, D.; Wang, J.; Nie, J.; Liu, S.; Cao, Y.; Jiang, Y. Aging Mechanism Diagnosis of Lithium Ion Battery by Open Circuit Voltage Analysis. *Electrochim Acta* **2020**, *362*, 137101. https://doi.org/10.1016/J.ELECTACTA.2020.137101.

(71) Wegmann, R.; Döge, V.; Sauer, D. U. Assessing the Potential of a Hybrid Battery System to Reduce Battery Aging in an Electric Vehicle by Studying the Cycle Life of a Graphite|NCA High Energy and a LTO|metal Oxide High Power Battery Cell Considering Realistic Test Profiles. *Appl Energy* **2018**, *226*, 197–212. https://doi.org/10.1016/J.APENERGY.2018.05.104.

(72) Zhang, Y.; Wang, C.-Y.; Tang, X. Cycling Degradation of an Automotive LiFePO 4 Lithium-Ion Battery. *J Power Sources* **2010**, *196*, 1513–1520. https://doi.org/10.1016/j.jpowsour.2010.08.070.

(73) Han, X.; Ouyang, M.; Lu, L.; Li, J.; Zheng, Y.; Li, Z. A Comparative Study of Commercial Lithium Ion Battery Cycle Life in Electrical Vehicle: Aging Mechanism Identification. *J Power Sources* **2014**, *251*, 38–54. https://doi.org/10.1016/J.JPOWSOUR.2013.11.029.

(74) Yang, N.; Zhang, X.; Shang, B.; Li, G. Unbalanced Discharging and Aging Due to Temperature Differences among the Cells in a Lithium-Ion Battery Pack with Parallel Combination. *J Power Sources* **2016**, *306*, 733–741. https://doi.org/10.1016/J.JPOWSOUR.2015.12.079.

(75) Gogoana, R.; Pinson, M. B.; Bazant, M. Z.; Sarma, S. E. Internal Resistance Matching for Parallel-Connected Lithium-Ion Cells and Impacts on Battery Pack Cycle Life. **2014**. https://doi.org/10.1016/j.jpowsour.2013.11.101.

(76) Baghdadi, I.; Briat, O.; Delétage, J. Y.; Gyan, P.; Vinassa, J. M. Lithium Battery Aging Model Based on Dakin's Degradation Approach. *J Power Sources* **2016**, *325*, 273–285. https://doi.org/10.1016/J.JPOWSOUR.2016.06.036.

(77) Delaille, A.; Grolleau, S.; Duclaud, F.; Bernard, J.; Revel, R.; Pelissier, S.; Redondo-Iglesias, E.; Vinassa, J.-M.; Eddahech, A.; Forgez, C.; Kassem, M.; Joly, S.; Porcellato, D.; Gyan, P.; Bourlot, S.; Ouattara-Brigaudet, M. SIMCAL Project: Calendar Aging Results Obtained on a Panel of 6 Commercial Li-Ion Cells. **2013**, 1 p.

(78) Grolleau, S.; Delaille, A.; Gualous, H.; Gyan, P.; Revel, R.; Bernard, J.; Redondo-Iglesias, E.; Peter, J. Calendar Aging of Commercial Graphite/LiFePO4 Cell – Predicting Capacity Fade under Time Dependent Storage Conditions. *J Power Sources* **2014**, *255*, 450–458. https://doi.org/10.1016/J.JPOWSOUR.2013.11.098.

(79) Dakin, T. W. Electrical Insulation Deterioration Treated as a Chemical Rate Phenomenon. *Transactions of the American Institute of Electrical Engineers* **1948**, *67*, 113–122. https://doi.org/10.1109/T-AIEE.1948.5059649.

(80) Wu, X.; Wang, W.; Sun, Y.; Wen, T.; Chen, J.; Du, J. Study on the Capacity Fading Effect of Low-Rate Charging on Lithium-Ion Batteries in Low-Temperature Environment. *World Electric Vehicle Journal 2020, Vol. 11, Page 55* **2020**, *11* (3), 55. https://doi.org/10.3390/WEVJ11030055.

(81) Burow, D.; Sergeeva, K.; Calles, S.; Schorb, K.; Börger, A.; Roth, C.; Heitjans, P. Inhomogeneous Degradation of Graphite Anodes in Automotive Lithium Ion Batteries under Low-Temperature Pulse Cycling Conditions. *J Power Sources* **2016**, *307*, 806–814. https://doi.org/10.1016/J.JPOWSOUR.2016.01.033.

(82) Rauhala, T.; Jalkanen, K.; Romann, T.; Lust, E.; Omar, N.; Kallio, T. Low-Temperature Aging Mechanisms of Commercial Graphite/LiFePO4 Cells Cycled with a Simulated Electric Vehicle Load Profile—A Post-Mortem Study. *J Energy Storage* **2018**, *20*, 344–356. https://doi.org/10.1016/j.est.2018.10.007.

(83) Single, F.; Latz, A.; Horstmann, B. Identifying the Mechanism of Continued Growth of the Solid–Electrolyte Interphase. *ChemSusChem* **2018**, *11* (12), 1950–1955. https://doi.org/10.1002/CSSC.201800077.

(84) Todeschini, F.; Onori, S.; Rizzoni, G. An Experimentally Validated Capacity Degradation Model for Li-Ion Batteries in PHEVs Applications. *IFAC Proceedings Volumes* **2012**, *45* (20), 456–461. https://doi.org/10.3182/20120829-3-MX-2028.00173.

(85) Cordoba-Arenas, A.; Onori, S.; Guezennec, Y.; Rizzoni, G. Capacity and Power Fade Cycle-Life Model for Plug-in Hybrid Electric Vehicle Lithium-Ion Battery Cells Containing Blended Spinel and Layered-Oxide Positive Electrodes. *J Power Sources* **2015**, *278*, 473–483. https://doi.org/10.1016/J.JPOWSOUR.2014.12.047.

(86) Saxena, S.; Hendricks, C.; Pecht, M. Cycle Life Testing and Modeling of Graphite/LiCoO2 Cells under Different State of Charge Ranges. *J Power Sources* **2016**, *327*, 394–400. https://doi.org/10.1016/J.JPOWSOUR.2016.07.057.

(87) Wang, J.; Liu, P.; Hicks-Garner, J.; Sherman, E.; Soukiazian, S.; Verbrugge, M.; Tataria, H.; Musser, J.; Finamore, P. Cycle-Life Model for Graphite-LiFePO4 Cells. *J Power Sources* **2011**, *196* (8), 3942–3948. https://doi.org/10.1016/J.JPOWSOUR.2010.11.134.

(88) Bloom, I.; Cole, B. W.; Sohn, J. J.; Jones, S. A.; Polzin, E. G.; Battaglia, V. S.; Henriksen, G. L.; Motloch, C.; Richardson, R.; Unkelhaeuser, T.; Ingersoll, D.; Case, H. L. An Accelerated Calendar and Cycle Life Study of Li-Ion Cells. *J Power Sources* **2001**, *101* (2), 238–247. https://doi.org/10.1016/S0378-7753(01)00783-2.

(89) Gao, Y.; Jiang, J.; Zhang, C.; Zhang, W.; Jiang, Y. Aging Mechanisms under Different State-of-Charge Ranges and the Multi-Indicators System of State-of-Health for Lithium-Ion Battery with Li(NiMnCo)O2 Cathode. *J Power Sources* **2018**, *400*, 641–651. https://doi.org/10.1016/J.JPOWSOUR.2018.07.018.

(90) Wikner, E.; Thiringer, T. Extending Battery Lifetime by Avoiding High SOC. *Applied Sciences 2018, Vol. 8, Page 1825* **2018**, *8* (10), 1825. https://doi.org/10.3390/APP8101825.

(91) Gantenbein, S.; Schönleber, M.; Weiss, M.; Ivers-Tiffée, E. Capacity Fade in Lithium-Ion Batteries and Cyclic Aging over Various State-of-Charge Ranges. *Sustainability 2019, Vol. 11, Page 6697* **2019**, *11* (23), 6697. https://doi.org/10.3390/SU11236697.

(92) Benavente-Araoz, F.; Varini, M.; Lundblad, A.; Cabrera, S.; Lindbergh, G. Effect of Partial Cycling of NCA/Graphite Cylindrical Cells in Different SOC Intervals. *J Electrochem Soc* **2020**, *167* (4), 040529. https://doi.org/10.1149/1945-7111/ab78fd.

(93) Preger, Y.; Barkholtz, H. M.; Fresquez, A.; Campbell, D. L.; Juba, B. W.; Romàn-Kustas, J.; Ferreira, S. R.; Chalamala, B. Degradation of Commercial Lithium-Ion Cells as a Function of Chemistry and Cycling Conditions. *J Electrochem Soc* **2020**, *167* (12), 120532. https://doi.org/10.1149/1945-7111/abae37.

(94) Naumann, M.; Spingler, F.; Jossen, A. Analysis and Modeling of Cycle Aging of a Commercial LiFePO4/Graphite Cell. *J Power Sources* **2020**, *451*. https://doi.org/10.1016/j.jpowsour.2019.227666.

(95) Wang, J.; Liu, P.; Hicks-Garner, J.; Sherman, E.; Soukiazian, S.; Verbrugge, M.; Tataria, H.; Musser, J.; Finamore, P. Cycle-Life Model for Graphite-LiFePO4 Cells. *J Power Sources* **2011**, *196* (8), 3942–3948. https://doi.org/10.1016/j.jpowsour.2010.11.134.

(96) Sarasketa-Zabala, E.; Gandiaga, I.; Martinez-Laserna, E.; Rodriguez-Martinez, L. M.; Villarreal, I. Cycle Ageing Analysis of a LiFePO4/Graphite Cell with Dynamic Model Validations: Towards Realistic Lifetime Predictions. *J Power Sources* **2015**, *275*, 573–587. https://doi.org/10.1016/j.jpowsour.2014.10.153.

(97) Groot, J.; Swierczynski, M.; Stan, A. I.; Kær, S. K. On the Complex Ageing Characteristics of High-Power LiFePO4/Graphite Battery Cells Cycled with High Charge and Discharge Currents. *J Power Sources* **2015**, *286*, 475–487. https://doi.org/10.1016/j.jpowsour.2015.04.001.

(98) Impact of Temperature and Discharge Rate on the Aging of a LiCoO 2 /LiNi 0.8 Co 0.15 Al 0.05 O 2 Lithium-Ion Pouch Cell. https://doi.org/10.1149/2.0401707jes.

(99) Petit, M.; Prada, E.; Sauvant-Moynot, V. Development of an Empirical Aging Model for Li-Ion Batteries and Application to Assess the Impact of Vehicle-to-Grid Strategies on Battery Lifetime. *Appl Energy* **2016**, *172*, 398–407. https://doi.org/10.1016/J.APENERGY.2016.03.119.

(100) Barcellona, S.; Piegari, L. Effect of Current on Cycle Aging of Lithium Ion Batteries. *J Energy Storage* **2020**, *29*, 101310. https://doi.org/10.1016/J.EST.2020.101310.

(101) Saldana, G.; Martin, J. I. S.; Zamora, I.; Asensio, F. J.; Onederra, O.; Gonzalez, M. Empirical Electrical and Degradation Model for Electric Vehicle Batteries. *IEEE Access* **2020**, *8*, 155576–155589. https://doi.org/10.1109/ACCESS.2020.3019477.

(102) Jalkanen, K.; Karppinen, J.; Skogström, L.; Laurila, T.; Nisula, M.; Vuorilehto, K. Cycle Aging of Commercial NMC/Graphite Pouch Cells at Different Temperatures. *Appl Energy* **2015**, *154*, 160–172. https://doi.org/10.1016/J.APENERGY.2015.04.110.

(103) Waldmann, T.; Wilka, M.; Kasper, M.; Fleischhammer, M.; Wohlfahrt-Mehrens, M. Temperature Dependent Ageing Mechanisms in Lithium-Ion Batteries – A Post-Mortem Study. *J Power Sources* **2014**, *262*, 129–135. https://doi.org/10.1016/J.JPOWSOUR.2014.03.112.

(104) Schuster, S. F.; Bach, T.; Fleder, E.; Müller, J.; Brand, M.; Sextl, G.; Jossen, A. Nonlinear Aging Characteristics of Lithium-Ion Cells under Different Operational Conditions. *J Energy Storage* **2015**, *1* (1), 44–53. https://doi.org/10.1016/J.EST.2015.05.003.

(105) Barré, A.; Deguilhem, B.; Grolleau, S.; Gérard, M.; Suard, F.; Riu, D. A Review on Lithium-Ion Battery Ageing Mechanisms and Estimations for Automotive Applications. *Journal of Power Sources*. 2013, pp 680–689. https://doi.org/10.1016/j.jpowsour.2013.05.040.

(106) Song, Z.; Hofmann, H.; Li, J.; Hou, J.; Zhang, X.; Ouyang, M. The Optimization of a Hybrid Energy Storage System at Subzero Temperatures: Energy Management Strategy Design and Battery Heating Requirement Analysis. *Appl Energy* **2015**, *159*, 576–588. https://doi.org/10.1016/j.apenergy.2015.08.120.

(107) Cordoba-Arenas, A.; Onori, S.; Rizzoni, G.; Fan, G. Aging Propagation in Advanced Battery Systems: Preliminary Results. *IFAC Proceedings Volumes* **2013**, *46* (21), 313–318. https://doi.org/10.3182/20130904-4-JP-2042.00122.

(108) Millner, A. Modeling Lithium Ion Battery Degradation in Electric Vehicles. *2010 IEEE Conference on Innovative Technologies for an Efficient and Reliable Electricity Supply, CITRES 2010* **2010**, 349–356. https://doi.org/10.1109/CITRES.2010.5619782.

(109) Lehtola, T. A.; Zahedi, A. Electric Vehicle Battery Cell Cycle Aging in Vehicle to Grid Operations: A Review. *IEEE J Emerg Sel Top Power Electron* **2021**, *9* (1), 423–437. https://doi.org/10.1109/JESTPE.2019.2959276.

(110) Käbitz, S.; Gerschler, J. B.; Ecker, M.; Yurdagel, Y.; Emmermacher, B.; André, D.; Mitsch, T.; Sauer, D. U. Cycle and Calendar Life Study of a Graphite|LiNi1/3Mn1/3Co1/3O2 Li-Ion High Energy System. Part A: Full Cell Characterization. *J Power Sources* **2013**, *239*, 572–583. https://doi.org/10.1016/J.JPOWSOUR.2013.03.045.

(111) Redondo-Iglesias, E.; Venet, P.; Pélissier, S. Influence of the Non-Conservation of SoC Value during Calendar Ageing Tests on Modelling the Capacity Loss of Batteries. *2015 10th International Conference on Ecological Vehicles and Renewable Energies, EVER 2015* **2015**. https://doi.org/10.1109/EVER.2015.7112987.

(112) Bloom, I.; Cole, B. W.; Sohn, J. J.; Jones, S. A.; Polzin, E. G.; Battaglia, V. S.; Henriksen, G. L.; Motloch, C.; Richardson, R.; Unkelhaeuser, T.; Ingersoll, D.; Case, H. L. An Accelerated Calendar and Cycle Life Study of Li-Ion Cells. *J Power Sources* **2001**, *101* (2), 238–247. https://doi.org/10.1016/S0378-7753(01)00783-2.

(113) Eddahech, A.; Briat, O.; Vinassa, J. M. Strategy for Lithium-Ion Battery Performance Improvement during Power Cycling. *IECON Proceedings (Industrial Electronics Conference)* **2013**, 6806–6811. https://doi.org/10.1109/IECON.2013.6700259.

(114) Broussely, M.; Herreyre, S.; Biensan, P.; Kasztejna, P.; Nechev, K.; Staniewicz, R. J. Aging Mechanism in Li Ion Cells and Calendar Life Predictions. *J Power Sources* **2001**, *97–98*, 13–21. https://doi.org/10.1016/S0378-7753(01)00722-4.

(115) Mirjalili, S. Genetic Algorithm. *Studies in Computational Intelligence* **2019**, *780*, 43–55. https://doi.org/10.1007/978-3-319-93025-1_4/COVER.

(116) Lambora, A.; Gupta, K.; Chopra, K. Genetic Algorithm- A Literature Review. *Proceedings of the International Conference on Machine Learning, Big Data, Cloud and Parallel Computing: Trends, Prespectives and Prospects, COMITCon 2019* **2019**, 380–384. https://doi.org/10.1109/COMITCON.2019.8862255.

(117) *Genetic Algorithms in Search Optimization and Machine Learning*. https://www.researchgate.net/publication/216545901_Genetic_Algorithms_in_Search_Optimization_and_Machine_Learning (accessed 2023-11-18).

(118) Tayfur, G. GA-Optimized Model Predicts Dispersion Coefficient in Natural Channels. *Hydrology Research* **2009**, *40* (1), 65–75. https://doi.org/10.2166/NH.2009.010.

(119) Kumar, M.; Husain, Dr. M.; Upreti, N.; Gupta, D. Genetic Algorithm: Review and Application. *SSRN Electronic Journal* **2010**. https://doi.org/10.2139/SSRN.3529843.

(120) *About Evolver*. https://help.palisade.com/v8/en/Evolver/About.htm (accessed 2023-11-18).

(121) Schmitt, J.; Maheshwari, A.; Heck, M.; Lux, S.; Vetter, M. Impedance Change and Capacity Fade of Lithium Nickel Manganese Cobalt Oxide-Based Batteries during Calendar Aging. *J Power Sources* **2017**, *353*, 183–194. https://doi.org/10.1016/J.JPOWSOUR.2017.03.090.

(122) Final Report MAT4BAT Project Final Report Grant Agreement Number: 608931 Project Acronym: ADVANCED MATERIALS FOR BATTERIES.

(123) Sun, Y.; Saxena, S.; Pecht, M. Derating Guidelines for Lithium-Ion Batteries. *Energies 2018, Vol. 11, Page 3295* **2018**, *11* (12), 3295. https://doi.org/10.3390/EN11123295.

(124) Liu, W.; Delacourt, C.; Forgez, C.; Pelissier, S. Study of Graphite/NCA Li-Ion Cell Degradation during Accelerated Aging Tests - Data Analysis of the SimStock Project. *2011 IEEE Vehicle Power and Propulsion Conference, VPPC 2011* **2011**. https://doi.org/10.1109/VPPC.2011.6043110.

(125) Keil, P. Aging of Lithium-Ion Batteries in Electric Vehicles.